University of Twente

Controlled Flow Excavation on cohesionless soil

Understanding the physical processes of Controlled Flow Excavation. Predicting the static and dynamic scour depth

Author:
R.A. Brinkers
(s2383225)

Faculty of Engineering Technology

Department of Civil Engineering

March 19, 2023

Bachelor of Science Thesis by

R.A. Brinkers

Controlled Flow Excavation on cohesionless soil

Understanding the physical processes of Controlled Flow Excavation. Predicting the static and dynamic scour depth

UT supervisor:
dr. ir. B.W. Borsje
Second assessor:
ir. M. Pena Acosta

Company supervisors:
Mayra Zaldivar
Quentin Bourdos

March 19, 2023

Public version

The original document of this thesis contains confidential information of the company DEME Offshore. This version is not confidential and open to the public. Therefore, the names of the excavation projects are changed and some equations are excluded. Some adjustments in figures are indicated with red square boxes.

Preface

This thesis is executed as a final assignment for achieving the degree Bachelor of Sciences in Civil Engineering at the University of Twente. This thesis is executed in cooperation with DEME Offshore, which is a department of the umbrella company DEME Group. The assignment that led to this thesis was proposed by DEME Offshore. They proposed building a tool that predicts a trench's static and dynamic scour depth using the sub-sea excavation method: Controlled Flow Excavation. I want to thank them for this opportunity. This report shows an understanding of all the processes that are involved in Controlled Flow Excavation and how these processes can be quantified.

First of all, I want to thank the whole examination committee in general for the clear guidance throughout the whole process. Each time when I approached you, your responses were quick and clear. This was really useful and reduced the time I was stuck on certain topics. When I had my ski accident during the Christmas break, you were sympathetic and compassionate. I was stressed about the continuation of my thesis, but you all assured me that everything would be fine and that a good recovery is most important. Thank you.

My special thanks to dr.ir. Bas Borsje for helping me find a subject, the guidance in the proposal phase, the guidance in the executing phase and for the critical but justified feedback on my deliverables. You were involved in the whole process, challenged me and understood my interest and capabilities very well. As well special thanks to my supervisors at DEME Offshore, Quentin Bourdos and Mayra Zaldivar. Quentin thank you for the extra brain power when Mayra and I were not sure about something. I think the main factor of the great working and pleasant atmosphere in the team is thanks to you. Mayra thank you for the daily guidance. There are too many things to mention I want to thank you for. I can't imagine getting this result without you. Last, thanks to the rest of the team at DEME Offshore for the funny conversations, endless snacks, bananas from downstairs, sandwich Wednesday and the long lunch break walks.

Enjoy the reading, Roel.

Abstract

Subsea excavation refers to the process of removing materials, such as sediment, rock, or debris, from the seabed floor or underwater structures. It is a technique used for a variety of purposes, including offshore oil and gas exploration, construction of underwater pipelines and cables, salvage operations, and archaeological excavations. This thesis focuses on a specific method that is used for the construction of underwater pipelines and cables on a seabed consisting of cohesionless soil. This seabed excavation method is Controlled Flow Excavation (CFE) using jetting. A CFE tool consists of a high-flow low-pressure pump with a small nozzle exerting a high-force flow on the seabed. This flow excavates materials scouring a semi-circular trench while maintaining precise control and minimizing the risk of damage to the surrounding area. There are two different scour depths. The dynamic depth is the maximum depth the flow reaches when the CFE tool is active. The static depth is reached when the CFE tool is no longer active and all the sand is settled. CFE is a complex and challenging process that requires specialized equipment and skilled operators. There is limited knowledge about the processes that take place during CFE, resulting in the possibility of achieving undesired trench dimensions. Process-based understanding is desired about the physical processes of CFE. This leads to the following main research question:

What are the physical processes of Controlled Flow Excavation and how can these processes be quantified?

The process of CFE starts when the flow exits the water pump system and is directed to the seabed. As the high-pressure water jet hits the seabed, it erodes the material and creates a depression or cavity in the seabed. The erosion potential depends on the mass properties dilantancy, permeability and slope of the bed and a stability factor. The water flow continues to erode the seabed and the dimensions of the flow increase due to entrainment. Eventually, the settling forces on a soil particle exceed the forces that initiated erosion and the particles in the suspension start to settle. The particles either settle in the trench or are transported out of the trench. There is little known about the capacity of this transport flow and the direction, making it hard to quantify the static depth after the dynamic depth is reached.

During this thesis, there are two tools built respectively for modeling the static and dynamic depth. The first model computes the dynamic depth and can be modeled by mapping all the different physical processes described in the literature into building blocks. These building blocks are jetting, erosion, entrainment and bed deformation. The second model computes the static depth and can be modeled by using the theory of the erosion parameter and empirical found relations. The results of the models are compared to the field data of the excavation projects: N, T and D. Prior to this comparison, it was found that this data was unreliable. The field data was not in line with theoretically expected trends. Therefore, no clear conclusions can be drawn about the accuracy of the models.

In the dynamic model, four different theories for erosion velocity are implemented. Winterwerp et al. (1992) showed unrealistic predictions and Leo C. van Rijn (1984) had an unusual pattern of results when a sensitivity analysis was conducted. The two theories left are Bisschop et al. (2010) and Mastbergen and Van Den Berg (2003), with respectively the second best and best results. The static model is calibrated to the field data in two ways. The first calibration is dependent on the input parameter the nozzle diameter and the other calibration is dependent on the trail velocity. There was not a significant difference in error between the two calibrations, but the nozzle diameter calibration had a large limitation for the input range of the eponymous input parameter. Therefore, the best method for modeling the static depth is applying the calibration method that is based on the trail velocity.

The main research question can be answered as follows: The physical process of CFE are the flow development in the free jet region, erosion, sedimentation and the entrainment of soil and water. Further, mass properties such as permeability, dilatancy and the slope of the bed need to be taken into account in determining the erosion potential. The flow development can be quantified by determining the discharge rate and the flow velocity. Erosion can be quantified by calculating the bed deformation which is dependent on the erosion velocity. In this research, sedimentation was neglected and therefore not quantified. Entrainment can be quantified by determining the increased discharge which is dependent on the soil and water entrainment rates.

At last, it needs to be addressed that the conclusions of the models are drawn on unreliable data. It is recommended to find a larger data set of reliable field data. Then the next steps are: research the effect of sedimentation in CFE modeling, compare the model to this new field data, and finally, make final conclusions on the best theories and methods for modeling CFE.

Contents

List of Figures

List of Tables

1 Introduction

1.1 General introduction

The offshore industry is developing rapidly due to the increasing demand for energy sources and globalization. The offshore industry has the potential to gain more oil, gas and energy from the ocean. This requires more facilities built in remote locations offshore, all depending on cables and pipelines for the transportation of these energy sources. Next to that, the increase of globalization requires larger networks of electricity and communication cables between countries and regions. The demand for cable and pipeline installation is increasing (Njock et al., 2020) (C et al., 2021).

The seabed is exposed to different kinds of environmental and external factors, such as currents, flows and drop and drag of anchors and fishing gear. These factors can damage cable and pipeline networks (Njock et al., 2020). Maintenance and reparations operations of these cables and pipeline networks are expensive and time-consuming. The cables and pipelines need to be protected to prevent damage. Multiple methods are available for the protection and installation of sub-sea cables and pipelines.

A method for installation and protection is Controlled Flow Excavation[1] (CFE). Controlled Flow Excavation is excavating a (sanded) seabed with a high-flow low-pressure pump. The CFE tool exerts a high water flow scouring a trench in the seabed. This way, a CFE process can be used for seabed clearance, route preparation, pre-lay dredging, post-lay-burial and trenching operations (DEME Offshore, 2022).

This report addresses the following subjects. First, context is given on the subject of CFE. Based on the problem statement and the assignment given by the commissioning party DEME Offshore, the research objective and main research question are established. Second, literature research has been done on all the processes that are relevant to CFE. Next to this, an in-house built model that predicts the static depth of CFE is assessed. Based on this and some other criteria, the methodology is determined for predicting the static and dynamic scour depth. These predictions are compared to available field data. Based on this comparison possible calibration methods are suggested in order to receive the best result. A sensitivity analysis of the models is conducted to analyze the quality of the model and the critical parameters are determined. Finally, the findings of this report are discussed, a conclusion is drawn and some recommendations are given for further research.

[1]The term Controlled Flow Excavation is introduced by DEME Offshore and is similar to the terminology Mass Flow Excavation (MFE) in other studies.

1.2 Context

Sub-sea excavation

There are three types of hazards that can damage cables and pipelines when a cable or pipeline is not protected (Njock et al., 2020) (Lu et al., 2021). The first one is environmental threats, e.g. currents that cause the cable or pipeline to move, resulting in deformation and internal stresses. The second type of threat is floating. A pipeline or cable has the possibility that it can start to float, also resulting in deformation and stresses. The third and last threat is external threats. These threats are caused by human interference. The cables or pipelines can be damaged by ships and drop and drag of anchors and fishing gear. The methodology of protecting cables and pipelines is to bury them under a specific layer of sand using sub-sea excavation. Sub-sea excavation refers to the process of removing materials, such as sediment, rock, or debris, from the seabed floor or underwater structures. It is a technique used for a variety of purposes, including offshore oil and gas exploration, construction of underwater pipelines and cables, salvage operations, and archaeological excavations.

Sub-sea excavation can be achieved through several methods (Nobel, 2013), including:

- Dredging: Involves using a dredger to scoop up sediments and materials from the seabed floor and depositing them into a barge or vessel.
- Jetting: Uses high-pressure water jets to loosen and remove sediments from the seabed floor.
- Suction: Involves using a suction pump to remove sediments and materials from the seabed floor.
- Mechanical excavation: Uses mechanical tools, such as excavators or backhoes, to dig and remove sediments and materials from the seabed floor.

In general, sub-sea excavation projects are considered to be complex, time-consuming and expensive. However, subsea excavation is of great importance in offshore engineering. A more general understanding of offshore engineering and its history is provided in Appendix-13.1.

Controlled Flow Excavation (CFE)

A relatively new method for seabed excavation is Controlled Flow Excavation using jetting. Unlike other excavation methods, CFE uses a powerful water jet to excavate materials while maintaining precise control and minimizing the risk of damage to the surrounding area. The CFE tool is hanging directly from a vessel or it is controlled by a Remotely Operated Vehicle (ROV) that is connected to a vessel. A CFE tool consists of a high-flow low-pressure pump with a small nozzle exerting a high force on the seabed. The CFE tool blows the seabed material away with its high flow. This high flow of water causes the sand particles to change from a static solid state to a more dynamic fluid state. This phenomenon is called fluidization or liquefaction (Stuyts et al., 2018).

CFE can be used for seabed clearance, route preparation, pre-lay dredging, trenching, and post-lay burial. It can also be used to de-bury cables to repair or remove them. Post-lay burial of a cable is the process of lowering a cable from the surface of the seabed to a certain depth. It can be achieved in two ways. Either by eroding the sand particles underneath the cable or fluidizing the sand beneath the cable causing the cable to sink due to its own weight. The most effective post-lay burial method is using a CFE tool with an inclined jet. One of CFE applications that was already mentioned is trenching. Trenching is an operation used before the actual installation of the cable. It scours a semi-circle trench for the cable, lowering the cable and removing the cable as a protrusion from the sea bed surface. The trench keeps the cable in place and protects the cable from threats. The dimensions of the trench must meet the depth of lowering requirements. It is therefore important to use the right CFE tool and operational parameters to create a trench sufficient for the dimension of the cable.

There are various types of CFE tools, each with its characteristic and settings. There are even CFE tools with multiple jets instead of one. The focus of this report is on a CFE tool with a single jet exerting the water flow perpendicular to the seabed used for trenching. Initially, it is thought that the effectiveness of the CFE tool and dimensions of the trench depends on the characteristics of the soil and jet, transverse velocity and offset distance of the CFE tool to the seabed and other external environmental factors. The results of this research should provide more insight into this.

The nozzle of the CFE tool exerts the water with a certain flow and pressure on a certain angle to the seabed. The static solid state of the sand changes into a dynamic fluid state. Sand is eroded and transported. The velocity of the sand particles decreases over time and the sand particles are re-deposited either in the trench or outside of the trench. The settlement in the trench occurs because the sand particles in the scour profile are liquefied, but can't exit the impingement zone due to impacts with other sand particles (hindered settlement further defined in section-2.3) and the created sand banks. After the jetting is stopped, these sand particles settle back in the trench and do not cause a change in profile. The jet can penetrate deep in the soil, exceeding the maximum slope angle of the soil and causing the sand particles to slide back down into the impingement zone. This all creates a certain profile which can be seen in figure-1.1. To conclude, there are two scour profiles. The first one, while the jet is active; the dynamic scour profile. The second one after the jet has stopped or moved; the static scours profile. After the jet has stopped or moved, the sand particles need some time to settle. This can take up to 0.5-1 minute for fine sand (Stuyts et al., 2018).

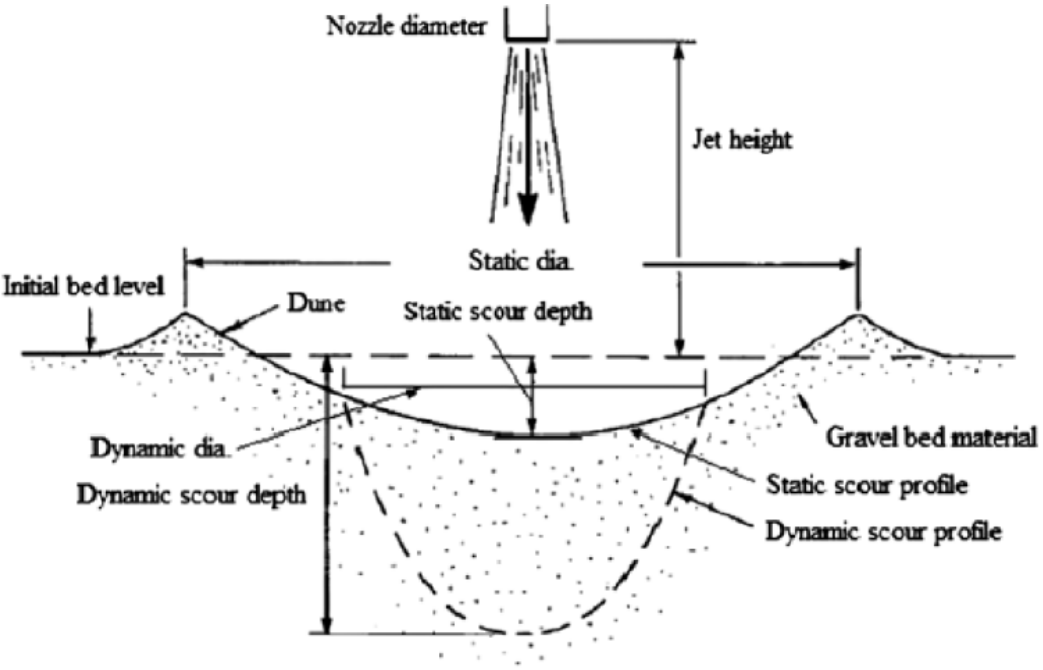

Figure 1.1: Sketch of a trench using CFE
Source: (Stuyts et al., 2018)

1.3 Problem statement

Controlled Flow Excavation is a complex and challenging process that requires specialized equipment and skilled operators. It is often carried out in harsh and challenging environments, such as deep-sea trenches or areas with strong currents, which can pose safety risks and make the excavation process more difficult. Therefore, proper planning, safety measures, and expertise are crucial for the success of sub-sea excavation projects. Cable and pipe laying installation projects including sub-sea excavations are expensive and time-consuming. The costs of the installation of pipelines/cables are in the order of 2 to 5 million pounds per kilometer (Gerrard, 2018). CFE has the potential to be more efficient than traditional excavation methods. More research is needed to optimize the technology in order to determine more accurate ways for various sub-sea environments.

At the beginning of a project, some requirements are set. These requirements include the minimum depth that needs to be excavated in order to achieve the burial or de-burial of a cable. It is possible that with low accuracy use of CFE, these requirements are not met. The vessel with the jet needs to do another pass over the trench, leading to more vessel time and as it was said in the beginning, sub-sea excavation projects are expensive.

There are possible causes for undesired trench dimensions. One can imagine that if the flow velocity of the jet is significantly low, almost no seabed erosion will occur. Another cause can be that the jet is located too far from the seabed and subsequently the flow does not interact with the soil. Based on the experience of engineers in the relevant field of this topic, it is observed that now and then the required trench dimensions are not met. There is a gap in knowledge on what processes take place after the flow has left the pump in the direction of the soil. What happens with the flow between the pump and soil, how does the flow interact with the soil and what factors determine the final trench dimensions? The gap in knowledge prevents the possibility to make accurate predictions which in consequence prevents achieving required trench dimensions in practice. To conclude, the problem can be stated as:

The gap in knowledge about the processes that take place during CFE prevents making accurate predictions and consequently results in the possibility of achieving undesired trench dimensions

1.4 Research objective

CFE is an interesting process that involves a lot of steps. From lowering the jet from the vessel to its designated location to actually excavating the soil. This whole process from the design table to the desired results takes a long time to plan and prepare. Following the problem statement, it is clear that more research needs to be done on the interaction between the jet and the soil. Based on this research and theory a correct assessment of these processes can lead to a better general understanding of subsea excavation using flows and jets.

The scope of this research is narrowed down to investigate the processes of CFE on cohesionless soil using a single jet that has a perpendicular angle with the seabed. If these processes are fully understood it can lead to an accurate prediction of how soil is deformed when it is exposed to a high flow. Ideally, a model can be developed that predicts the static and dynamic scour depth of the trench. To achieve this, the objective of this research can be stated as follow:

To understand and quantify the physical processes that take place during CFE

The use of the model provides more insight into CFE so other engineers can use this research as information for relevant projects. This research could be beneficial for all projects including sub-sea excavation with jetting. The final product of this thesis is very specific, but the theory and separate parts elaborated in this research could contribute to further research on the topic of sub-sea excavation.

1.5 Research questions

The objective is clear, more need to be known about the physical processes of CFE and how this can be quantified. The main research question is established based on the objective.

Main research question

1. What are the physical processes of Controlled Flow Excavation and how can these processes be quantified?

The main research question is divided into sub-research questions so that all the steps that need to be taken for answering the main research question are covered. The sub-research questions are:

Sub-research questions

1.1. What is known about Controlled Flow Excavation in literature?

1.2. How can Controlled Flow Excavation be implemented in modeling and how can the model(s) be calibrated?

1.3. What is the accuracy of the developed model(s) when it is compared to the field data from the Controlled Flow Excavation projects?

1.4. Which parameters/factors have the highest influence on the sensitivity of the result?

The sub- and main research questions are answered in the conclusion.

2 Literature research

In this section, literature research is conducted on the subject of Controlled Flow excavation. All the relevant processes to this subject are extensively researched and elaborated. First, all the phenomena that occur during CFE are mapped. Then each phenomenon is in-depth elaborated. Also, some equations are given that are useful for the quantification of the phenomenon.

2.1 Process of Controlled Flow Excavation

CFE is a complex process where multiple phenomena occur simultaneously and influence each other. The pump of the jet, with a certain trail velocity and flow exit velocity, exerts a low-pressure high water flow to the seabed. At multiple locations, sand is taken from the seabed or settled back onto the seabed. In order to map this in an understandable way, the path and direction of a flow are followed and described in chronological order. A description is given in figure-2.1.

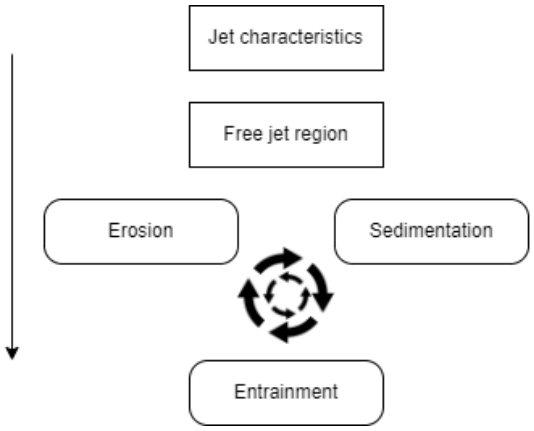

2.1.a. Description of the CFE processes in chronological order

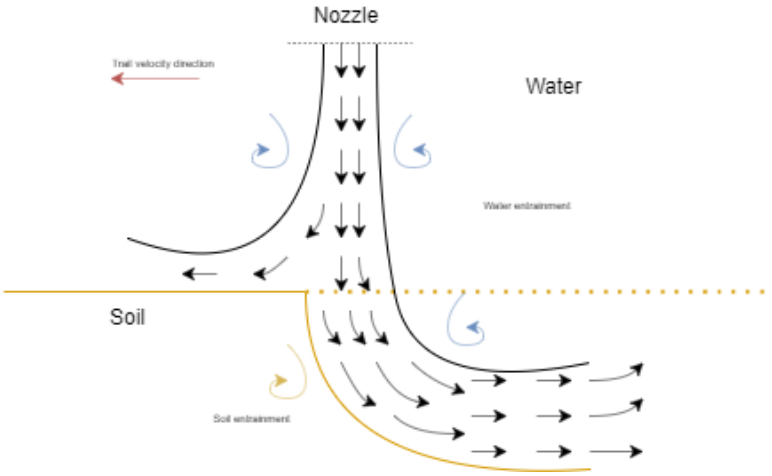

2.1.b. Schematization of CFE processes

Figure 2.1: Overview of CFE processes

This research starts when a free circular jet is active and starts pumping water in the direction of the seabed. The pump has a certain power that affects the pressure and flow rate of the water flow. The water flow is affected by the surrounding water that has no or a significantly lower flow velocity. This creates Reynolds shear stresses at the boundary of the flow and the surrounding water. These stresses can be compared to friction forces. Due to this friction, more water is entrained, the discharge increases and the velocity decreases. Additionally, the radius of the circular jet flow increases. Eventually, if the force of the water is large enough, the water flow will impede the soil. A hydraulic gradient moves down in the soil. If the flow pressure is equal to or larger than critical failure pressure, erosion occurs. Erosion is defined as *the process of gradual destruction of the surface of something* (Dey, 1996). The soil is in suspension and the sand is transported away with the flow.

The jet is moving in a horizontal direction. The velocity of this movement is called the trail velocity. In a 2D scenario when the jet starts impeding the soil the flow entrains soil on both sides. When the jet starts moving to the left, it will only erode more sand on the left. The flow does not reach any soil on the right side, because it is moving away from this. So after some initial setup time, it can be assumed that the flow is surrounded by water on one side and soil on the other side. This can be seen in the right figure of figure-2.1. This results in two types of entrainment: soil entrainment and water entrainment. These entrainment rates have a similar effect on the flow as the water entrainment before the flow reaches the soil. These effects were an increasing discharge, decreasing velocity and increasing width of the flow.

The maximum depth of the flow (dynamic depth) is dependent on the ratio between the trail velocity and the flow exit velocity. Due to the entrainments and the trail velocity, the direction of the flow starts to bend backward (the opposite direction in which the jet is moving). The maximum depth (dynamic depth) is reached, when the

direction of the flow exceeds the horizon or when the flow does not impede the soil any deeper.

After some time, the settling forces on a particle exceed the initial forces of the flow and the soil in the suspension starts to settle. Sedimentation occurs. Sedimentation is the process of particles that settle to the bottom of a body or water flow. Due to the dynamic depth and the banks on the sides of the trench, some percentage of the soil in the suspension can't settle outside the dimensions of the trench, resulting in a back-fill of the trench. The rest settles outside of the trench. When no soil is in suspension anymore, the static depth is reached.

2.2 Erosion

In the context of CFE, erosion can be described as the process of gradual destruction of the surface of the seabed by the flow of water. This occurs when the jet penetrates the soil and the forces exerted by the flow exceed the critical stability of the soil. This section starts by briefly mentioning which forces act on a single grain. After this, the most well-known stability factor will be discussed. The stability factor can be used to indicate and quantify the scour profile of the erosion process by calculating the erosion velocity in m/s. The erosion velocity describes the bed deformation. It indicates the erosion potential of a jet and will later be used to quantify erosion in the dynamic model.

2.2.1 Forces acting on a soil particle

The two forces that act vertically on a spherical sand particle are the gravity force (F_g) and the drag force (F_{dv}). There are also forces acting horizontally on a spherical sand particle. These forces are the drag force (F_{dh}), shear force (F_s) and lift force (F_l). These forces can be calculated with equations-13.1-13.5 in appendix-13.2.1.

If a sand particle is stable, all the forces around the center of the particle are in equilibrium. The drag force and shear forces are equal to the shear force and the gravitational force is equal to the lift force. Movement starts when the equilibrium of these forces is disrupted. The exerted water on the seabed causes the pore pressure of the soil to increase. This results in an increasing drag force, shear force and lift force. A force exceeds a critical resistance force. The forces on a sand particle are no longer in equilibrium and the sand particle starts to move.

2.2.2 Stability factor: Shields parameter

After the jet penetrates the soil, a sand particle starts to move when the instantaneous fluid force on a single particle exceeds the resisting force (Shahmohammadi et al., 2021). The resisting force depends on multiple factors such as the friction coefficient and particle weight. The most well-known stability factor is the Shield parameter (θ) (-). The basic Shield equation is as follows (Shahmohammadi et al., 2021) (Schoen, 2014):

$$\theta = \frac{\tau_{bed}}{(\rho_s - \rho_w) * g * D_{50}} = \frac{u_*^2}{g * \Delta * D_{50}} = \frac{u^2}{{C_{ch}}^2 * \Delta * D_{50}}$$

Where :

$$\begin{aligned}
\theta &= \text{Shields parameter [-]};\\
\tau_{bed} &= \text{bed shear stress } [N/m^2];\\
\rho_s &= \text{Density of the soil } [kg/m^3];\\
\rho_w &= \text{Density of water } [kg/m^3];\\
g &= \text{gravitational acceleration } [m/s^2];\\
D_{50} &= \text{Diameter of soil grain } [m];\\
u_* &= \text{Overall bed-shear velocity } [m/s];\\
C_{ch} &= \text{Chézy coefficient } [\sqrt{m/s}];\\
\Delta &= \text{Relative density } [-] = (\rho_s - \rho_w)/(\rho_w);
\end{aligned} \tag{2.1}$$

The critical point at which a particle starts to move can be described with the critical Shields parameter (θ_{cr}) [-]. No erosion will take place if the Shields parameter is below this critical value. When the Shields parameter is

equal to this critical value the critical point is reached. This critical point is called the state of incipient motion or critical condition (Shahmohammadi et al., 2021). The critical value can be calculated similarly to equation-2.1 with equation-2.2:

$$\theta_{cr} = \frac{\tau_{bed_cr}}{(\rho_s - \rho_w) * g * D_{50}} = \frac{{u_{*cr}}^2}{g * \Delta * D_{50}} = \frac{{u_{cr}}^2}{{C_{ch}}^2 * \Delta * D_{50}} \tag{2.2}$$

Leo C. van Rijn (1984) altered equation-2.2 to derive a new equation that calculates the critical Shields parameter. The critical Shields parameter is dependent on a dimensionless critical diameter that can be derived from equation-2.3. Subsequently, the critical Shields parameter can be derived from equation-2.4 (Schoen, 2014). This last equation only holds when the dimensionless critical diameter is between the values 20 and 150.

$$\begin{aligned} D_* &= D_{50} * (\frac{\Delta * g}{\nu^2})^{\frac{1}{3}} \\ &\text{Where :} \\ D_* &= \text{Critical diameter [-];} \\ \nu &= \text{Viscosity of water } [10^3 Pa]; \end{aligned} \tag{2.3}$$

$$\theta_{cr} = 0.013 D_*^{0.29} \text{ for } 20 < D_* < 150 \tag{2.4}$$

2.2.3 Hindered erosion according to Bisschop et al. (2010)

The theory of the Shield parameter does not take hindered erosion into account. Hindered erosion decreases the erosion potential of high velocities due to the properties of soil as a mass. These properties of soil mass are the angle of the sand bed, permeability, and dilatancy. Schoen (2014), W.D. Regout (1996) and Bisschop et al. (2010) address some adjustment factors to take mass properties into account in the process of erosion.

Slope angle of the bed
At the start of the CFE process, the jet exerts the water on the soil perpendicular to the top layer of the sand bed. It is assumed that at the start of this process, the soil is flat. The jet penetrates the soil and some sand is eroded and transported away from its original place. The angle of the bed (α_{bed}) [deg] will increase along the direction of the jet. The stability of the soil decreases and sand is then with less effort eroded. The critical angle at which the soil is unstable and the soil breaches with the absence of a jet flow is called the angle of internal friction (ϕ) [deg]. In this situation, each particle is already on the threshold of movement. Theoretically, if the angle of internal friction is met, infinite erosion takes place Schoen (2014). However, in practice this is different due to the influence of dilatancy (Yuan et al., 2019).

Permeability and dilantancy
With high velocities, particles are not eroded particle by particle but in layers. The top layer is exposed to shear forces. When this top layer is sheared, the positioning of the particles is altered due to deformation in all directions. Due to this shearing, the particles need to move upwards in order to enhance the horizontal displacement. The porosity increases. The soil needs to fill these arisen pores with water in order to maintain its shape, resulting in a hydraulic gradient (Van Rhee, 2010). Theoretically, this hydraulic gradient can push either the top or lower layer with a certain force to the other layer. The direction of the force depends on the direction of the hydraulic gradient. Bisschop et al. (2010) stated that dilatancy retard the erosion potential of a layer. For CFE this means that the top layer is pushed down to the lower layer. With this theory of dilantancy applied, the shear stress needed to erode needs to be higher than proposed in earlier theories, e.g. Leo C. van Rijn (1984). Figure-2.2 illustrates dilatancy.

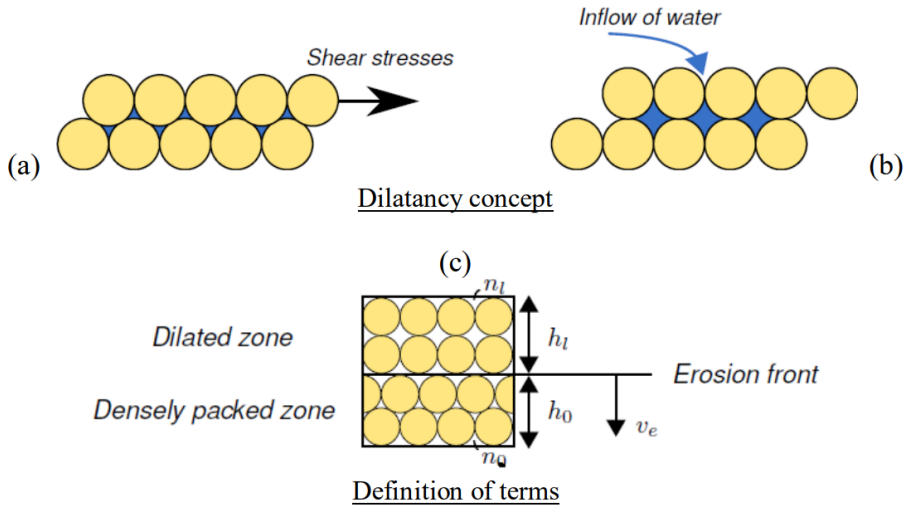

Figure 2.2: Process of dilatancy
The soil is subject to a shear force (a). This increases the pore volumes driving the inflow of water into these pore volumes (b). The result is that the lower layer is more densely packed than its original state (c)
Source: (Elsayed and Goseberg, 2020)

Permeability is an indication of the ease of movement of a liquid through the soil. Permeability is dependent on the particle size, porosity and composition of the soil. Bisschop et al. (2010) derived an equation to take the properties of dilantancy and permeability into account.

The porosity of the top layer is hard to determine. According to Van Rhee (2010), n_i can be altered to the maximum porosity n_{max}. The max porosity for fine sand (grain diameter between 0.075 to 0.425mm) is 0.46 (Geotechdata.info, 2013). Taking the slope of the bed, the permeability and the dilantancy into account the critical Shields parameter ($\theta_{cr}{}^*$) [-] can be adjusted. This factor is shown in equation-2.5. How this equation is derived can be found in appendix-13.2.2.

$$\theta_{cr}{}^* = \theta_{cr} * \left(\frac{sin(\phi) + sin(\alpha_{bed})}{sin(\phi)} * \frac{\nu_e}{k} * \frac{n_{max} - n_0}{1 - n_{max}} * \frac{1}{\Delta * (1 - n_0)}\right)$$

Where :

$$\begin{aligned} \phi &= \text{angle of internal friction [°]};\\ \alpha_{bed} &= \text{Angle of the sea-bed [°]};\\ i &= \text{Hydraulic gradient [m/s]};\\ \nu_e &= \text{Erosion velocity [m/s]};\\ k &= \text{Permeability [m/s]};\\ n_0 &= \text{in-situ porosity [-]};\\ n_{max} &= \text{Maximum Porosity [-]}; \end{aligned} \tag{2.5}$$

2.3 Sedimentation

In the context of CFE, sedimentation can be described as the process of soil particles that are in the suspension of the flow that settles to the surface of the seabed. In most of the erosion velocity theories discussed later in section-2.4, it is assumed that sedimentation is relatively small when erosion occurs. Sedimentation is therefore neglected in those theories. Due to this reason, it is less relevant for this research and the theory about sedimentation is limited. Nevertheless, research was done on the topic of sedimentation. The goal of this research was to find any theory or relevant information that says that sedimentation can't be neglected. No clear statements or relevant theories were found that could substantiate that sedimentation had to be included. Therefore, sedimentation in this report is left out of further research. The research on the topic of sedimentation can be found in appendix-13.2.3.

2.3.1 Hindered sedimentation and erosion according to Winterwerp et al. (1992)

Erosion increases the number of sand particles within a flow. This means that the sand concentration (c) is increased. If the presence of sand particles in a flow is higher, the chance of collisions between the particles increases. A sand particle with a certain movement direction will be altered into a new direction and/or slowed down, because of this collision. The collision of sand particles in water-sand mixture causes two phenomena: hindered settlement and hindered erosion. Note that the hindered erosion here is different than the hindered erosion mentioned in section-2.2.3. That hindered erosion is affected by mass soil properties and this hindered erosion is affected by the concentration level of sand within a flow. The hindered settling according to Winterwerp et al. (1992) is analogous to hindered erosion. Hindered settling can be described as the obstruction and collision between sand particles within a flow that prevents the sand particle to settle onto the sea bed. The sand particle tries to settle by a downward movement but collides with slower settling particles or just eroded sand particles trying to move upwards. Contra-wise hindered erosion is the phenomenon of an eroding particle that is hindered by slower-moving eroded particles or settling particles.

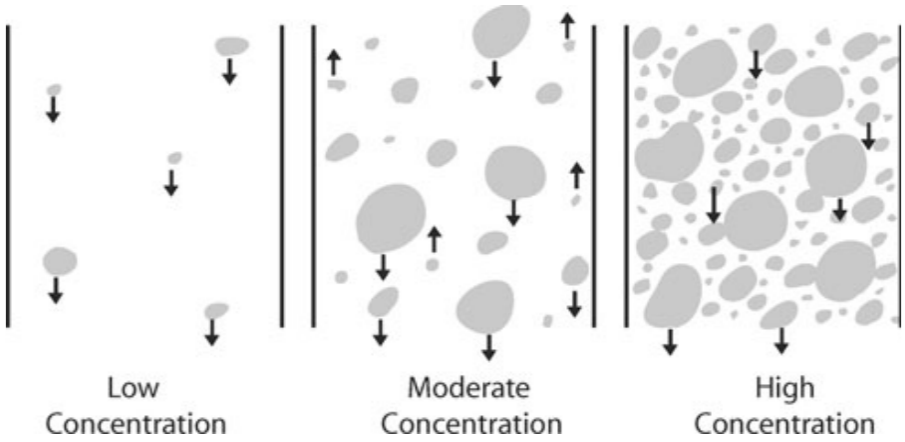

Figure 2.3: Hindered settling
Source: (Major, 2003)

2.4 Pick-up functions - Erosion velocity

The theory mentioned in the previous sections describes erosion and sedimentation, but how can the net displacement of the bed level be quantified? The potential displacement can be expressed as erosion velocity (ν_e) in $[m/s]$. The general way of computing the erosion velocity can be calculated by subtracting the pick-up flux (E) from the settling flux (S) and dividing that by the density of the solid, the in-situ porosity and the concentration level near the bed. The equation is shown below:

$$\nu_e = \frac{E - S}{\rho_s * (1 - n_0 - c_b)} \text{ or } \nu_e = \frac{E}{\rho_s * (1 - n_0)} \text{ when S} = 0$$

Where :

$$\begin{aligned} \nu_e &= \text{Erosion velocity } [m/s]; \\ E/\phi_p &= \text{Pick-up flux } [kg/m^2 s]; \\ S/\phi_s &= \text{Settling flux } [kg/m^2 s]; \\ c_b &= \text{Concentration of the bed level [-]}; \end{aligned} \tag{2.6}$$

The pick-up flux is the mass of sand that is eroded from the bed level into suspension. The settling flux is the mass of sand that settles from the suspension to the bed level of the soil. Figure-2.4 shows the relation between the pick-up flux and settling flux. Both these fluxes are expressed in $kg/m^2 s$. The bed level decreases when the pick-up flux is larger than the settling flux. The bed level decreases when the settling flux is lower the pick-up flux.

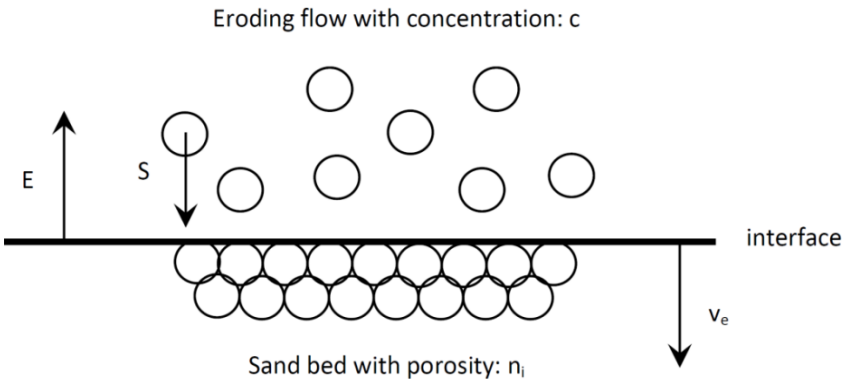

Figure 2.4: Relation between pick-up flux and settling flux
Source: (Van Rijn et al., 2019)

There are four theories found in the literature that describes how erosion velocity can be calculated. Each paper has a different approach and different limitations. In this section, each theory and its limitations will be elaborated. The main points relevant are shown here. How each erosion velocity equation is derived can be found in appendix-13.2.4. The four different theories are:

- Leo C. van Rijn (1984)
- Bisschop et al. (2010)
- Winterwerp et al. (1992)
- Mastbergen and Van Den Berg (2003)

2.4.1 Leo C. van Rijn (1984)

The sediment pick-up function is an equation developed by Leo C. van Rijn (1984) to quantify the sediment transport rates in rivers. It considers the influence of flow velocity and grain size on sediment erosion and deposition. The equation predicts the sediment transport rate in rivers with varying flow and sediment properties. Leo C. van Rijn (1984) did research in the pick-up process of single sand particles He conducted experiments with relatively low flow velocities ranging from 0.5 to 1.5 m/s and soil types with diameters ranging from 100 to 1500 μm. Based on the data obtained from the experiments, equation-2.7 which calculates the erosion velocity was derived. How this equation was derived can be found in appendix-13.2.4.1.

$$\nu_e = \frac{0.00033 * \rho_s * \sqrt{\Delta * g * D_{50}} * D_*^{0.3} * T^{1.5} - S}{\rho_s * (1 - n_0 - c_b)} \tag{2.7}$$

The theory is based on the erosion and sedimentation of single sand particles. In this case, if a sand particle is eroded then the settling flux is equal to zero. The theory of Leo C. van Rijn (1984) is seen as one of the best-known sediment/erosion functions. However, the applicability is very limited for CFE. Normally, in CFE the jet flow (+ 1.5 m/s) is higher than the flow (0.5 - 1.5 m/s) used in Leo C. van Rijn (1984). Also, the perspective of deriving the theory based on single particles is not a good representation of the CFE process. In CFE erosion does not take place particle by particle.

2.4.2 Bisschop et al. (2010)

In the last part of the previous section, it is described that the function of Leo C. van Rijn (1984) is very limited in its application. In the theory of Leo C. van Rijn (1984), Bisschop et al. (2010) found that the pick-up flux is significantly over-estimating if higher flow velocities of +1.5 m/s are applied. Therefore (Bisschop et al., 2010) derived a new method that is applicable to situations with higher flow velocities. This method can be used for applications with higher flow velocities (e.g. dike breaching and CFE). Bisschop et al. (2010) states that the erosion of sand particles depends on soil mass properties instead of single sand properties. These soil mass properties are

described by hindered erosion described in section-2.2.3. Bisschop et al. (2010) uses the adjusted critical Shields parameter (θ^*_{cr}) of equation-2.5 in the method of Leo C. van Rijn (1984) in order to take the mass soil properties (slope of the bed, dilatancy and permeability) into account.

Bisschop et al. (2010) derived two equations and equated them. It was found that the erosion velocity (ν_e) was present on both sides. This problem couldn't be solved analytically. Therefore, Bisschop et al. (2010) derived a simplification. This simplification is equation-2.8 and can be used to calculate the erosion velocity. How exactly this equation is derived can be found in appendix-13.2.4.2.

$$\nu_e = \alpha^{0.4} * D_*^{0.12} * (\frac{\theta - \theta_{cr}}{\theta_{cr}})^{0.6} * (\frac{k}{\delta})^{0.6} \tag{2.8}$$

In equation-2.8 the permeability is directly related to the erosion velocity with a factor of $(k)^{0.6}$. The dilatancy is related to the erosion velocity with a factor of $(\frac{1}{\delta})^{0.6}$. From this, it can be concluded that a higher volume increase due to shearing results in a higher factor of dilatancy and causes a lower erosion rate. In Bisschop et al. (2010) the equation is compared to data obtained from a large-scale dike breach experiment conducted in 1994 in the Zwin-channel. This comparison showed that the model could predict erosion rates with high accuracy for high flow velocities ($> 4m/s$).

2.4.3 Winterwerp et al. (1992)

Winterwerp et al. (1992) researched the erosion effects of relatively small and specific flow rates of 0.01 m^3/s and 0.3 m^3/s over a sand bar with a gentle slope. The goal was to gain more insight into the erosion and sedimentation processes. For example, with this insight dikes could be strengthened with correctly placed sand and more knowledge could be gained by knowing more about dike breaching and how it can be prevented. Experiments were conducted by Winterwerp et al. (1992) with flows containing a high concentration of sediment. From this, it was discovered that the erosion and sedimentation processes are limited by a maximum concentration of sediment within a flow. These phenomena are called "hindered erosion" and the opposite "hindered erosion" due to particle-particle interaction both already briefly elaborated in section-2.3. NB: not to confuse this with the "hindered erosion" due to mass properties mentioned in section-2.2.3.

Similar to the conclusion of Bisschop et al. (2010), Winterwerp et al. (1992) concluded that the theory of Van Rijn et al. (2019) was over estimating the pick-up flux. Therefore, a new empirical equation was derived for the pick-up flux based on experiments conducted on the lee side of the bar by Winterwerp et al. (1992). This pick-up flux also takes the factor of the angle of the bed into account. Eventually, by substituting and combining equations the final equation was derived that could calculate the erosion velocity. How this equation actually is derived can be found in appendix-13.2.4.2.

$$\nu_e = \frac{0.012 * (\Delta * g * D_{50})^{0.5} * (\theta^{0.5} - 1.3) * D_*^{0.3}}{(1 - n_0)} \tag{2.9}$$

2.4.4 Mastbergen and Van Den Berg (2003)

Mastbergen and Van Den Berg (2003) researched the effect of "breaching" during erosion processes. Breaching is the process of gradual retrogressive failure of very steep subaqueous slopes (Mastbergen and Van Den Berg, 2003). This shear deformation is caused by forces originated by gravitation and/or a flow. Pore volumes increase when soil is eroded. This results in the creation of negative pore pressures and shear dilatancy that work counterproductive for erosion rates. Mastbergen and Van Den Berg (2003) derived a new pick-up function to provide a quantification analysis of the breaching of non-cohesive soil. Mastbergen and Van Den Berg (2003) continued on the theory proposed by Winterwerp et al. (1992). Mastbergen and Van Den Berg (2003) found that the pick-up flux can be expressed with equation-2.10. The coefficients are determined based on experiments/field data.

$$\Phi = A * (\theta - \theta_{cr})^m * D_*^n$$

Where :

Φ = Dimensionless pick-up flux [-]
A = Coefficient [-]
m = Shear stress power in erosion function [-]
n = Grain size power in erosion function [-]

(2.10)

If the flow velocity is low, the diameter of the particles is relatively large or has a high permeability and the sand bar has a mild slope, the classic erosion equation-2.10 holds. In the case that there are high erosion rates or fine sand with relatively low permeability, dilantancy occurs. The final equation to calculate the erosion velocity according to Mastbergen and Van Den Berg (2003) can be expressed as:

$$\nu_e = \sqrt{\frac{A * (\theta - \theta_{cr})^m * D_*^n * k * \sqrt{\Delta^3 * g * D_{50}}}{\Delta n}}$$

Where :

Δn = Difference in in-situ porosity and max porosity [-]

(2.11)

The values for the coefficients are empirically determined by Mastbergen and Van Den Berg (2003) and shown below:

- Coefficient A [-] ~ 0.018
- Shear stress power m [-] ~ 1.5
- Grain size power n [-] ~ 0.3

It is not stated in the paper of Mastbergen and Van Den Berg (2003) and other papers (such as Mastbergen (2009) for which conditions these parameters hold. Therefore, it is assumed that these parameters are applicable for every input condition, but optionally can be altered and calibrated. The method of Mastbergen and Van Den Berg (2003) was tested by W.D. Regout (1996) and showed that this theory holds for flow velocities ranging from 2 to 5 m/s.

2.5 Water jet

The water is exerted by a circular free jet. This jet is hanging from a special vessel and is moving in a horizontal direction with a velocity normally ranging from 0.01 to 0.2 m/s. The nozzle of the jet is circular and has a certain distance to the seabed, called the distance offset (SOD). The jet exerts a flow in the direction of the seabed with a certain velocity, called the flow exit velocity (u_0). Most of the time the flow exit velocity of the water flow is known, but it can occur that this data is missing. Then equation-13.38 found in appendix-13.2 can be used to determine the flow exit velocity. With this exit flow velocity the discharge at the nozzle can be calculated with equation-2.12:

$$Q_0 = u_0 * (\frac{D_0}{2})^2 * \pi$$

Where :

Q_0 = Discharge at the nozzle $[m^3/s]$;
u_0 = Uniform flow velocity at nozzle exit $[m/s]$;
D_0 = Diameter nozzle $[m]$;

(2.12)

The velocity of the water exiting the jet is significantly higher than the current velocity of the surrounding water. This causes a shear force and subsequently, a turbulent flow at the boundary between these layers. The surrounding water is entrained, the discharge and radius of the flow increase, but the flow velocity decreases. More information about water and soil entrainment can be found in section-2.6.

There are two regions that can be distinguished: the development region and the fully developed region (Weegenaar et al., 2015). These two regions are shown in figure-2.5

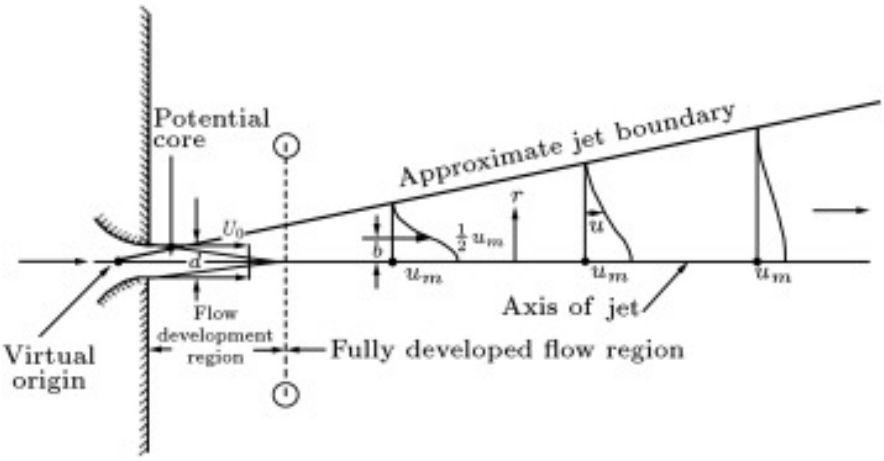

Figure 2.5: The two jet regions: development region and fully developed region
Source: (Sedaghat et al., 2012)

2.5.1 Development region

The flow has a cone-shaped form when it is in the development region. In the core of the flow, the maximum velocity is equal to the jet exit flow. As the depth increases, the turbulence flow gradually penetrates in the direction of the core of the flow. Eventually, the turbulence reaches the core of the flow. After this point, the flow is in the fully developed region. The length of the development region is approximately six times the diameter of the nozzle of the jet ($6 * D_0$). The border between the development region and the fully developed region can be calculated with the following condition:

$$\begin{aligned} s &< \sqrt{\frac{k_j}{2}} * D_0 = \text{Development region} \\ s &> \sqrt{\frac{k_j}{2}} * D_0 = \text{Fully developed region} \\ &\text{Where :} \\ s &= \text{Variable distance of the jet to the seabed [m];} \\ k_j &= \text{Emperical constant with average of 77 [-] (Nobel, 2013);} \end{aligned} \tag{2.13}$$

The discharge with a certain distance from the nozzle (s) can be calculated with equation-2.14

$$\begin{aligned} Q_j &= Q_0 * (1 + 0.082 * \frac{s}{D_0} + 0.013 * (\frac{s}{D_0})^2) \\ &\text{Where :} \\ Q_j &= \text{Discharge at distance s } [kg/m^3]; \end{aligned} \tag{2.14}$$

and the radius of the flow can be calculated with equation-2.15

$$\begin{aligned} r_{flow} &= \sqrt{\frac{1}{2 * k_j}} * s + \frac{s}{D_0} \\ &\text{Where :} \\ r_{flow} &= \text{Radius of the flow } [m]; \end{aligned} \tag{2.15}$$

2.5.2 Fully developed region

When the core is gone, the turbulence has penetrated through the core of the flow and so the maximum flow velocity will decrease. The discharge in the fully developed region with a certain distance from the nozzle (s) can be calculated with equation-2.16

$$Q_j = Q_0 * (\sqrt{\frac{8}{k_j}} * Q_0 * (\frac{s}{D_0})) \tag{2.16}$$

and the radius of the flow for the fully developed region can be calculated with equation-2.17

$$r_{flow} = \sqrt{\frac{2}{k_j}} * s \tag{2.17}$$

2.5.3 Erosion parameter and jet regimes

Another way of describing the erosion potential of a jet flow is the dimensionless Erosion parameter (E_c). The erosion parameter is used as a simplification to represent the ratio between an inertial force and the resistance of soil particles. It is hard to represent and map all the different phenomena that occur during the jetting process. This erosion parameter simplifies these processes into one variable. Multiple papers such as Yeh et al. (2009) and first defined in Aderibigbe and Rajaratnam (1996) use this parameter to predict the static scour depth, radius, and width using a stationary jet in their models. This equation is derived from the ratio of the material densimetric Froude number and the impinging distance. The equation for the Erosion parameter is shown in equation-2.18:

$$E_c = V_j * \frac{d/h}{\sqrt{g * D_{50} * \Delta\rho/\rho}}$$

Where :

$$\begin{aligned} V_j &= \text{Exit velocity [m/s];} \\ d &= \text{Nozzle Diameter [m];} \\ h &= \text{Distance Offset [m];} \\ g &= \text{Gravity } [m/s^2]; \\ D_{50} &= \text{Grain size [m];} \\ \Delta\rho &= \text{Submerged water density } [kg/m^3]; \\ \rho &= \text{Water density } [kg/m^3]; \end{aligned} \tag{2.18}$$

It is not always known how the soil interacts with the flow. A jet flow and the interaction with the soil can be distinguished into two characteristics: strongly or weakly deflecting. In total there are four regimes. In which regime the jet is can be determined with the erosion parameter. However, the regimes are not relevant to the physical process of CFE and/or how they can be quantified. Therefore this is further elaborated in appendix-13.2.6.

2.6 Entrainment of water and sand

The entrainment of water and soil causes the discharge to increase and the velocity of the flow to decrease over time. The direction of the flow is dependent on the ratio between the flow velocity and the trail velocity. If the flow velocity decreases, the trail velocity becomes relatively larger, resulting in the direction of the flow bending backward (the opposite direction in which the jet is moving). The flow velocity can be calculated at every point with equation-2.19.

$$
\begin{aligned}
u_n &= \frac{I_n}{\rho_{jn} * Q_n} \\
&\text{Where :} \\
u_n &= \text{Flow velocity at point n } [m/s]; \\
I_n &= \text{Jet momentum at point n } [kg.m/s^2]; \\
p_{jn} &= \text{Density of the jet flow at point n } [kg/m^3]; \\
Q_n &= \text{Discharge at point n } [m^3/s];
\end{aligned}
\tag{2.19}
$$

In order to determine the flow velocity at a point, the discharge, jet momentum and jet flow density must be known. All these parameters are, however, affected by the entrainment rates. The flow in the free jet region the flow is circular. When the jet impedes the soil, it is assumed that half of the circular flow entrains water and the other half entrains soil. This can be assumed based on the theory provided in section-2.1 in its third paragraph. The total entrainment can be calculated with equation-2.20.

$$
\begin{aligned}
\frac{\Delta Q}{\Delta s} &= \frac{\Delta Q_w}{\Delta s} + \frac{\Delta Q_s}{\Delta s} \\
&\text{Where :} \\
\Delta Q &= \text{Total entrainment discharge } [m^3/s]; \\
\Delta Q_w &= \text{Water entrainment discharge } [m^3/s]; \\
\Delta Q_s &= \text{Soil entrainment discharge } [m^3/s]; \\
\Delta s &= \text{Distance difference between step n and n-1 } [m];
\end{aligned}
\tag{2.20}
$$

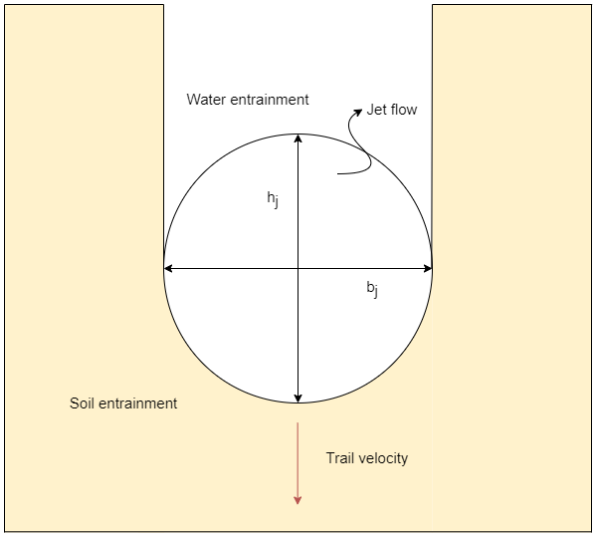

Figure 2.6: Top down view: Entrainment of soil and sand

The entrainment rates can't be determined immediately at a certain depth s, but needs to be calculated iterative step by step with Δs. The entrainment rates are dependent on the dimensions of the jet flow. Soil entrainment is different than water entrainment. Over time this changes the circle shape of the flow to an oval shape, since water is more easily entrained. In order to calculate the entrainment rates the jet width and height of the jet flow must be determined.

The entrainment rates are a large part of the prediction of the dynamic depth and need to be elaborated extensively in order to be fully understood. Therefore, to avoid repetition, it is further elaborated on how the entrainment rates for both the soil and water are calculated in section-7.2.4 which is part of the sections that explain the model that predicts the dynamic depth.

3 Available trench data

3.1 Excavation projects

There are some trench dimensions data available from subsea excavation projects. These projects are the N, T and D projects. The field data will be used for two purposes. First, the field data is used to assess the accuracy of the dynamic and static predictions. Second, the field data is used to calibrate the models. The determined level of accuracy is the critical factor for assessing calibration possibilities. All the data points with their input parameters can be found in appendix-13.4. The field data per project with their depths are shown in figure-3.1.

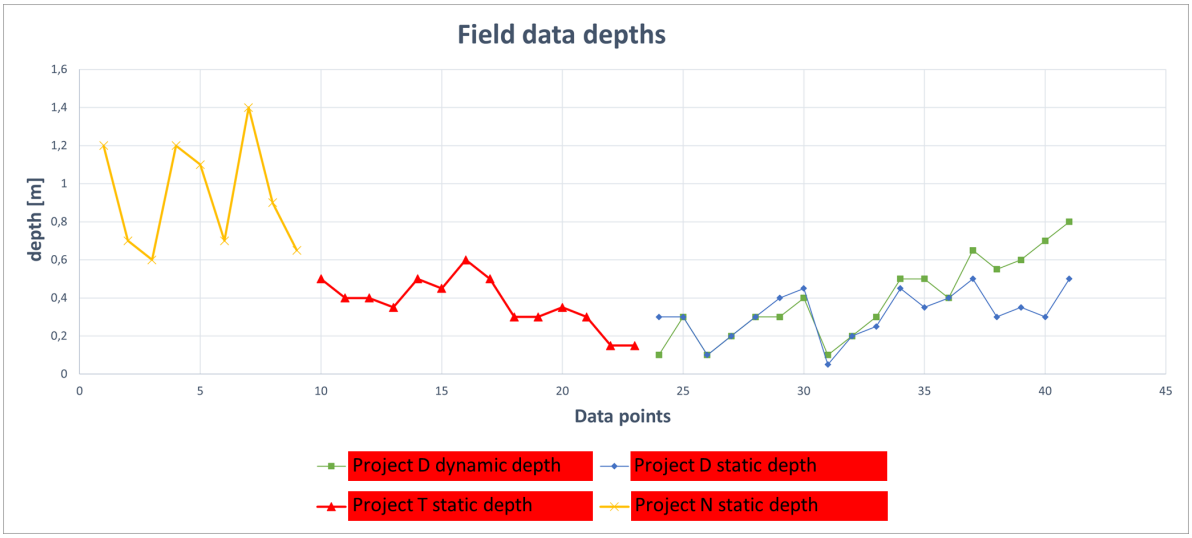

Figure 3.1: The field data per project and their cohering depths

3.2 Reliability assessment of the data

It is important to check the reliability of the data, because there is a possibility that some data is not reliable. Surveying data is a process with limitations and where errors are easily made. These limitations and errors can be caused by different factors. For example, a possible limitation may be the inaccuracy of the surveying products or not matching the time and date of logging.

In this section, the reliability of the data is assessed based on the theory elaborated in section-2. The argument that the field data is unreliable can also be proven by finding two opposite trends in the field data. The best way to explain this is by giving an example.

> Assume that: data point A has a lower uniform flow velocity than data point B. Data point A has a higher static depth than data point B. This does not match the theory. Data point C has a lower uniform flow velocity than data point D. Data point C has a lower static depth than data point D. Now the model contradicts itself because it is both showing opposite trends.

All of the data points are investigated. The complete assessment can be found in appendix-13.4. In particular two data points stood out. The discrepancy of these two data points was not logical at all. Therefore these two data points were considered an outlier and removed from the data set. Further, Assuming that the theoretical trends are correctly defined, it was found that there are a lot of discrepancies. Also, the trends found in each discrepancy could be refuted by showing the opposite trend within the data points. It was tried to find the opposite trend within the same project that the discrepancy was found in, to maintain the same conditions and subsequently exclude other external factors and/or coincidences.

It is hard to provide a quantification of the reliability of the data. To provide an understanding of the level of reliability, or let's say the level of unreliability, a summary is given of all the discrepancies per project for the static and dynamic depth based on the extensive assessment in appendix-13.4.

3.2.1 Conclusion on the available data

The data showed that there are trends in the data that are not in line with the theory and that some trends in the data can be refuted by the opposite trend, also found in the same data set. The data is not consistent in the following trends.

- For the N project, the data does not have a clear trend based on the stand off distance. The theoretically expected trend was that an increasing stand off distance would result in a decreasing static depth.
- For the static depths of the T and D projects, the data does not have a clear trend based on the uniform flow velocity and trail velocity. The theoretically expected trend was that an increasing uniform flow velocity and a decreasing trail velocity would result in an increasing static depth.
- For the dynamic depth of the D project, there was no clear trend for the uniform flow velocity. The theoretically expected trend was that an increasing uniform flow velocity would result in an increasing dynamic depth.
- In all three projects, there were some discrepancies based on identical parameters with different scour depths and identical scour depths with identical parameters except for one parameter. The two expected theoretically expected trends are: identical input parameters would result in similar scour depths and second identical input parameters except for one parameter, would result in various scour depths.

Reliability can't be expressed in a value and consequently can't be quantified. An indication can be made by determining the percentage of data points that are part of a discrepancy. From the total 39 data points that have a static depth, 36 data points could be linked to a discrepancy. This is a percentage of 92%. From the total 18 data points that have a dynamic depth, 5 data points could be linked to a discrepancy. This is a percentage of 25%. A quick overview of the conclusion of the discrepancies found is given in table-3.1. From the complete assessment of this section, it can be concluded that the data is unreliable.

Table 3.1: Overview discrepancies data

	Discrepencies static	Discrepencies dynamic	Total data points
Project N	9	-	9
Project T	11	-	12
Project D	16	5	18
Total	36		39

4 Inhouse-build static model assessment

4.1 Commissioning party: DEME Offshore

The commissioning party for this bachelor thesis is the company DEME Offshore. One of the core expertise of DEME offshore is the installation of inter-aray/HVDC export cables and pipelines on a seabed. DEME offshore can manage and execute the complete process, from determining the requirements to the actual installation of the cables and pipelines. This includes: "the supply of the cables, accessories and cable protection systems, execution of seabed clearance and route preparation, pre-lay dredging, trenching, cable laying, post-lay burial and protection of crossings and construction of landfalls" (DEME Offshore, 2022). An accurate prediction of the scour depth and width of a CFE tool can be beneficial for most of these activities. DEME offshore is also capable of the removal and testing of cables/pipelines. More general information about DEME Offshore is given in Appendix-13.1.

Currently, DEME Offshore is in possession of an empirical model that predicts the static depth and width of CFE. built by the company confidential in 2013. During the N project trial data was obtained with DEME's Offshore CFE tool. This data is used to calibrate the theory obtained from the paper Yeh et al. (2009). Unfortunately, it turned out that this in-house built model couldn't be used to predict static scour depths and width because of its high inaccuracy. The in-house built model is decomposed, analyzed and assessed in this section. The low level of practicality of this in-house built model is one of the reasons that led to the proposition for this bachelor thesis.

4.2 Decomposing

The main theory behind this model is the use of the dimensions less erosion parameter E_c. The model is decomposed using the Boon & Knuuttila (B&K) technique proposed by Boon and Knuuttila (2009). The steps of this method are shown in figure-13.5 in appendix-13.3. Following this technique, a model can be functionally decomposed and its role within a modeling study can be analyzed. This helps to better understand how the model works and it has the potential to expose weaknesses and strengths. The whole decomposition of the model is shown in appendix-13.3.

The model is decomposed into the following two building blocks: the erosion parameter (E_c) and the erosion depth/radius (E_m/r_m). A flowchart of the model is shown in figure-4.1.

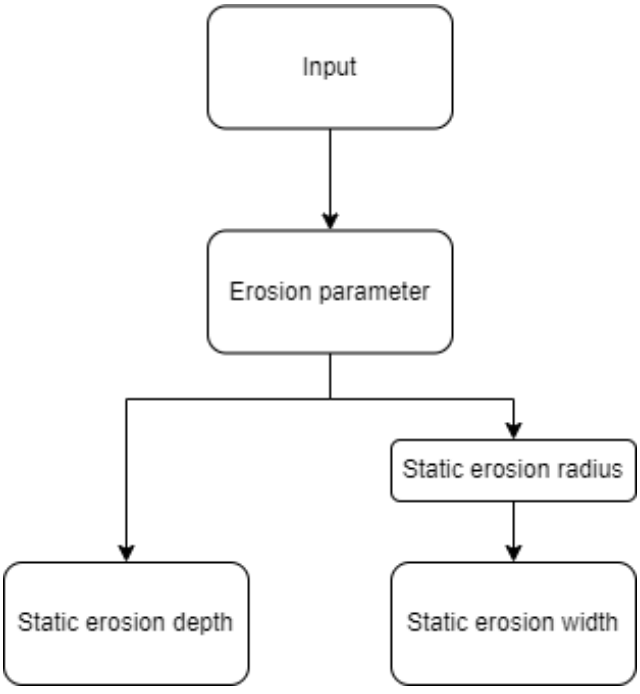

Figure 4.1: Flowchart in-house built model

In the first building block is the erosion parameter described. This is done by using equation-2.18 (Aderibigbe and Rajaratnam, 1996). The erosion parameter is already explained in section-2.5.3 and can be quantified by

equation-2.18. The second building block is related to the calculation of the static erosion depth and radius. The static scour depth and width are calculated with equation-4.1.

EQUATION CONFIDENTIAL (4.1)

A full description on how these equations are derived can be found in appendix-13.3.

4.3 Accuracy of the in-house built model

The accuracy of the in-house built model is calculated in this section. This basis level of accuracy can, later on, be used to see if the improved model is more accurate. There are a lot of statistical methods to determine the difference between collected field data and calculated data. In this research the goal is to investigate the level accuracy. Therefore the following method is chosen. The accuracy of the model for the depth will be determined by calculating the Mean Absolute Percentage Error (MAPE) between the field values (F_x) with the calculated values (C_x). It is important to take an absolute value for the error, otherwise, some negative and positive errors will balance each other out. Equation-4.2 is used (Rogojan, 2018):

$$\begin{aligned} \text{MAPE} &= \left[\frac{1}{n} * \sum \frac{|F_x - C_x|}{F_x}\right] * 100\% \\ &\text{Where :} \\ \text{MAPE} &= \text{Mean Absolute Percentage Error;} \\ n &= \text{number of data points;} \\ F_x &= \text{value of field data;} \\ C_x &= \text{value of calculated;} \end{aligned} \tag{4.2}$$

The closer the value of the MAPE to zero, the more accurate the calculations are compared to the field data. The higher the value, the more inaccurate the calculations are compared to the field data. The MAPE of each project and all the data combined is calculated and shown in table-4.1. The total MAPE is 110.76%.

Table 4.1: in-house built model - MAPE

	MAPE
Project N	14.95 %
Project T	136.68 %
Project D	141.38 %
Total	**110.76 %**

4.4 Preliminary-conclusion

The Mean Absolute Percentage Error shown in table-4.1 is considered to be too high in order to solve the problem context. A prediction with this level of inaccuracy can't be used in the application. It will not provide any correct insight into the static dimensions of a trench using Controlled Flow Excavation. The model is calibrated to the data obtained in the N project. The MAPE for the N project is 14.95%. This level of accuracy is considered to be relevant for future applications. Therefore, the recommendation is to use this model only when the soil conditions and the jet settings are the same as the soil conditions and jet settings used in the N project. However, the chances of this are really low.

The application of the model is very limited and does not fully fill the research objective due to the low accuracy. The theory behind the model seems to be correctly implemented according to some validation and verification tests. Further, the model is very concise and simple to use. The abstractions, assumptions and simplifications do not prevent the model from the opportunity to meet the research objective. The main fallback of the model is that it is only calibrated to the N project and not compared/calibrated to other data from other projects.

5 Models specifications

The objective of the thesis is to understand and quantify the physical processes that take place during CFE. Ideally, a tool can be built that predicts the dynamic and static depth. Therefore, two models are built that respectively predict the static and dynamic depth. In order to correctly built these models, it is advantageous to define the model requirements, study area and preliminary assumptions upfront. The model requirements are mainly established by the commissioning party DEME Offshore.

5.1 Requirements

The epistemic purpose of the models is that it predicts the static and dynamic depth of CFE. A requirement for the model is that it needs to be variable to the input parameters mentioned below so it is widely applicable in practice:

- The exit velocity of the water flow exerted by the jet (uniform jet flow velocity)
- The distance of the nozzle of the CFE tool to the seabed (distance offset or SOD)
- The horizontal traveling velocity of the CFE tool (trail velocity)
- Diameter of the nozzle of the jet
- Diameter of the grain
- Porosity of the soil
- Density of the soil

The parameters mentioned above need to be adjustable in a wide range so that the model can be used in multiple scenarios. Further, the model needs to be reliable, robust and practical as much as possible.

5.2 Study area, boundary conditions and assumptions

The study area is a 3D representation of the area that is influenced by the CFE tool. The process of lowering the CFE tool by the vessel is not taken into account. The focus of this report is on the erosion of the seabed soil and not on the effect on its surrounding. Therefore changes in water flows, not relevant for sand erosion or sedimentation, are left out of the study.

Some boundary conditions and assumptions can be set beforehand. These boundary conditions and assumptions simplify the model so that obtaining a realistic prediction is feasible. It is important to keep these assumptions and boundary conditions in mind.

1. It is assumed that the direction of the water flow is unaffected by the transverse velocity of the jet until the flow reaches the soil.
2. The input parameters are fixed, e.g. the CFE tool has no vertical movement resulting in a fixed nozzle to seabed distance.
3. There are no environmental factors such as water currents, taken into account.
4. The sea bed consists of cohesionless sand particles. There is no vegetation or other wildlife taken into account.
5. The bathymetry of the seabed is flat initially
6. There are no frictional losses in the jet momentum until the jet flow reaches the soil

6 Static scour model

6.1 Static model - Approach and method used

In the literature a lot of information is found on how to calculate and represent separate processes of sub-sea excavation. It is complicated to map all these processes in the correct order so a model can be made to predict the static depth.

Information is found on how to jet impedes the soil, water and soil are entrained, the flow velocity step by step decreases and how the jet reaches a certain depth, the dynamic depth. In this part of the process, sedimentation is relatively low compared to erosion and is therefore assumed to be zero. Thus for modeling the dynamic depth, it can be neglected. For modeling the static depth the sedimentation part is of high importance. After the jet has reached a maximum depth the jet momentum is decreased to a certain extent so that the sedimentation process can't be neglected anymore. The vertical downward forces on a grain, described in section-2.2.1, are larger than the vertical upward forces and sand particles start to settle on the seabed. The concentration of sand particles within the jet starts to decrease and the level of the seabed increases. The extent of theory on the process after the jet has reached maximum depth is minimum. An attempt can be made to calculate the static depth and width by combining all the processes in the correct order following the concise theory. However, taking the limited timeframe of the thesis research and the difficulty into account, it is predicted not to be feasible to achieve a trustworthy prediction at the end of the research with this approach.

It is chosen to look at another option. An option that simplifies and generalizes all the separate processes. The erosion parameter E_c described in equation-2.18, is a good alternative to use in order to describe the static depth and width of CFE. The Erosion parameter simplifies all the processes in one practical equation. Knowing all this, the approach that confidential used in its model can be considered as a good possible method to describe the static scour depth CFE. Currently, the accuracy of the in-house built model is too low as already elaborated in section-4.3. The in-house built model is originally calibrated on data only from the N project. Now a larger data set containing data points from the T and D projects is available.

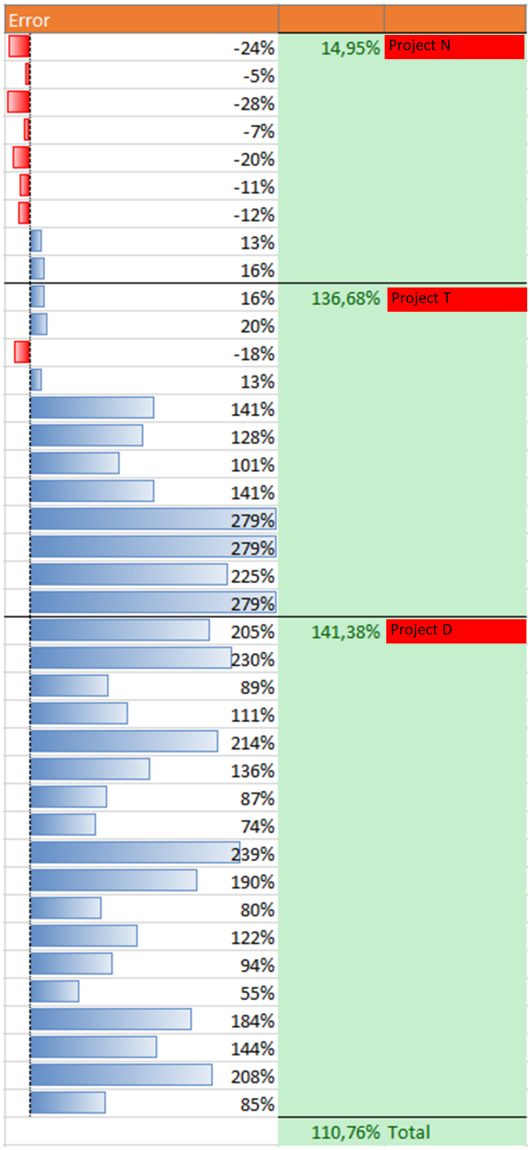

Figure 6.1: Error per data point when the in-house built model is compared to the field data

6.2 Analysis of the results from the in-house built model

6.2.1 Results in-house built model

The approach for the static model is to use the theory described in the in-house built model as a basis and then calibrate the result based on the three projects; N, T and D. Without the calibration, the model is on average over-estimating. This means that on average the predicted value is higher than the value of the field data. The results per data point can be seen in figures-6.1 and 6.2. For figure-6.1, a positive percentage (blue bar) means overestimation and a negative percentage (red bar) means underestimation. For figure-6.2 a dotted line represents calculated model values and a consistent line represents the field data.

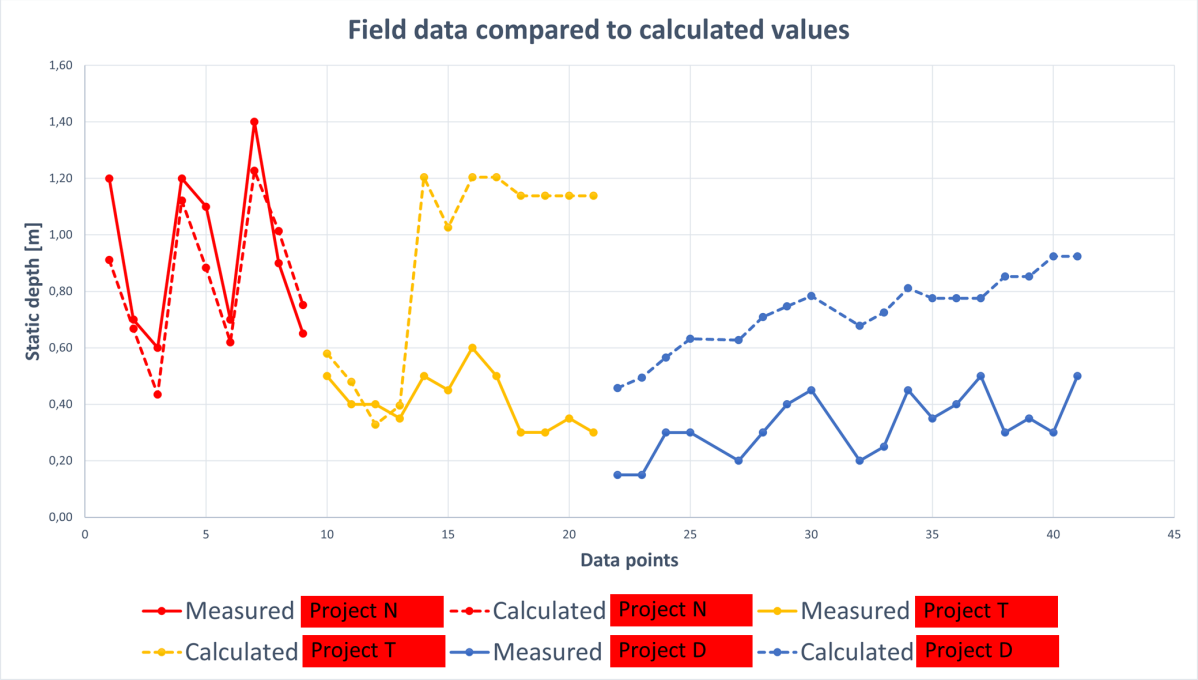

Figure 6.2: Field data compared to calculated data expressed in static depth

6.2.2 Calibration coefficient

The static model consists of multiple equations that need to be determined in a specific order. All these equations are shown in appendix-13.3. The sensitivity of the static depth was determined by manually changing the results of the different equations. In other words, it was investigated what the impact on the static depth value is when the results of the different equations are manually changed. Equation-2.18 is chosen not to be calibrated because different papers use the erosion parameter and do not question the reliability and accuracy. Then equation-6.1 that calculates the static depth for stationary jets was assessed. It was found that a relatively high percentage change in the static depth for stationary jets, does not have a significant impact on the static depth. So equation-6.1 does not contribute a lot to the value of the static depth. The sensitivity is shown in figure-6.3. If the value of equation-6.1 is changed with +100% then the static depth only changes <20%. A significant calibration must be achieved (based on the original errors of the in-house built model) in order to bring the high inaccuracy down. The calibration will be done on equation-6.2. For clearness the equation is repeated here:

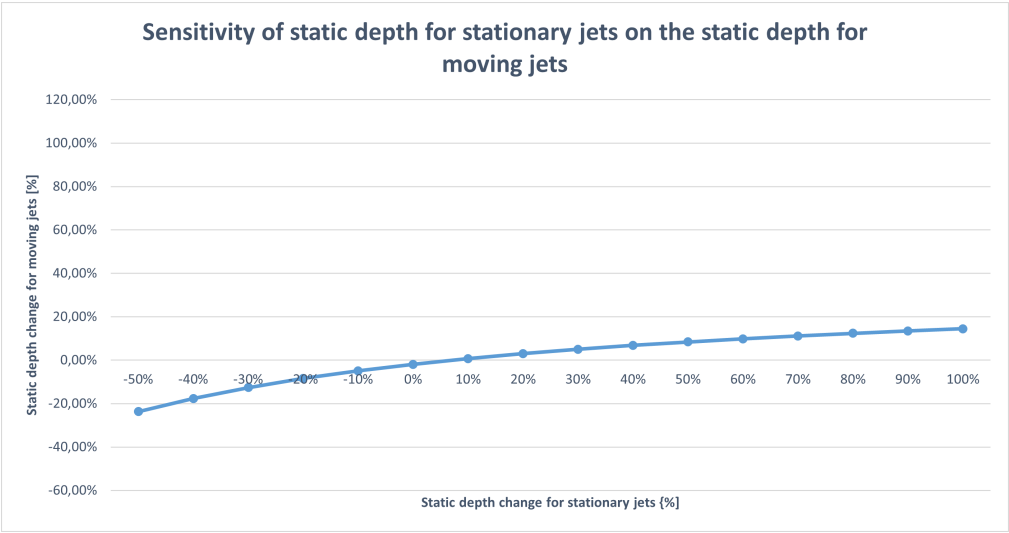

Figure 6.3: Sensitivity of static depth for stationary jets on the static depth for moving jets

EQUATION CONFIDENTIAL (6.1)

EQUATION CONFIDENTIAL (6.2)

Many different ways of calibrating this equation were tried manually. Eventually, altering the value of 190 in the numerator part of the equation is the best way to calibrate the model. This value has the best sensitivity on the static depth that matches the error range of the in-house built model. The value of 190 is now further addressed as the calibration coefficient in this report. In order to find the best value for the calibration coefficient, it is necessary to look at when the model is over or under-estimating and which parameters have the highest relation with over or under-estimating.

6.2.3 Relations between parameters and over- and underestimation

Based on the results, it is determined whether there are relations between the level of error and specific parameters. The parameters, trail velocity, uniform velocity, velocity ratio, impingement ratio, diameter nozzle and the stand off distance were plotted against the error. A linear trend line and its cohering coefficient of determination R^2 which shows the goodness of fit were implemented in each graph. The trendline shows the relation between the level of error and the specific parameter. All graphs for the above-mentioned parameters can be found in appendix-13.5.

The steeper the angle of the trendline, the higher the coefficient of determination and the better the relation is between the error and the parameter. Based on this information the two parameters nozzle diameter and trail velocity had the highest relation with the errors. These graphs can be seen in figure-6.4 and 6.5. The coefficients of determination were respectively, 0.299 and 0.4181.

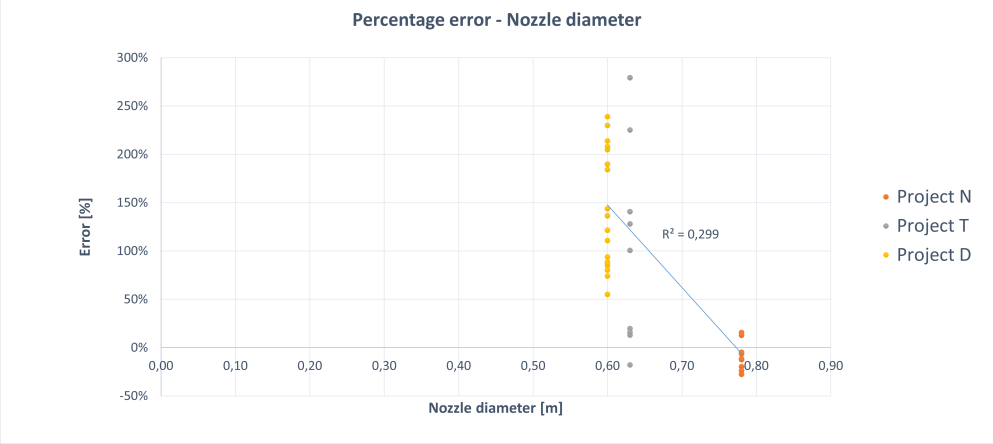

Figure 6.4: Error against nozzle diameter

Figure 6.5: Error against trail velocity

For the nozzle diameter, the following trend is found in all of the field data. When the nozzle diameter is low, the error is relatively high. When the diameter increases, the error decreases. The trail velocity shows a similar trend. If the trail velocity is relatively low, then the error is high. When the trail velocity increases, the error decreases.

It was also investigated if there was a relation between the input parameters and over- or underestimating, with the data set being split. The data set was split into three projects; N, T and D. No clear significant relation was found. In all of the graphs, there was a flat line found as trendline. It was therefore chosen to not continue with this approach.

6.3 Determination of calibration coefficient

The trail velocity and nozzle diameter have a negative relation with the error. Based on the found trends the following needs to be done. For relatively low trail velocities and nozzle diameters, the model needs to be calibrated so the overestimations are reduced and for higher parameter values the model needs to be calibrated so the smaller overestimations and underestimations are reduced. This can be achieved if the calibration coefficient is changed into an equation dependent on either one of two parameters trail velocity or nozzle diameter.

6.3.1 Range calibration coefficient

The equation for the calibration coefficient is determined by dividing the data set into bins. For each bin, the optimum value of the calibration coefficient is manually determined. But before this was carried out, a large range of values (0-5000) for the calibration coefficient was plotted against the percentage change of static depth to analyze how the static depth changes for different values of the calibration coefficient. The full analysis can be found in appendix-13.5. This analysis is used as an indication for manually determining the optimum values for each bin. It also provides an indication of to what extent the static depth can be altered. With different values for the calibration coefficient for different nozzle diameters, the change of static depth ranges from +115% to -93%. With different values for the calibration coefficient for different trail velocities, the change of static depth ranges from +200% to -95%. These percentage changes in the static depth were compared to data point N.2 which had the lowest error before calibration. With this analysis, it can be concluded that not all errors can be covered since some errors do not fall within these ranges as is shown in figure-6.1.

6.3.2 Creating bins and determining the optimum value for the calibration coefficient

The data is divided into bins. The optimum value for each bin with the lowest MAPE is determined and shown in the third column in figures-6.66.6.a. and 6.76.7.a.. The calibration was done manually with the help of the sensitivity analysis of the calibration coefficient. In the fourth column in figures-6.66.6.a. and 6.76.7.a. the MAPE's can be found with the optimum value applied to each bin.

The found optimum calibration coefficient values are plotted against the values that created the bins in a graph, shown in figure-6.66.6.b. and 6.76.7.b.. In other words, the values of the second column are plotted in the graph on the y-axis and the values of the third column are plotted in the graphs on the x-axis. The best-fitting trendline (highest value for the coefficient of determination R^2) is added to these graphs as well. In the sixth column in figures-6.66.6.a. and 6.76.7.a. the MAPE's can be found with this best-fitting trendline substituted for the calibration coefficient.

ID	Bin Nozzle	Optimum value	Error	MAPE	Error with equation	MAPE
N.1	0,78	160	-19%	12,79%	-19%	12,78%
N.4			-2%		-2%	
N.7			-9%		-9%	
N.2			4%		4%	
N.8			19%		19%	
N.5			-14%		-14%	
N.3			-19%		-19%	
N.9			26%		26%	
N.6			-2%		-2%	
T.5	0,63	2700	-5%	35,21%	-5%	35,21%
T.8			-5%		-5%	
T.7			-21%		-21%	
T.12			20%		20%	
T.9			20%		20%	
T.10			20%		20%	
T.11			3%		3%	
T.1			-79%		-79%	
T.6			-46%		-46%	
T.2			-83%		-83%	
T.4			-86%		-86%	
T.3			-91%		-91%	
D.11	0,6	1700	43%	30,91%	43%	30,91%
D.12			30%		30%	
D.13			-16%		-16%	
D.14			-10%		-10%	
D.15			-21%		-21%	
D.16			-37%		-37%	
D.17			20%		20%	
D.18			3%		3%	
D.19			34%		34%	
D.20			-19%		-19%	
D.6			0%		0%	
D.7			-21%		-21%	
D.8			-37%		-37%	
D.9			-40%		-40%	
D.1			-32%		-32%	
D.2			-24%		-24%	
D.3			-55%		-55%	
D.4			-48%		-48%	
Total:				27,94%		27,94%

6.6.a. Error per data point - Nozzle diameter

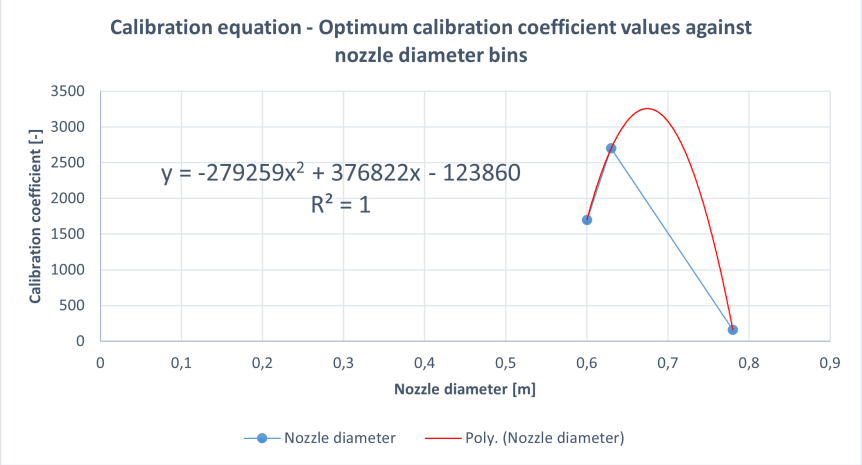

6.6.b. Optimum calibration coefficient values against nozzle diameter

Figure 6.6: Equation for calibration coefficient - Nozzle diameter

ID	Bin velocity	Optimum value	Error		Error with equation	
T.5	0,02	2500	0%	5,61%	3%	6,67%
T.7			-17%		-14%	
T.8			0%		3%	
D.11	0,03	2600	11%	23,38%	24%	26,76%
D.12			-2%		9%	
D.13			-36%		-29%	
T.12			23%		45%	
T.9			23%		45%	
T.11			6%		24%	
T.10			23%		45%	
D.14			-33%		-19%	
D.15			-41%		-29%	
D.16			-53%		-43%	
D.17			-11%		8%	
D.18			-23%		-7%	
D.19			0%		21%	
D.20			-40%		-27%	
D.6	0,05	1200	29%	36,40%	7%	43,14%
D.7			1%		-16%	
D.8			-19%		-32%	
D.9			-23%		-36%	
T.1			-59%		-67%	
T.6			-1%		-18%	
N.1			-74%		-79%	
N.4			-62%		-68%	
N.7			-59%		-65%	
D.1	0,1	700	41%	39,95%	33%	39,63%
D.2			54%		46%	
D.3			-9%		-14%	
D.4			3%		-2%	
T.2			-46%		-49%	
N.2			-61%		-63%	
N.5			-62%		-65%	
N.8			-42%		-45%	
T.3	0,2	190	-18%	17,12%	-15%	16,68%
T.4			13%		17%	
N.3			-28%		-24%	
N.6			-11%		-8%	
N.9			16%		19%	
Total:				27,61%		30,34%

6.7.a. Error per data point - Trail velocity

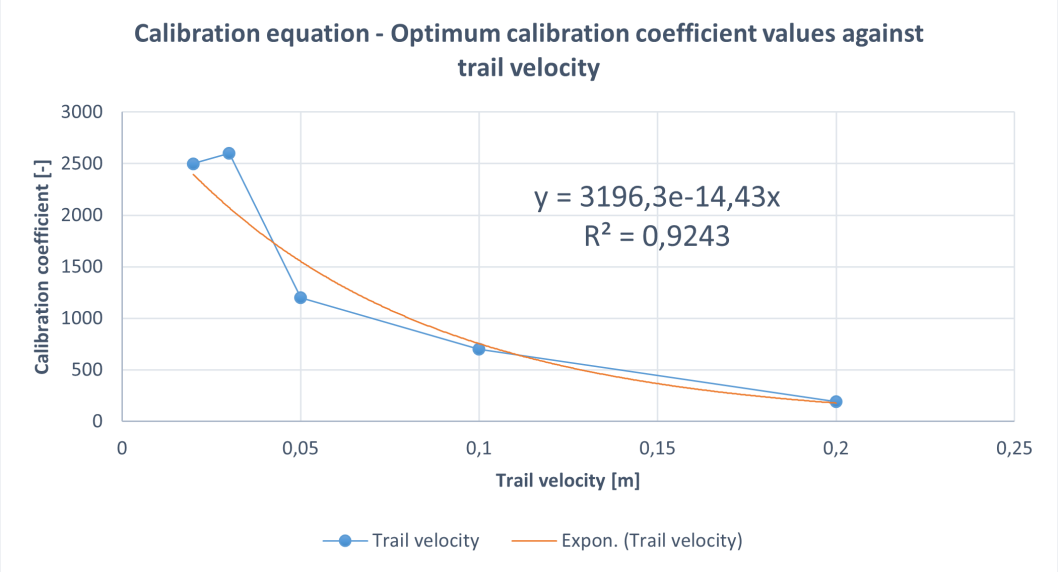

6.7.b. Optimum calibration coefficient values against trail velocity

Figure 6.7: Equation for calibration coefficient - Trail velocity

6.3.3 Result calibration

From the plotted trendlines the following equations can be determined for the optimum value of the calibration coefficient. The equations are added to the static depth equation and the new results are then calculated and added to the columns called "Error with equation" in figures-6.66.6.a. and 6.76.7.a..

EQUATION CONFIDENTIAL (6.3)

EQUATION CONFIDENTIAL (6.4)

After this calibration both results from the calibrations were randomly over and under-estimating. Again, it was determined if there was a relation between one of the input parameters and the over or underestimation of the model. No further relations were found. The trendlines of the graphs were near flat and the coefficients of determination were low (< 0.13). Nevertheless, some calibration attempts were made based on the small relations that were found. Unfortunately, without success. These calibrations did not reduce the MAPE. The final MAPE's for the static depth was reduced from initially a MAPE of 110.76% to 27.94% (nozzle diameter calibration) and 30.34% (trail velocity calibration). Both errors are very close to each other and do not significantly differ from each other. Based on the results thus far which is only the level of error, a preliminary conclusion can be drawn. This is in favor of the calibration depending on the nozzle diameter since this calibration has a lower error. However, there are more things to assess that contribute to the final conclusion on which calibration method is better. For example, the applicable input range of the parameters. These things need to be investigated first before final conclusions can be drawn.

7 Dynamic scour model

7.1 Dynamic model - Approach and method used

For the dynamic model, no generalization or simplification method is used. Instead, the different processes that contribute to the maximum depth that are part of CFE are addressed separately and then combined into one model. To make the dynamic clear and understandable, the model is decomposed into building blocks that each describe a different process of CFE. In section-6.1 it was already touched upon, but the dynamic depth can briefly be described as: water is pumped from the jet towards the soil with a high-flow low-pressure pump, the water impedes the soil, water and soil is entrained as it goes further in the soil, the flow velocity decreases as the depth increases, the direction of the flow gradually bends backward until the angle of the flow exceeds the horizontal line. Resulting in the maximum trench depth. This process is mapped in figure-7.1.

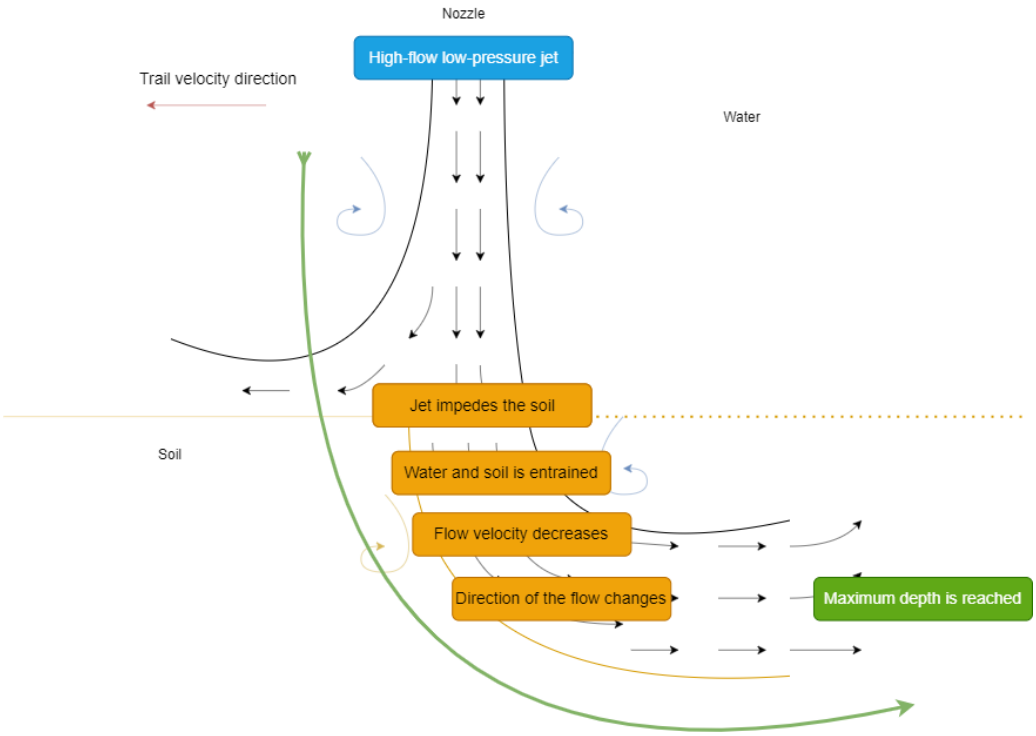

Figure 7.1: Side view of the processes of CFE with text blocks

This process of CFE now is divided into building blocks. The building blocks are: jetting, erosion, entrainment and bed deformation. Each building block has its own content of equations, needed input parameters and output. A general overview of how these building blocks relate is shown in figure-7.2.

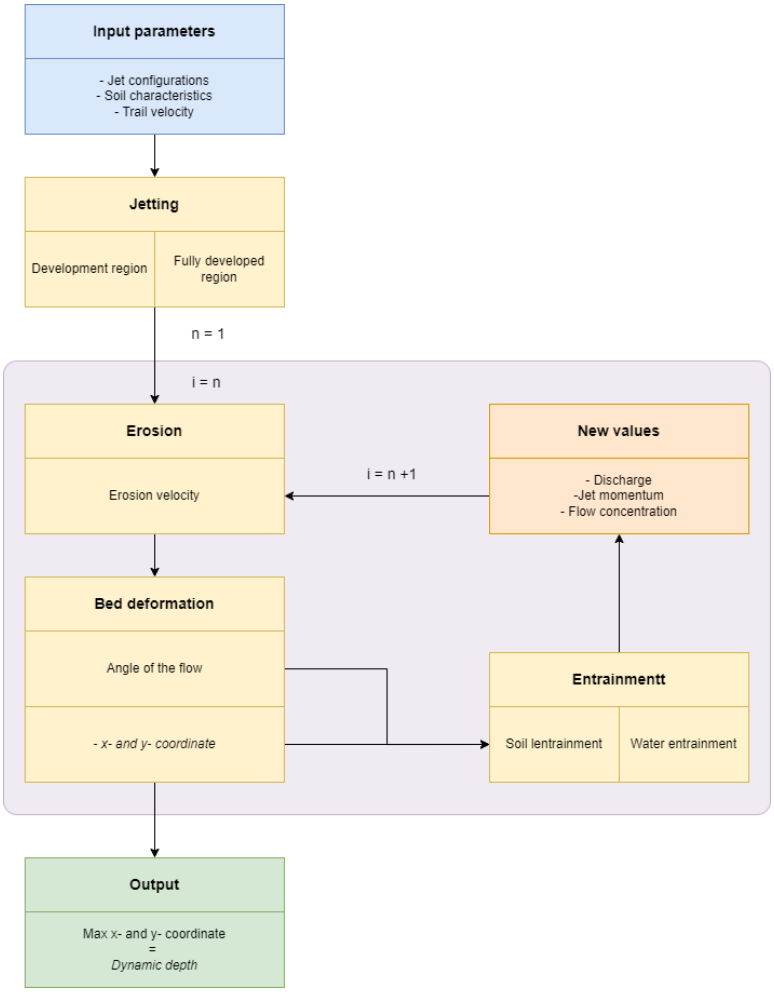

Figure 7.2: General overview of the model - Building blocks

7.2 Building blocks

The goal of the dynamic model is to calculate the trajectory of the flow through the soil. This is done by calculating for each step (n) the x- and y-coordinate of the flow from a 2D side perspective, similar to figure-7.1. The direction of the flow depends on the angle between the trail and erosion velocity. With step size (Δs) which is expressed in meters and the known angle, the grid points for each step (n) can be calculated. The erosion velocity decreases with each step (n+1) due to the entrainment of soil and water. Resulting in a decreasing angle and a specific trajectory of the flow through the soil.

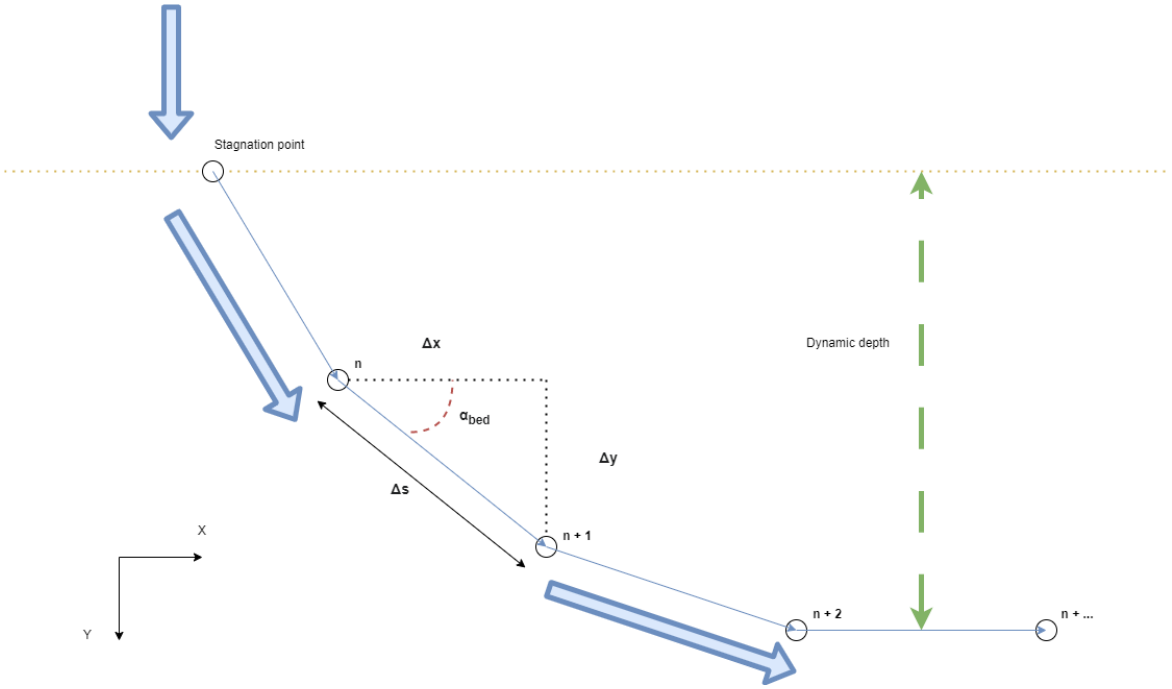

Figure 7.3: Trajectory of the flow through the soil divided into steps n

7.2.1 Jetting

The first building block is jetting. The water is with a high-flow and low-pressure pumped out of the circular jet in the direction of the soil with a certain discharge (Q_0) and jet momentum (I_0). It is assumed that the jet momentum does not decrease till the flow reaches the soil. This means that the jet momentum at the nozzle is equal to the jet momentum at the stagnation point. The jet momentum at the nozzle can be calculated with equation-7.1

$$I_0 = (\frac{\pi}{4}) * \rho * u_0^2 * D_0^2$$
$$\text{Where :} \tag{7.1}$$
$$I_0 = \text{Jet momentum } [kg.m/s^2];$$

The angle between the flow direction and the soil is perpendicular. After some time the flow reaches the soil and the discharge is increased due to the entertainment of the surrounding water. This results in a lower flow velocity. When the flow reaches the soil, the flow is either in its development region or in its fully developed region. For both regions, the discharge (Q_j) and radius (r_{flow}) of the flow can be calculated for each stand off distance. These equations can be found in section-2.5. The used equations for this are equations-2.12, 2.14, 2.15 and 2.16 and 2.17.

7.2.2 Erosion

Erosion occurs when the Shields parameter exceeds the critical Shields parameter. This Shields parameter is dependent on the force exerted by the flow velocity, the chézy-coefficient, the relative density between the soil and water and the grain size. The flow velocity for each step of n can be calculated with equation-7.2.

$$u_n = \frac{I_n}{\rho_{j_n} * Q_n}$$

Where :

$$\begin{aligned} u_n &= \text{Uniform flow velocity for step n } [m/s]; \\ I_n &= \text{Jet momentum for step n } [kg.m/s^2]; \\ \rho_{j_n} &= \text{Density of the jet mixture } [kg/m^3]; \\ Q_n &= \text{Discharge for step n } [m^3/s]; \end{aligned} \tag{7.2}$$

The chézy-coefficient can be calculated with equation-7.3. The roughness coefficient is a coefficient that takes the roughness of the individual particle and the soil as a whole into account. The value of the roughness coefficient for a regular bed can be approximated with $6 * D_{50}$ (Schoen, 2014). It is assumed that the bed of the model is a regular bed.

$$C_{ch} = 18 * \log(3 * \frac{b_{j_n}}{k_{rg}})$$

Where :

$$\begin{aligned} C_{ch} &= \text{chézy-coefficient } [m/s]; \\ b_{j_n} &= \text{Width of jet flow } [m]; \\ k_{rg} &= \text{Grain roughness coefficient } [m]; \end{aligned} \tag{7.3}$$

Now that all the input values are known, the Shield parameter can be calculated for every step n with equation-2.1. The critical Shields parameter can be calculated with equation-2.4.

In section-2.4 four different theories for the erosion velocity are elaborated. In the model the four final equations for the erosion velocity are taken into account. This means that the model will predict four different dynamic depths. In a later part of this report, these results are compared to each other. Where these equations can be found, is shown in table-7.1.

Table 7.1: The four different erosion velocities

Theory	**Erosion function #**	**Referred equation**
Leo C. van Rijn (1984)	1	Equation-2.7
Bisschop et al. (2010)	2	Equation-2.8
Winterwerp et al. (1992)	3	Equation-2.9
Mastbergen and Van Den Berg (2003)	4	Equation-2.11

7.2.3 Bed deformation

The different erosion velocities can be calculated with the equations in table-7.1. The direction of the flow is dependent on the ratio between the trail and the erosion velocity. The direction of the erosion velocity is always perpendicular to the deformation of the bed. The trail velocity is constant in a horizontal direction. The angle of the bed can be calculated with equation-7.4 (Schoen, 2014).

$$a_{bed} = \arcsin\left(\frac{\nu_e}{\nu_{trail}}\right)$$

Where :

$$\begin{aligned} a_{bed} &= \text{Angle of the bed deformation } [\pi]; \\ \nu_{trail} &= \text{Trail velocity } [m/s]; \end{aligned} \tag{7.4}$$

With this angle the next grid point can be determined. The next grid points for the x- and y-coordinate can be calculated respectively with equations-7.5 and 7.6.

$$
\begin{aligned}
x_n &= x_{n-1} + \Delta s * \cos(a_{bed}) \\
&\text{Where :} \\
\Delta s &= \text{Step size [m];} \\
x_{n-1} &= \text{x-coordinate of step n-1 [m];}
\end{aligned}
\tag{7.5}
$$

$$
\begin{aligned}
y_n &= x_{y-1} + \Delta s * \sin(a_{bed}) \\
&\text{Where :} \\
y_{n-1} &= \text{y-coordinate of step n-1 [m];}
\end{aligned}
\tag{7.6}
$$

7.2.4 Soil and water Entrainment

In section-2.6 it was already elaborated on how the flow water and soil entrains. Here in this section, it is elaborated on how the entrainment rates can be quantified. These quantifications are mainly determined by Schoen (2014). With these entrainment rates, new values can be assigned to the discharge, jet momentum and density of the flow, resulting in a new flow velocity for each distance step n+1.

Both the entrainment rates for water and soil is dependent on the width flow. The initial value for the width of the flow can be calculated by multiplying the radius, which can be calculated by equation-2.15 and 2.17, by two. After the initial step, the increasing width is calculated by equation-7.7 (Schoen, 2014).

$$
\begin{aligned}
b_{j_n} &= b_{j_{n-1}} + \nu_e * (\frac{\Delta x}{\nu_{trail}} + \frac{\Delta y}{\Delta s} * \frac{\Delta b_{j_{n-1}}}{\nu_{trail}}) \\
&\text{Where :} \\
\Delta x &= \text{Difference between } x_n \text{ and } x_{n-1} \text{ [m];} \\
\Delta y &= \text{Difference between } y_n \text{ and } y_{n-1} \text{ [m];} \\
\Delta s &= \text{Difference between } b_{j_n} \text{ and } b_{j_{n-1}} \text{ [m];}
\end{aligned}
\tag{7.7}
$$

The entrainment of water is higher than the entrainment of soil. This explains the gradual change of the circular flow to a more oval shape. According to Schoen (2014) the added entrainment rates for step n can be described with equations-7.8 and 7.10.

$$
\begin{aligned}
\Delta Q_w &= (\frac{1}{2} * a_{mom} * \pi * b_{j_n} * u_n + \frac{\Delta y}{\Delta s} * b_{j_n} + n_0 * \nu_{trail}) * \Delta s \\
&\text{Where :} \\
\Delta Q_w &= \text{Entrainment rate for water for step size n } [m^3/s]; \\
a_{mom} &= \text{Entrainment coefficient for water [-];}
\end{aligned}
\tag{7.8}
$$

in which:

$$
a_{mom} = \sqrt{\frac{1}{2 * k_j}}
\tag{7.9}
$$

$$
\begin{aligned}
\Delta Q_s &= (1 - n_0) * \nu_{trail} * (\frac{\Delta y}{\Delta s} * b_{j_n} + \frac{\Delta b_{j_n}}{\Delta s} * y_n) \\
&\text{Where :} \\
\Delta Q_s &= \text{Entrainment rate for soil for step size n } [m^3/s];
\end{aligned}
\tag{7.10}
$$

The total entrainment rate can now be calculated with equation-2.20. Add this entrainment rate to the discharge of step n and the total discharge is calculated for step n+1.

The density of the jet is before soil entrainment equal to the density of the flow. Now that soil entrainment takes place, the mixture of the water will contain floating soil particles. A mass balance is used to solve the unknown value of the jet density for step n+1 (Schoen, 2014). The new jet density increases with the ratio of soil entrainment to the total entrainment rate. Add the previous jet density to the increased density and the jet density can be calculated for step n+1.

$$\Delta\rho_{j_n} = (\frac{(\Delta Q_w * \rho) + (\Delta Q_s * \rho_s)}{Q_n}) \tag{7.11}$$

In some equations of the erosion velocities, the concentration near the bed needs to be determined. This can be done by assuming that the average concentration can be measured in the middle of the height of the flow. This implies that the concentration at the surface is zero and the near the bed concentration is two times the average concentration (Schoen, 2014). In practice, the different concentrations levels are more complex. A more complex way of calculating the concentration near the bed is described in W.J. Siteur (2012). The average concentration can be calculated by equation-13.23.

Lastly, the new value for the jet momentum needs to be determined. The jet momentum is decreased by the shear stress between the flow and the soil. Therefore, the jet momentum can be calculated by equation-7.12. Add this difference to the previous jet momentum and the jet momentum for step n+1 is calculated. Note that the jet momentum decreases with increasing steps (n+..).

$$\begin{aligned} \Delta I_n &= -\frac{1}{2} * \pi * b_{j_n} * \tau_n \\ &\text{Where :} \\ \tau_n &= \text{Shear stress } [Pa]; \end{aligned} \tag{7.12}$$

in which τ_n can be calculated by equation-7.13.

$$\begin{aligned} \tau_n &= \frac{u_n^2 * g * \rho_w}{C_{ch}^2} \\ &\text{Where :} \\ u_n &= \text{Uniform flow velocity } [m/s]; \end{aligned} \tag{7.13}$$

7.2.5 Iterative steps

The initial values for the discharge, jet momentum and jet width are can now be calculated. Before the flow hits the soil, no soil is entrained yet and therefore the jet density equals the density of water. Given these values, the first iteration i the erosion velocity can be calculated. Subsequently, the bed angle and the grid points. Now that the first grid points are known, the next grid points can be determined by calculating the new values for the equation that determines the uniform flow velocity. In the model, it is chosen for a relatively low step size Δs which results in a smoother trajectory. The iterations are repeated until the angle of the bed is almost zero. The lowest y-coordinate is then taken as the maximum depth. This value is the dynamic depth.

7.3 Main dynamic model assumptions

To make the model work, some assumptions for certain factors and general assumptions are made. These assumptions are specific to the dynamic model and are on top of the initial assumptions mentioned in section-5.2. Some of them are already mentioned, but they are repeated here to make the research more easily reproducible. These assumptions and the corresponding factors are shown below.

- Sedimentation is neglected
- No jet momentum of the flow is lost between the exit of the nozzle and the soil.
- The near bed concentration is two times the average concentration (Schoen, 2014).

- The value of k_j is assumed to be 77 (Schoen, 2014)
- The roughness coefficient k_{rg} is six times the D_{50}
- The max porosity n_{max} for fine sand (grain diameter between 0.075 to 0.425mm (HPD Construction, 2021)) is 0.46 (Geotechdata.info, 2013).
- Half of the jet flow is subject to soil entrainment and the other half is subject to water entrainment.

8 Results

8.1 Results static model

The static model is built upon the theory that was implemented in the in-house built model. The in-house built model uses the erosion parameter to generalize all the different physical processes in CFE. Two ways of calibration were added to the equation that calculates the static depth for moving jets. After the calibration, it was found that the errors were reduced from 110.76% to 27.94% and 30.34% respectively for the calibration dependent on the nozzle diameter and trail velocity. The results are shown in figure-8.1.

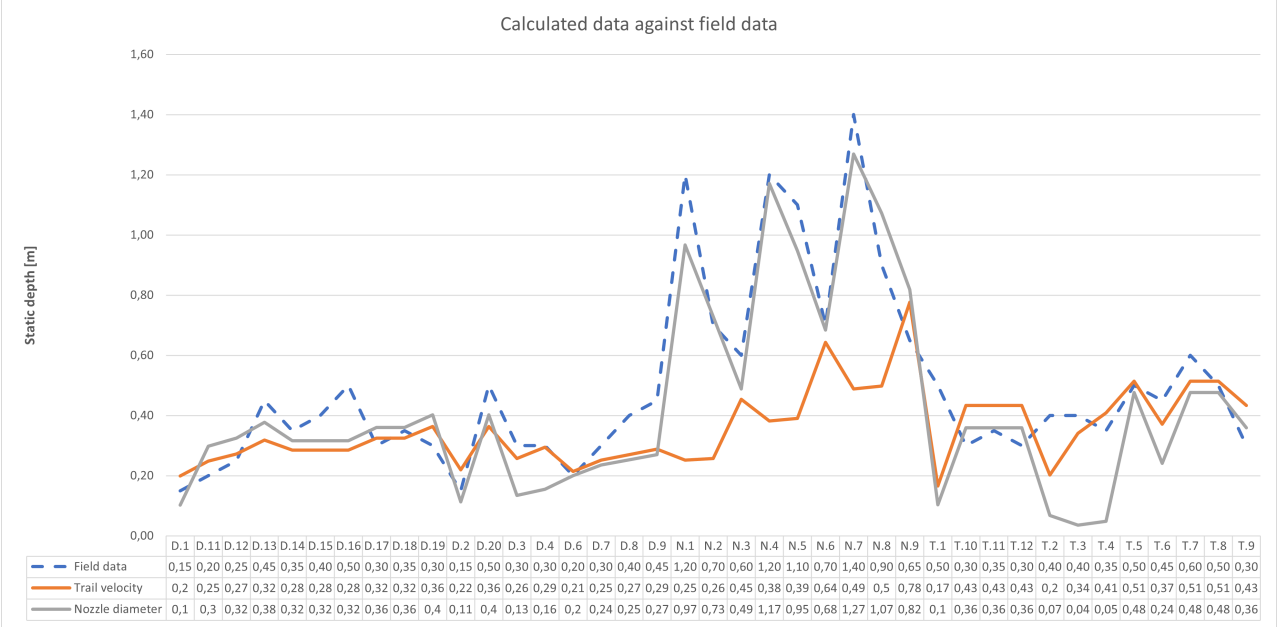

Figure 8.1: Results static depth model - Static depth per data point

The errors of both models are very close to each other. Apart from a few exemptions, the general trends of the three lines behave the same. Overall both calibration methods are mainly under-estimating (the blue dotted line is most of the time higher than the two other lines). Only in some cases, one or two calibration methods predict a higher static depth than the field data indicates. This is random and no clear relation was found that could clarify this. Another thing that could be seen from this graph is that for the different projects either one calibration method predicts consistently higher depths than the other. For the D and N projects the calibration based on the nozzle diameter predicts higher values and for the T project, the calibration based on the trail velocity predicts higher values.

Another thing that stands out is the low prediction of the calibration method dependent on the trail velocity for the N project. Additionally to this, it is also not following the same trend as the other two lines. In fact, it seems that when the other two lines are decreasing (compared to their previous data point) the prediction of the calibration depending on the trail velocity is increasing. The opposite is also shown. When the other two lines are increasing, the prediction of the calibration depending on the trail velocity is decreasing. On the other hand, the calibration method dependent on the nozzle diameter has a high accuracy compared to the field data.

In section-6.3.3 some preliminary conclusions were drawn based on the value of the MAPE. Now in this section also the individual data points are shown and compared to the field data. The high inaccuracy of the calibration method dependent on the trail velocity for the N project adds up to the conclusion that the calibration method dependent on the nozzle diameter is better. However, similar to the previous preliminary conclusion, there are more things to assess that contribute to the final conclusion on which calibration method is better. These things need to be investigated first before final conclusions can be drawn.

8.2 Results dynamic model

The results of the dynamic depth model are compared to the data set of the D project for each erosion velocity. The accuracy is determined with the Mean Absolute Percentage Error (MAPE), similar to the static depth model. The results are shown in table-8.1 and figure-8.2.

Table 8.1: MAPEs of dynamic depth model

Theory	**MAPE**
Leo C. van Rijn (1984)	99.75 %
Bisschop et al. (2010)	58.93 %
Winterwerp et al. (1992)	97.65 %
Mastbergen and Van Den Berg (2003)	30.34 %

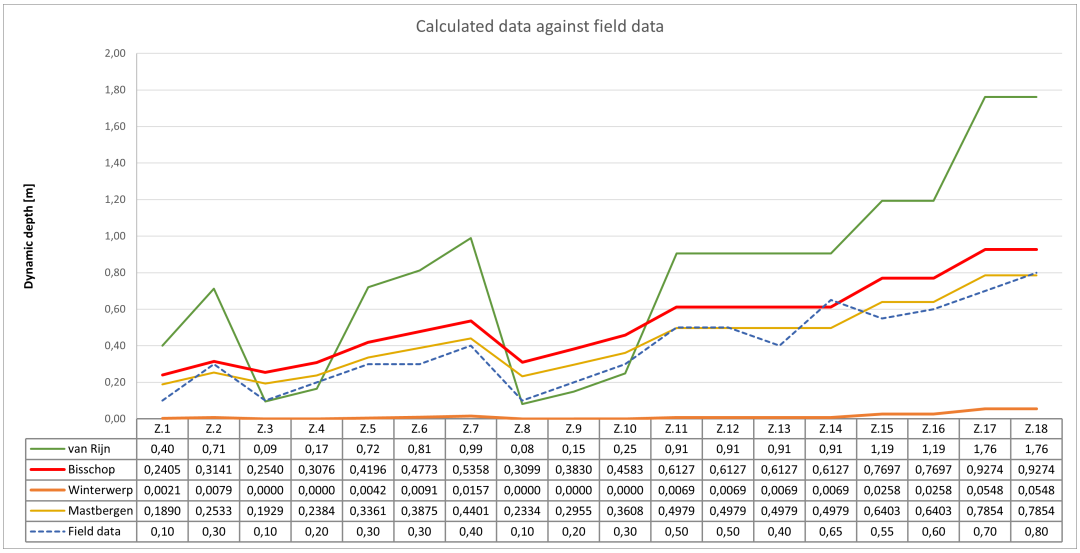

	Z.1	Z.2	Z.3	Z.4	Z.5	Z.6	Z.7	Z.8	Z.9	Z.10	Z.11	Z.12	Z.13	Z.14	Z.15	Z.16	Z.17	Z.18
van Rijn	0,40	0,71	0,09	0,17	0,72	0,81	0,99	0,08	0,15	0,25	0,91	0,91	0,91	0,91	1,19	1,19	1,76	1,76
Bisschop	0,2405	0,3141	0,2540	0,3076	0,4196	0,4773	0,5358	0,3099	0,3830	0,4583	0,6127	0,6127	0,6127	0,6127	0,7697	0,7697	0,9274	0,9274
Winterwerp	0,0021	0,0079	0,0000	0,0000	0,0042	0,0091	0,0157	0,0000	0,0000	0,0000	0,0069	0,0069	0,0069	0,0069	0,0258	0,0258	0,0548	0,0548
Mastbergen	0,1890	0,2533	0,1929	0,2384	0,3361	0,3875	0,4401	0,2334	0,2955	0,3608	0,4979	0,4979	0,4979	0,4979	0,6403	0,6403	0,7854	0,7854
Field data	0,10	0,30	0,10	0,20	0,30	0,30	0,40	0,10	0,20	0,30	0,50	0,50	0,40	0,65	0,55	0,60	0,70	0,80

Figure 8.2: Results dynamic depth model - Dynamic depths per data point

From these results it can be concluded that the three theories of Leo C. van Rijn (1984), Bisschop et al. (2010) and Mastbergen and Van Den Berg (2003) generally overestimate the dynamic depth. They all do follow the same general trend as the field data. This means that when the dynamic depth of the field data increases/decreases compared to the previous point, generally these three theories follow this trend.

The dynamic depths calculated following the theory found by Winterwerp et al. (1992) is the one that stands out of the others in a negative way. The calculated depths are underestimated with an average factor of 44.85, not taking the values of 0 into account. Initially, it was thought that Winterwerp et al. (1992) was incorrectly implemented in the model. However, no error was found.

A preliminary conclusion can be drawn based on these results. In general, the results of the dynamic model are considered to be significantly different compared to the field data from the D project. The MAPEs are too high to provide an accurate prediction of the scour depths. Nevertheless, if something needs to be said about the best erosion velocity theory it can be concluded that the theories of Bisschop et al. (2010) and Mastbergen and Van Den Berg (2003) are the most reliable. Both theories have an error that is in a reasonable range. The other two theories are not. The best theory is the erosion velocity according to Mastbergen and Van Den Berg (2003). Note that this is a preliminary conclusion only based on the value of the errors. Similar to the preliminary conclusion of the static depth. There are more things to assess that contribute to the final conclusion. These things need to be investigated first before final conclusions can be drawn.

9 Sensitivity analysis

A sensitivity analysis is carried out on both the static and the dynamic model. Each parameter is changed with a specific representative range that is considered realistic for CFE applications. The sensitivity analysis can be divided into three steps. The first step is to check whether the theory is correctly implemented in the model. The second step is to see if the trends from the model are matching the trends in the field data. The third and final step is to determine the sensitivity between the parameters and the results.

9.1 Trends in the models

Following the theory, certain theoretical trends are expected. It was manually assessed if these trends were correctly implemented in both the static and dynamic model. The parameters that are investigated are: diameter nozzle, uniform flow velocity, trail velocity, stand off distance, density solid, porosity and diameter grain. Almost all the theoretical trends that were expected were manually confirmed. The only unexpected trend or unusual finding is mentioned below but could be explained.

Stand off distance
When the trend of the stand off distance to the depths was investigated, something remarkable stood out. The trend for the dynamic model showed that when the stand off distance increases, the dynamic depth decreases. The trend for the static model showed an opposite relation. The static depth increases with an increasing stand off distance. At first, it was thought that the trend shown in the dynamic model should apply to both models, but this difference can be explained. When the jet is close to the soil, the jet is in a strongly deflected regime. This means a high dynamic depth, but due to the large angle of the sides of the sand can't be transported outside of the trench. This means a low static depth. When the stand off distance increases, the regimes change and the dynamic depth decreases. The angles of the side of the trench are lower and sand is more easily transported out of the trench.

9.2 Sensitivity of parameters compared to field data

To keep it comprehensible the following part is divided into the static and dynamic models. But first, representative ranges for the parameters need to be determined. These ranges are determined based on data from recent excavation projects and logical values based on expert knowledge. A quick overview of these ranges is given in table-9.1

Table 9.1: Representative ranges for the parameters

Parameter	**Range**
Grain diameter	0.002 - 2 mm
Porosity	0.01 - 0.40
Density solid	1500 - 3000 kg.mˆ3
Uniform flow velocity	2-10 m/s
Nozzle diameter	0.4 - 1.2 m
Trail velocity	0.01 - 0.2 m/s
Stand off distance	1 - 5 m

Something that needs to be addressed one more time before the sensitivity is compared to the data is that the reliability of the data is questionable. The purpose of this assessment is to see which relations or trends can be confirmed with the field data. Accuracy is not important here in this part. Also, some preliminary conclusions can already be made about which calibration or erosion velocity theory is better for a wide range of input parameters.

9.2.1 Static model - Sensitivity of parameters compared to field data

All the analyses of the parameters that are used for the static model are shown in appendix-13.6.1. The best trendline (lowest value for R^2) is plotted and the equation is shown in these graphs. There were no matching trendlines found between the field data and the model. From this, it can be concluded that there is no strong relation between the field data and the static model for both calibration ways. There are some smaller relations found that only hold for a specific part of the representative range. For instance, for the part $SOD > 3$ the model and the data hold the same trend. This relation is depicted with the green transparent box in figure-9.1. The trend

that is seen here is that the stand off distance increases, the depth increases as well.

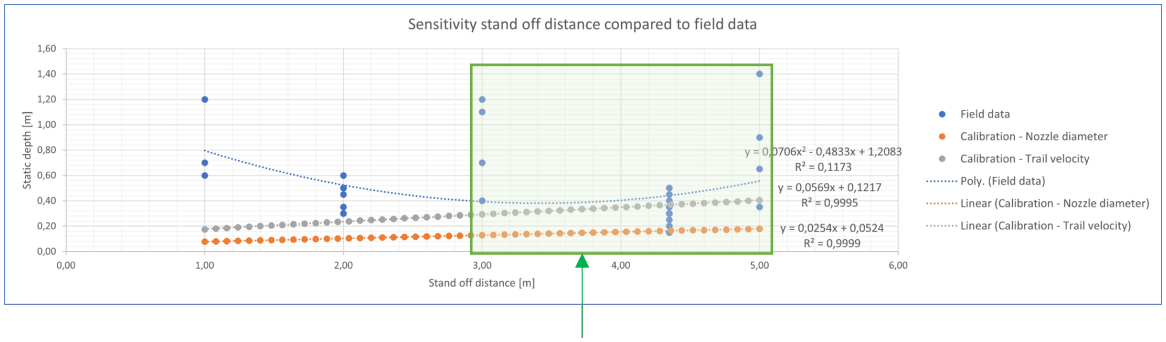

Figure 9.1: Sensitivity of stand off distance compared to the field data

Another example is the range $u_n < 8$. This relation is depicted with the purple transparent box in figure-9.2. Here the model and the field data both increase when the uniform flow velocity increases. With this last trend, it has to be mentioned that these data points in this range are all from the T project. There might be a chance that other factors play a role and this trend is not caused by the uniform flow velocity.

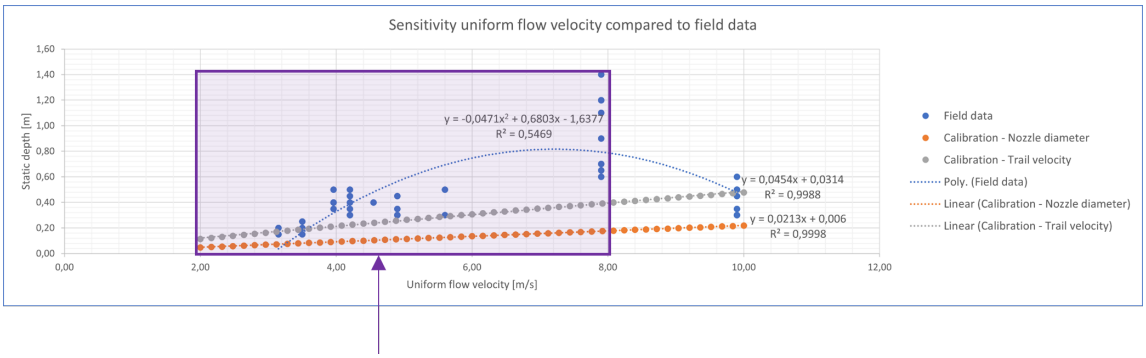

Figure 9.2: Sensitivity of Uniform flow velocity compared to the field data

The two calibration ways act in the same way for all the parameters, except for one parameter. That they act similarly was along the expectation since most of the methods are similar. The one thing that stood out was found when the sensitivity of the nozzle diameter was determined. The calibration method for the nozzle diameter has some strong outliers with some extremely negative depths. This is caused by the characteristic of the equation chosen for the calibration coefficient. This is a limitation of the calibration based on the nozzle diameter method for the static model and is further elaborated on in the discussion.

9.2.2 Dynamic model - Sensitivity of parameters compared to field data

The dynamic model can only be compared with the data from the D project. The D project has fixed values in all of its input parameters, except for the trail and uniform velocity. If the data has fixed values in its input parameter, there is no trend in the field data. Therefore, the sensitivity of the parameters can only be compared for the trail and uniform velocity parameters. Nevertheless, the graphs for each parameter can be found in appendix-13.6.1. The graphs for the trail and uniform velocity can be found in figure-9.3 and 9.4.

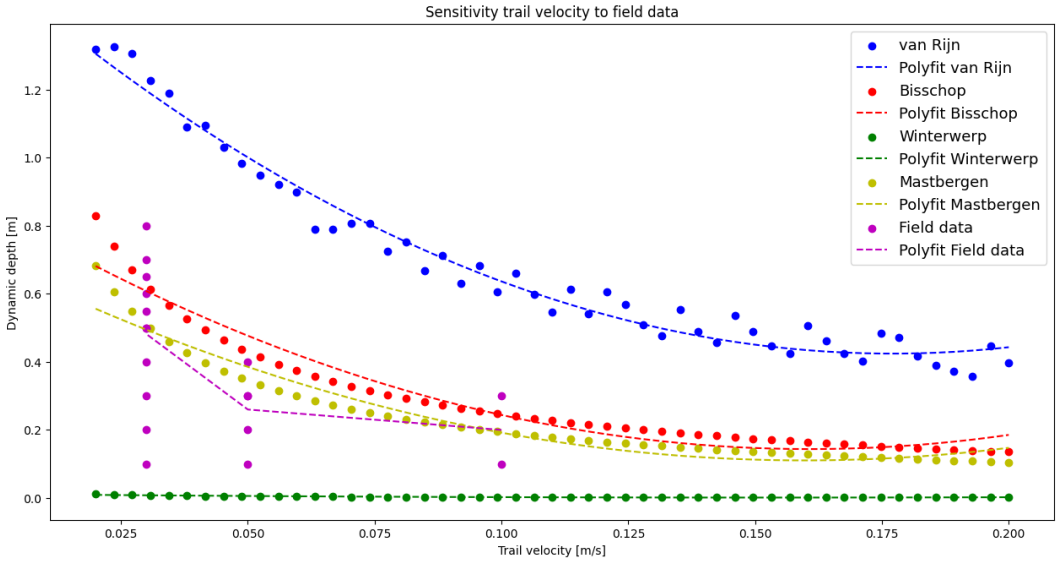

Figure 9.3: Sensitivity of parameters compared to field data - Trail velocity

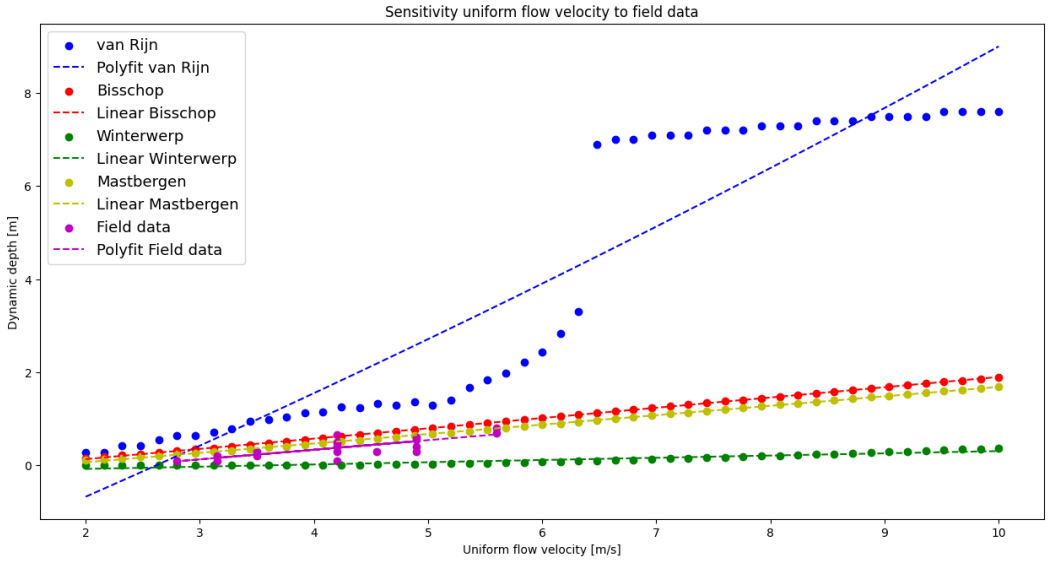

Figure 9.4: Sensitivity of parameters compared to field data - Uniform flow velocity

Unlike the static model, there are similar trends found in the data as in the sensitivity analysis. Note that Winterwerp et al. (1992) is included in the graphs, but again shows unrealistic results. The results were briefly assessed, but nothing beneficial that could contribute to the objective of this thesis could be found. Therefore the sensitivity analysis of Winterwerp et al. (1992) is not taken into account in further analysis. For the trail velocity, the theories showed a polynomial curve. When the trail velocity decreases, the static depth decreases as well. The same can be found in the field data. For the uniform flow velocity, a linear increasing trend could be seen for both the theories as the field data.

Another thing that needs to be addressed is the unusual pattern of the theory of Leo C. van Rijn (1984). Based on the graphs it can be seen that the results are not smooth as the other theories. It is expected the curve shows

a smooth and consistent pattern. It can be concluded that there is something off with the implementation of Leo C. van Rijn (1984). This can have multiple causes that are described in the discussion.

The last thing that needs to be addressed is the unusual behavior of the theory of Mastbergen and Van Den Berg (2003) when the sensitivity of the dynamic model for the parameter diameter grain is assessed. This sensitivity analysis is shown in figure-9.5. The values differ from unrealistic values up to ≈ 40 meters and more realistic values up to ≈ 2 meters as the diameter of the grain increases. This pattern is not expected and is highly unusual. The possible cause of this unusual pattern is described in the discussion. At last, the nod in the line of the Diameter grain - Mastbergen in figure-9.7 can also be explained by this unusual pattern.

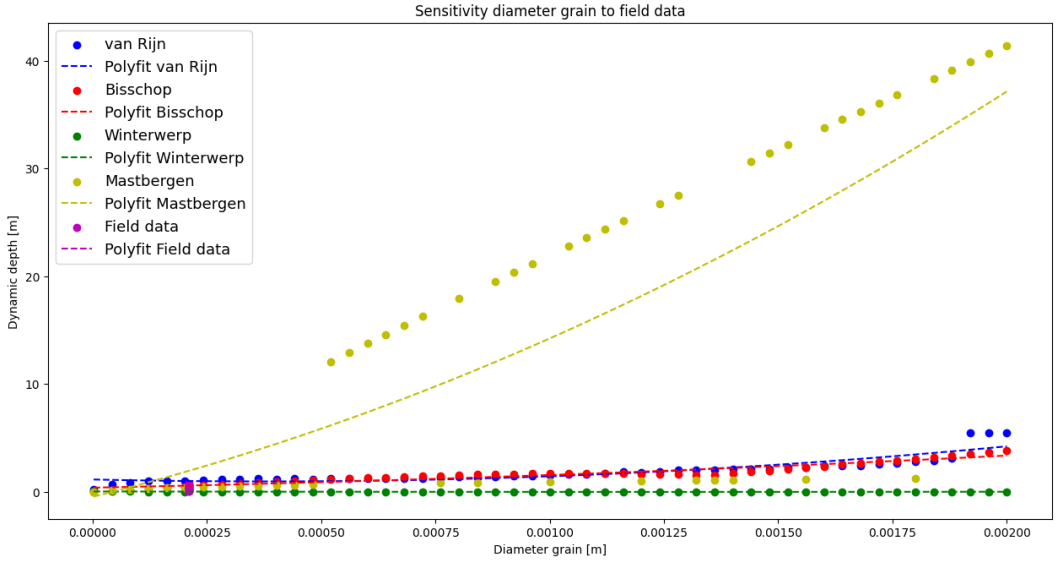

Figure 9.5: Model and field data comparison - Dynamic model - Diameter grain

9.3 Critical parameters of the models

In the third and final step, it is determined which parameters have the highest influence to the sensitivity of the output of the models. The sensitivity is expressed in percentage change compared to a reference data input. The median of a representative parameter range is chosen as a reference point for each analysis. Figure-9.6 and figure-9.7 show the results of this sensitivity analysis.

For figure-9.6 the two calibration methods are both shown in the graph. For figure-9.7 the two erosion velocities are both shown in the graph. The theories of Leo C. van Rijn (1984) and Winterwerp et al. (1992) are deliberately excluded in the sensitivity analysis of the dynamic model. These theories had unrealistic results and the implementation of these theories in the sensitivity analysis would not have been useful.

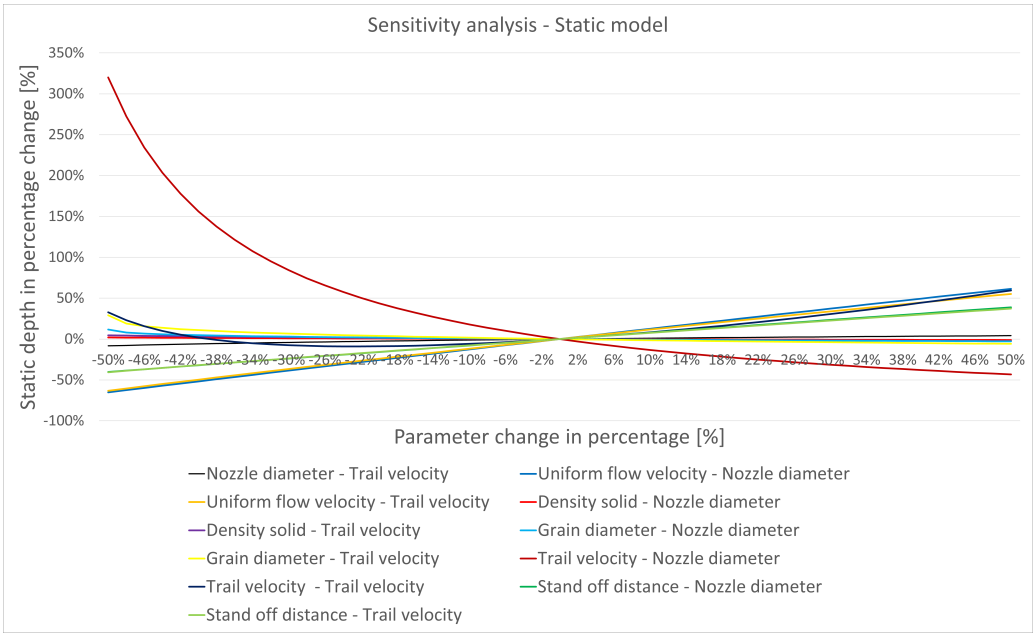

Figure 9.6: Critical factor analysis - static model
The first part of the names in the legend indicates the parameter that is assessed and the second part, after the "−" indicate the calibration method.

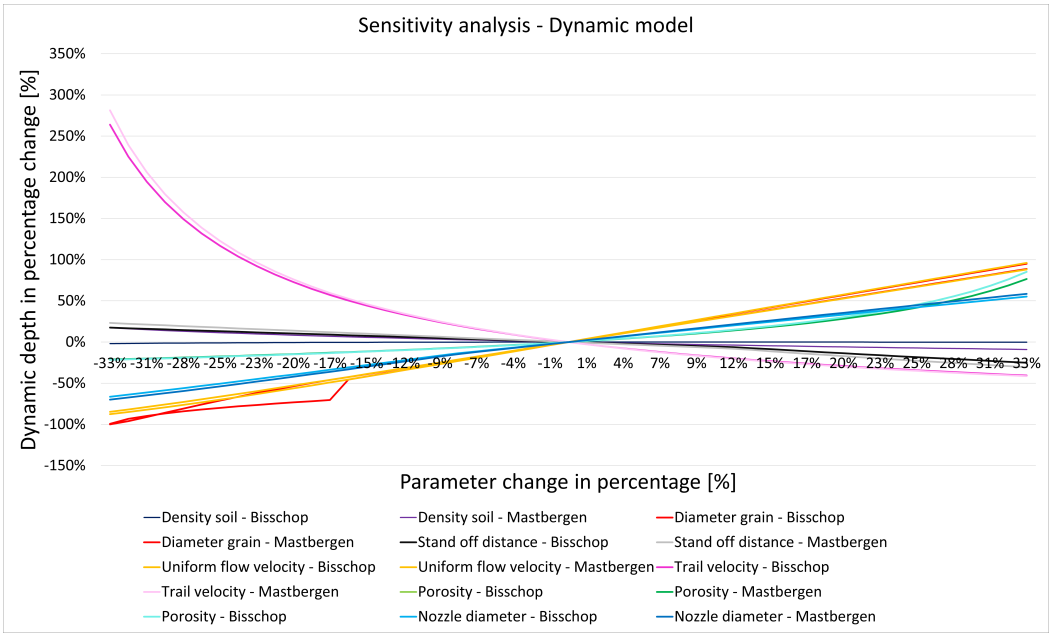

Figure 9.7: Criticial factor analysis - dynamic model
The part of the names in the legend indicates the parameter that is assessed and the second part, after the "−" indicates the theory that is applied.

From this analysis it can be concluded which critical parameters have the highest influence on the static and dynamic depth. The sensitivity intervals of the parameters are shown in tables-9.2 and 9.3. The intervals are based on a parameter change of [-50%;50%] and [-33%;33%], respectively for the static and dynamic models. The higher the parameter in the table, the more influence it has on the result of the models.

Table 9.2: Static model - Sensitivity intervals for a parameter interval change of [-50%;50%]

	Trail velocity		**Nozzle diameter**		
	Left boundary	Right boundary	Left boundary	Right boundary	
Uniform flow velocity	-29%	27%	-31%	30%	Nr. 1
Trail velocity	-9%	18%	44%	-23%	Nr. 2
SOD	-20%	18%	-21%	19%	Nr. 3
Density soil	5%	-3%	2%	-1%	Nr. 4
Nozzle diameter	-4%	3%	-	-	Nr. 5
Diameter grain	3%	-2%	1%	-1%	Nr. 6

Table 9.3: Dynamic model - Sensitivity intervals for a parameter interval change of [-33%;33%]

	Bisschop		**Mastbergen**		
	Left boundary	Right boundary	Left boundary	Right boundary	
Uniform flow velocity	-42%	42%	-45%	46%	Nr. 1
Nozzle diameter	-42%	36%	-45%	38%	Nr. 2
Trail velocity	39%	-22%	40%	-22%	Nr. 3
Diameter grain	-28%	28%	-30%	30%	Nr. 4
Porosity	-10%	15%	-10%	14%	Nr. 5
SOD	8%	-10%	11%	-13%	Nr. 6
Density soil	-2%	0%	17%	-9%	Nr. 7

In the above analysis only some part of the input parameters are assessed. There are some assumptions made for certain factors that contribute to the results of the dynamic model that are not analyzed. Manually, a few of these factors were altered to determine the change in dynamic depth. It was found that some of these factors do contribute a lot to the dynamic depth. For instance, the max porosity is a critical factor when the theory of Bisschop et al. (2010) is applied. Changing the max porosity from 0.46 to 0.50 changes the error from 58.93% to 23.02%. Other found factors that depend on assumptions are the roughness coefficient k_{rg}, empirical constant k_j and the concentration near bed c_b.

10 Discussion

10.1 Reflection and application of the objective

Before the results are discussed, it is good to reflect on the objective of this paper. More elaboration is needed on how this research and models will contribute to the application of CFE. Prior to the execution phase of this research, it was thought that the best result of the models is achieved by lowering the absolute error as much as possible. But is this really the best result for the application of these models for CFE? And how will this research contribute to CFE practices?

What is defined as the best result for the models?

The models will be used to predict the depths of the trench for both the dynamic and static parts. With this information, the correct configurations of the jet and trail velocity can be determined upfront in order to receive the required minimal trench dimensions. If the minimum requirements are not met, another pass of the jet tool is needed over the seabed, increasing costs and time. If the trench dimension is deeper and wider to a certain extent, the minimal requirements of the depth and width are still achieved. From this, it can be concluded, that it is desired that the prediction is rather underestimating (to a certain extent), rather than overestimating.

Of course, the underestimating can't be significant and needs to be within a certain range. If the under-estimation is too large, the process is not optimized resulting in more vessel time and consequently expenses. For instance, the model predicts that a relatively low trail velocity is needed for the (de-)burial of a cable. The model is underestimating with a large factor, so actually, a higher trail velocity could be used to reduce vessel time.

The best result for the models can be defined now as a prediction that has a low error that is also slightly underestimating values instead of overestimating. Based on this statement some preliminary conclusions are drawn on what the best results of the models are in the conclusion.

10.2 Discussion points

10.2.1 Data and assumptions

- **Reliability data**
  A major factor that plays a role in the assessment of the models, is the reliability of the field data. In section-3 the field data was analyzed. From this assessment, it was concluded that the field data is not reliable. Yet the models are compared to this field data. It is possible that the results of the models are actually more accurate or less accurate. This uncertainty has multiple consequences.
  - The field data is not reliable enough to represent CFE practices. The goal of the model is to predict the scour depth of CFE for practical uses. If the models can't be compared to CFE in practice, no clear conclusions can be drawn about the exact accuracy. Nevertheless, the models provide some indication of which theory or calibration method is better. Therefore some cautious conclusions are drawn in the conclusion. Before clear and final conclusions can be drawn on which theory or calibration method is the best for CFE, reliable data needs to be available. The requirements for this data are given in the recommendations.
  - The static model is calibrated on the field data. It is possible that the field data is so far off real CFE practices, that the calibration methods only increase the inaccuracy. If this is the case, then calibration made the models worse. One can assume that if you calibrate a model on unreliable field data, you get an unreliable model. This can only be confirmed by gathering more reliable field data and comparing the results. Again, the requirements and recommendations for this extra data are given in the recommendations.
  - The amount of data points for the dynamic model is even less than for the static model. Add this to the conclusion that the data is unreliable, it was chosen not to calibrate the dynamic model. More about the decision not to calibrate the dynamic model is elaborated on in a later discussion point.

These are some consequences because of the unreliability of the data. At last, there is one further thing that needs to be addressed regarding the available data set. The amount of data points that are available is debatable. In total there were 39 usable data points. Ideally, you have a significantly larger data set that you can choose from so that the chosen data points match the assumptions that were set for the models. A data set with more data points would increase the reliability of the accuracy.

- **Assumptions and generalizations**
  For both models, assumptions and generalizations are made. These assumptions and generalizations make CFE a consistent and easier process so that it can be modeled. These assumptions bring some uncertainty with them.

  For the models, it was said that the input parameters are fixed. However, in real life, they are not fixed. Take for instance, the stand off distance. The assumption is that this variable is fixed. In CFE application, this is a target that is tried to be met. If a deviation is detected, then the height is changed to bring the distance back to its target level.

  The field data that was used in this research was considered to be unreliable by looking at the trends based on the fixed input parameters. It could be the case that discrepancies in the field data were caused by external factors. For instance, if two data points have similar input parameters but different depths, it was concluded that this was a discrepancy. However, it is possible that more factors have been involved. Maybe, a strong current, the presence of vegetation, or a rapidly changing bathymetry of the seabed can explain the discrepancy. The larger the presence of these external factors, the less the situation becomes suitable for modeling.

  The main thing that can be concluded from the previous discussion point about the data, is that the models need to be compared with more reliable data. It should be taken into account that there is a chance that there is no 100% reliable data. The models are based on assumptions and simplification. With the approach taken in this research, there will always be assumptions and generalizations and these bring uncertainties with them. The only solution to this is then to increase the amount of data points with a significant factor so that averages can be taken.

10.2.2 Erosion velocity theories

- **Under estimation erosion velocity Winterwerp et al. (1992)**
  The results of the dynamic depths of the different erosion theories show that the erosion theory according to Winterwerp et al. (1992) is underestimating the dynamic depths with a large factor. For that reason, it has been investigated what the cause is of this big error. The following two causes were investigated. Either there is an error in the implementation of the model or the theory of Winterwerp et al. (1992) is not applicable to the situation of CFE that is described in this research. The implementation of the theory into the model was manually checked multiple times. Intermediate steps were tested, but no error was found. The theory of Winterwerp et al. (1992) that is described in section-2.4.3, mentions that research is conducted on the erosion effects of relatively small and specific flow rates of 0.01 m^3/s and 0.3 m^3/s over a sand bar with a gentle slope. The flow rates used in CFE practices are in another order of magnitude ($> m^3/s$ when the flow impedes the soil). These outlined situations do not match. This can be a cause for the high underestimation of the erosion velocity according to Winterwerp et al. (1992).

- **Neglection sedimentation**
  The building blocks that are included in the dynamic model are jetting, erosion, entrainment and bed deformation. The papers that describe the different theories mentioned that the sedimentation velocity is low compared to the erosion rate using high flow velocities. Therefore it was neglected in this research. A reason for the high overestimation of the three theories could be that sedimentation is not taken into account. Sedimentation namely reduces the erosion velocity and subsequently, the dynamic depth. Maybe sedimentation can't be neglected in CFE. From the small research that was done on the topic, it was already found that for example hindered settlement applies to CFE to some extent. Further research needs to be done on the implementation of sedimentation in CFE and how it affects the scour depth.

- **Unusual pattern of the erosion velocity according to Leo C. van Rijn (1984)**
  When the sensitivity of the input parameters of the erosion velocity of Leo C. van Rijn (1984) was analyzed it was found that the theory is acting unusually. The trend is changing constantly and no clear pattern was visible. This is clearly an error since this is not expected based on theoretical trends. On the other hand, the other theories of Bisschop et al. (2010) and Mastbergen and Van Den Berg (2003) show clear trends. There are several possibilities that cause this error. There might be an error in the assumptions and generalizations or in the implementation of the model. The implementation was double-checked to find this error. Unfortunately, without success.

  There is one factor that is taken into account in the theory of Leo C. van Rijn (1984), which can be a possible cause for this unusual pattern. In the equation that calculates the erosion velocity the concentration level near the bed is taken into account. It is assumed that this concentration level near the bed is twice the average concentration Schoen (2014). This is a simplification because in practice it is more complex to determine. Sethi (2018) focuses more on the sedimentation part of the sub-sea excavation and described another method to calculate the concentration level near the bed. For further research, it is recommended to use this method. Nevertheless, it can't be confirmed that this method will have a positive result on the unusual pattern if it is the cause. However, it will definitely create a more realistic representation of the concentration level near the bed, which is always good.

- **Unusual behavior of the theory of Mastbergen and Van Den Berg (2003) for the sensitivity of the dynamic model for the parameter diameter grain**
  Figure-9.5 shows an unusual behavior of the erosion velocity theory of Mastbergen and Van Den Berg (2003). There are three possible causes for this. The first cause, there could be an error in the assumptions and generalizations. The second cause, there could be an error in the implementation of the model. The third cause, could be a limitation of the theory. However, nothing is found in the papers about this. Therefore it is expected that the error is either in one of the two first two mentioned causes. Next to that, the implementation of the theory in the model is double-checked, but no error was found. In order to see if the error is in the assumptions or generalizations, more research must be done first.

- **Calibration potential for the erosion velocity according to Mastbergen and Van Den Berg (2003)**
  The equation to calculate the erosion velocity according to Mastbergen and Van Den Berg (2003) includes three coefficients. Unfortunately, it couldn't be found where those coefficients were determined on. The paper of Mastbergen and Van Den Berg (2003) only mentions the values of these coefficients without giving any information on the origin of these parameters. It is assumed that these coefficients are empirically determined based on experiments or field data. The circumstances that are sketched in the paper match realistic CFE practices. For that reason, the values of these coefficients have been taken for the dynamic model without altering them.

10.2.3 Calibration

- **Calibration of the dynamic model**
  It is already determined that sedimentation needs to be part of dynamic modeling and that the amount of data points is not enough and is unreliable. Being aware of the three things mentioned, it is decided not to calibrate the dynamic model to the field data of the D project. Calibrating will only enlarge the errors when the model is compared to other data or when the sedimentation is taken into account. To avoid time wasting, it is recommended to first research the effect of sedimentation in CFE modeling, compare the model to more reliable data points and then calibrate it to these data points.

- **Calibration method for the static model based on the nozzle diameter parameter**
  The calibration for the static model is done based on the parameter nozzle diameter. The calibration coefficient was substituted for an equation dependent on the nozzle diameter. One of the characteristics of this equation is that it has two vertical asymptotes. If another equation was chosen, the application range of this calibration method would have been better. The disadvantage is that this would increase the error. The consideration between a better application or lower error is open for discussion in further research.

- **Calibration method for the static model based on the trail velocity parameter**
  The calibration method, based on the trail velocity shows a large inaccuracy when it is compared to the N

project. Based on the way how it is calibrated, it was assessed whether the N project has trail velocity input values that are significantly different from the other two projects. This could have been an explanation for the large inaccuracy and consequently a limitation of the calibration method. However, the values of the trail velocity are not significantly different from the other two projects. A similar approach was followed for the other input parameters and it was found that these input parameters are also not significantly different than the input used in the other two projects. To conclude, no cause could be found that explains this large inaccuracy.

- **Manually assessing best method for calibrating the static model**
  It was assessed manually what the best way is to calibrate the static model. This was mostly done on trial and error. The method for calibration in this research was chosen because it had the highest effect on the sensitivity of the static depth that matched the original error ranges of the in-house build model. The other possibilities had less influence on the static depth and could cover less of the original error ranges. All in all, no specific calibration method based on literature was applied. There is probably literature on how to calibrate models, but this was not investigated in this research. Since that there are a lot of ways to calibrate, it can't be guaranteed that every possibility is checked manually and that the best method was chosen. It might be the case that there is an alternative that is better, resulting in better accuracy of the models.

10.2.4 Sensitivity analysis

- **Difference in critical factors between the static and dynamic model**
  There were some differences in the order of which parameter has the highest influence on the sensitivity of the output between both models. At first, it was expected that this order would be similar, but the sensitivity analysis showed the opposite. This provides us with important information for further research. For the static model, it was chosen not to map the physical processes but to use the erosion parameter and empirically found relations. There was a gap in theory found in the literature that couldn't describe the amount of sand that is transported out of the trench. With the sensitivity analysis of the static model, it was found that the nozzle diameter and diameter of the grain are less relevant for the static depth compared to the dynamic depth. This information can be used for further research on how to map the physical process that occurs after the dynamic depth is reached, which results in the static depth.

- **Critical parameters**
  Some parameters that influence the performance of CFE can be categorized as soil characteristics. Before a CFE process is executed, it is investigated what the characteristics of the soil are. Since these characteristics have an influence on the output of the models, these characteristics need to be determined with some accuracy. Usually, soil investigations are available. These soil investigations tell you the type of soil per layer, the particle distribution, the porosity, etc. The degree of detail of these soil investigations increases when the executing phase becomes closer. But how accurately does this information needs to be and how important is the accuracy of the soil characteristics for CFE?

  The other parameters are configurations. These configurations are determined upfront to receive the required dimensions. In the model, it is assumed these values are fixed. However, in CFE projects these values are targets trying to be maintained. What are the influences of these outliers on the dimensions of the trench? These questions are answered based on the results from the sensitivity analysis in section-9.

  The result of the critical sensitivity analysis shows the most important parameters that have the highest influence on the sensitivity of the result. From this analysis, it can be concluded that the soil characteristics are on average less important than the configuration parameters. With this information, the focus during the preparation phase can be pointed to the most important parameters instead of the less important ones.

10.2.5 Process

- **Limited time frame**
  A lot of assumptions had to be made and the scope had to be narrowed down a lot in order to build working models. The main consequence of this was that for the static model, a relatively easy approach was chosen. Describing the physical processes to the point that leads to dynamic depth is already challenging. Describing the physical processes after this point until the static depth did not fit within the time frame. Another consequence was the limited research in sedimentation. From the intermediate analysis of the results, it was found that the erosion velocities were overestimated. With more time available, more research would have been done on sedimentation.

- **Unavailability of the data**
  The importance of a large reliable data set is already emphasized for the quality of the result. But it also had some effect on the quality of the process of this research. Namely, the lacking of a significant amount of reliable data slowed down the process. A lot of time was lost in the search for finding reliable and relevant data. There is a lot of information available about previous trenching projects by DEME Offshore, but the key is to find relevant information that was useful for this research. Unfortunately, there is no clear structure and overview of this information and everything is spread across an internal server. A lot of time was lost in finding the data that is used in this research. It was quickly realized that the found data was not enough, so more time was spent trying to find more data. Even DEME Offshore colleagues helped to find useful data. Eventually, due to the limited timeframe, it was chosen not to look any further for more data but to continue with the data that was found.

11 Conclusion

The objective of this research is to understand and quantify the physical processes that take place during CFE. This led to the following main research question:

What are the physical processes of Controlled Flow Excavation and how can these processes be quantified?

This main research question was divided into four sub-research questions. In this chapter, the main and sub-research questions are answered.

1.1. What is known about Controlled Flow Excavation in literature?

Controlled Flow Excavation is an excavation method used for the burial and de-burial of cables and pipelines. There are four main processes into which CFE can be divided. The free jet region, erosion, sedimentation and entrainment. Erosion can be described as the process of gradual destruction of the surface of the seabed by the flow of water. Sedimentation is the process of soil particles settling on the surface of the seabed. Entrainment is the interaction of the flow with its surrounding material creating shear stresses.

When the forces of the flow exceed the critical stability of the soil, the soil erodes. The stability of the soil is determined by the mass properties dilantancy, permeability, angle of the bed, and the most commonly used stability factor the shields parameter. The force of the flow gradually decreases as it entrains more water and soil. The erosion parameter can predict the overall erosion potential of a jet flow. The erosion parameter is used as a simplification that represents the ratio between and inertial force and the resistance of soil particles.

The bed deformation can be quantified by computing the erosion velocity. The erosion velocity can be explained as the bed level change in meters per second. There are four theories found that describe a way to calculate erosion velocity. These four theories are: Leo C. van Rijn (1984), Bisschop et al. (2010), Winterwerp et al. (1992) and Mastbergen and Van Den Berg (2003). In all of those theories, sedimentation is neglected.

1.2. How can Controlled Flow Excavation be implemented in modeling and how can the model be calibrated?

CFE can be implemented in modeling by separating the static and dynamic scour depth into two different models.

The dynamic depth can be modeled by mapping all the different physical processes described in the literature into building blocks. The model is built around the idea to calculate the erosion velocity. The building blocks are: jetting, erosion, entrainment and bed deformation. When the interrelationships of these building blocks are known, the dynamic depth can be computed.

This approach neglects sedimentation and is therefore left out as a building block in the model. The data set of dynamic scour depths is small and unreliable. Being aware of the three things mentioned, it is decided not to calibrate the dynamic model to the field data of the D project. It is recommended to first research the effect of sedimentation in CFE modeling, compare the model to more reliable data points and then calibrate it to these data points.

The static model can be modeled by using the theory of the erosion parameter and empirical found relations. Calibration can be done by determining the factor in the equations that have the highest influence on the sensitivity of the output. One coefficient was found that had the best result. For this coefficient, an equation was determined dependent on a parameter that has the highest influence on the over- and/or underestimation of the model. It was found that two parameters trail velocity and nozzle diameter had the highest influence. Therefore two calibrations were done. This resulted in the two final equations for modeling the static depth:

EQUATION CONFIDENTIAL (11.1)

EQUATION CONFIDENTIAL (11.2)

1.3. What is the accuracy of the developed model(s) when it is compared to the field data from the Controlled Flow Excavation projects?

The field data that is available for the comparison is taken from three projects: N, T and D. Prior to this comparison, it was found that this data was not reliable. The field data showed many conflicting trends that were not in line with theoretically expected trends. The data set also showed opposing trends when mutual points were compared. It was tried to find more reliable data but without success. Therefore, the models are compared to this field data and some conclusions are drawn. Overall, to draw final conclusions and recommendations it is recommended first to find a significant amount of reliable data points.

The four different erosion velocities theories are implemented in the dynamic model, creating four different results. The Mean Absolute Errors (MAPEs) for the theories Leo C. van Rijn (1984), Bisschop et al. (2010), Winterwerp et al. (1992) and Mastbergen and Van Den Berg (2003) are respectively, 99.95%, 58.93%, 97.65% and 30.34%. The theory of Winterwerp et al. (1992) was too far off actual realistic predictions and Leo C. van Rijn (1984) showed an unusual pattern in the sensitivity analysis. Therefore these theories are not taken into account in further analysis. The two theories that are left, showed overall an overestimation compared to field data. Two possible reasons for this could be the neglect of sedimentation or the unreliability of the data. Based on the whole assessment of the theories, including the sensitivity analysis and the error, the best theory to describe the erosion velocity is first the theory according to Mastbergen and Van Den Berg (2003) and second the theory according to Bisschop et al. (2010).

The static model is calibrated in two ways, creating two different results. The MAPEs for the calibration methods based on the nozzle diameter and trail velocity are respectively, 27.94% and 30.34%. Both the calibration methods are randomly over and under-estimating when they are compared to the field data. The calibration method based on the nozzle diameter showed a limitation when the sensitivity of the result was analyzed by altering the input values of the nozzle diameter. The difference in error between both calibration methods weighs less than the limitation of the nozzle diameter. Therefore, the conclusion can be drawn that the best calibration method is dependent on the trail velocity.

1.4. Which parameters/factors have the highest influence on the sensitivity of the result?

The parameters with the highest sensitivity to the dynamic depth are from high to low: uniform flow velocity, nozzle diameter, trail velocity, diameter grain, porosity, stand off distance and density of the soil. The parameters with the highest sensitivity to the static depth are from high to low: uniform flow velocity, trail velocity, stand off distance, density soil, nozzle diameter and diameter grain. It can be concluded that the soil characteristics are on average less important than the configuration parameters for both the static and dynamic depths.

Not all the factors that were included in the dynamic model were taken into account in this analysis. There are some assumptions made for these factors and consequently, have some level of uncertainty. These factors are the max porosity n_{max}, the roughness coefficient k_{rg}, empirical constant k_j and the concentration near bed c_b. Manually, it was found that these factors have a high influence on the sensitivity of the dynamic depth.

Main research question - 1. What are the physical processes of Controlled Flow Excavation and how can these processes be quantified?

The first physical process of CFE is the flow development in the free jet region. The next physical processes all occur simultaneously when the flow impedes the soil. These physical processes are erosion, sedimentation and the entrainment of soil and water. Further, mass properties such as permeability, dilatancy and the slope of the bed need to be taken into account in determining the erosion potential.

The flow development can be quantified by determining the discharge rate and the flow velocity. Erosion can be quantified by calculating the bed deformation which is dependent on the erosion velocity. In this research, sedimentation was neglected and therefore not quantified. Entrainment can be quantified by determining the entrainment rates of soil and water. With these entrainment rates, an increased discharge of the flow can be calculated.

12 Recommendations

Recommendations for further research are given in this section. Most of these recommendations have arisen from the points of discussion.

- The data set only consists of 39 usable data points. It can be considered that this is not enough. Ideally, there is an infinite amount of field data. It is therefore recommended to find a significant amount of reliable data points and compare them with both the static and dynamic models.

  It is required that the following parameters are known: trail velocity of the jet, jet exit flow velocity, distance offset, nozzle diameter, the diameter of the soil type particle, normal porosity, maximum porosity and density of the soil. The data set should have a wide range of input parameters. Hereby, different trends in the field data can be validated. If the data set has a fixed value for a particular parameter then nothing can be said about the expected trend. The outputs that are required are dynamic and static depth expressed in meters with at least two decimals. In most of the CFE practices the trail velocity, jet exit flow velocity and distance offset are logged based on the targets that were predetermined before execution. It is better to log the actual values that were used during CFE because they usually have small deviations from the targets that were set.

  Ideally, there is a system that continuously logs the mentioned input parameters and output parameters. This results in a significant amount of data points. Averages from these data points can be taken to lower the influence of unreliable data, provided that on average the data is reliable.

  The importance of finding a significant amount of reliable data points need to be addressed one more time. Without this, no clear conclusions can be drawn about the best approaches and theories to use for quantifying the physical processes of CFE. **Therefore, this is one of the recommendations with top priority.**

- In the sensitivity analysis the sensitivity of the result for different parameters was determined. However, not all factors were assessed. It was found that some of these factors do contribute a lot to the dynamic depth. These factors are the max porosity n_{max}, the roughness coefficient k_{rg}, empirical constant k_j and the concentration near bed c_b. These factors are based on assumptions and consequently, have some level of uncertainty. It is therefore recommended to determine the sensitivity of the dynamic model for these factors and to do more research on the most sensitive factors in order to reduce the assumptions.

- In the dynamic model sedimentation is neglected. The two best erosion velocity theories were slightly overestimating. Sedimentation increases the bed level and works counterproductive for erosion. It is possible that the neglection of sedimentation causes a slight overestimation of the model. More in-depth research is recommended on the influence of sedimentation during CFE and how it can be quantified. It is also recommended to keep in mind that the quantification of sedimentation should fit in the dynamic model. This means that the interrelationship between the building blocks and the new building block *sedimentation* should be taken into account.

- Currently, the models work because some things are assumed and simplified. This reduces the level of representation CFE in the models. In order to receive the best result the models need to have a high level of representing CFE processes. It is recommended to reduce the extent and/or number of assumptions and simplifications and replace it with well-founded calculations and/or explanations.

- The method for calibrating the static model was manually found and the calibration was manually done as well. This questions the statement that the method found is the best way for calibration. There was no literature used to substantiate the chosen method. It is recommended to further assess the calibration possibilities and substantiate them by theories and methods found in the literature. This will probably result in a better calibration. There is no calibration done on the dynamic model, but this recommendation also holds for the dynamic model.

It was concluded that there is a limitation in the calibration method based on the nozzle diameter. This limitation is caused by the type of equation that is used and replaced for the calibration coefficient. This limitation can be removed by implementing another type of equation, but this will increase the inaccuracy of the model results. Nonetheless, there is no guarantee that this limitation will be removed because implementing another type of equation can cause another limitation. This needs to be researched. It is recommended to investigate the limitations and the accuracy of different equations for the calibration method based on the nozzle diameter for the static model.

- A unusual pattern of the dynamic depth occurred in the sensitivity analysis when the theory of Leo C. van Rijn (1984) was applied. The error can either be caused by the wrong assumption for the factor concentration near the bed c_b or by a wrong implementation of the theory in the dynamic model. It is therefore recommended to further research the two mentioned topics and check them for errors.

- The theory of Mastbergen and Van Den Berg (2003) acted unusual when the sensitivity of the dynamic depth was assessed for the parameter diameter grain. This is shown in figure-9.5. There are three possible causes mentioned in the discussion in the paragraph named *Unusual behavior of the theory of Mastbergen and Van Den Berg (2003) for the sensitivity of the dynamic model for the parameter diameter grain.* More research must be done on these causes to find the error of the unusual behavior.
- The average errors of the dynamic models are taken and shown as results in this thesis. The individual errors per specific data point are not assessed. Conclusions could be made for which ranges of input parameters the different erosion velocity theories perform better or worse if this was done. The reason why this is not included in this thesis is that sedimentation needs to be researched and enough reliable data needs to be found. After this, it is recommended to assess the dynamic model results per data point to make conclusions about which erosion velocity theory performs better for certain input ranges.
- The result shows that the theory of Mastbergen and Van Den Berg (2003) has the highest accuracy compared to the field data. No calibration was done on the theories, but it was manually assessed if altering these coefficients change the dynamic depth significantly. This is the case. It has the possibility to increase the models accuracy. It was found that the coefficient A has the most influence on the outcome between the range of 1-2 (Mastbergen and Van Den Berg, 2003). This leaves room for a possible calibration method so that the accuracy of the model can be increased.

References

Aderibigbe, O. O. and Rajaratnam, N. (1996). Erosion of loose beds by submerged circular impinging vertical turbulent jets. *Journal of Hydraulic Research*, 34(1):19–33.

Bisschop, F., Visser, P. J., Van Rhee, C., and Verhagen, H. J. (2010). Erosion due to high flow velocities: a description of relevant processes. Technical report.

Boon, M. and Knuuttila, T. (2009). *Models as epistemic tools in engineering sciences: a pragmatic approach*. Elsevier/North Holland.

C, O. M. H., Shadman, M., Amiri, M. M., Silva, C., Estefen, S. F., and La Rovere, E. (2021). Environmental impacts of offshore wind installation, operation and maintenance, and decommissioning activities: A case study of Brazil.

Cossette, D. (2016). Erodibility and Scour by a Vertical Submerged Circular Turbulent Impinging Jet in Cohesive Soils.

DEME GROUP (2022). About us.

DEME Offshore (2022). DEME Offshore Brochure.

Dey, S. (1996). Sediment pick-up for evolving scour near circular cylinders. *Applied Mathematical Modelling*, 20(7):534–539.

Einsten, H. A. (1951). The Bed-Load Function for Sediment Transportation in Open Channel Flows. Technical report, United States Deparment of Agriculture, Washington D.C.

Elsayed, S. M. and Goseberg, N. (2020). ROLE OF SPATIAL VARIABILITY OF SOIL RESISTANCE IN ALONGSHORE VARIABILITY OF COASTAL BARRIERS RESPONSE TO SUPERSTORM SURGES. *Coastal Engineering Proceedings*, (36v):41.

F., R. J. (1954). Sedimentation and Fluidisation : Part I. *Transactions of the Institution of Chemical Engineers*, 32:35–53.

Geotechdata.info (2013). Soil void ratio.

Gerrard, G. (2018). Cable laying.

Hazen, A. (1917). XXIII. SOME PHYSICAL PROPERTIES OF SANDS AND GRAVELS, WITH SPECIAL REFERENCE TO THEIR USE IN FILTRATION.

HPD Construction (2021). Types of Sand Used in Construction.

Imfeld, T. (1996). Dental erosion. Definition, classification and links.

Leo C. van Rijn (1984). Sediment Pick-Up Functions. *Journal of Hydraulic Engineering*, 110:1494–1502.

Lu, Z., Cao, C., Ge, Y., He, J., Yu, Z., Chen, J., and Zheng, X. (2021). Research on improving the working efficiency of hydraulic jet submarine cable laying machine. *Journal of Marine Science and Engineering*, 9(7).

Major, J. J. (2003). Hindered settling. In Middleton Gerard V.
}and Church, M. J., Mario, C., A., H. L., and J, L. F., editors, *Encyclopedia of Sediments and Sedimentary Rocks*, pages 358–360. Springer Netherlands, Dordrecht.

Mamatsopoulos, V. A., Michailides, C., and Theotokoglou, E. E. (2020). An analysis tool for the installation of submarine cables in an s-lay configuration including "in and out of water" cable segments. *Journal of Marine Science and Engineering*, 8(1).

Mastbergen, D. (2009). Oeverstabiliteit bij verdieping waterbodems: Rekenmodel HMBreach.

Mastbergen, D. R. and Van Den Berg, J. H. (2003). Breaching in fine sands and the generation of sustained turbidity currents in submarine canyons. *Sedimentology*, 50(4):625–637.

Mazurek, K. A. and Rajaratnam, N. (2005). Erosion of sand beds by obliquely impinging plane turbulent air jets. *Journal of Hydraulic Research*, 43(5):567–573.

Meijers, A., Boon, M., and Knuuttila, T. (2009). *Philosophy of technology and engineering sciences*. Elsevier/North Holland.

Miedema, S. A., Warringa, S., van Rhee, C., and Visser, C. (2019). MODELLING THE CABLE TRENCHING PROCESS ON SAND DUNES. Technical report, DEME Offshore, Delft.

Njock, P. G. A., Zheng, Q., Zhang, N., and Xu, Y. S. (2020). Perspective review on subsea jet trenching technology and modeling.

Nobel, A. J. (2013). *On the excavation process of a moving vertical jet in cohesive soil*. PhD thesis, Technische Universiteit Delft, Delft.

PERNG, A. T. H. and CAPART, H. (2008). Underwater sand bed erosion and internal jump formation by travelling plane jets. *Journal of Fluid Mechanics*, 595:1–43.

Rogojan, B. (2018). How To Measure the Accuracy Of A Predictive Model Or Algorithm Part 1.

Sargent, R. G. (2008). Verification and validation of simulation models. In *Proceedings - Winter Simulation Conference*, pages 157–169.

Schmidt, V. A., Crager, B., and Rodenbusch, G. (2017). Historical Development of the Offshore Industry. In *Encyclopedia of Maritime and Offshore Engineering*, pages 1–17. John Wiley & Sons, Ltd.

Schoen, J. J. (2014). *Removal of a dumped rock cover with a low pressure jet - MSc Thesis Report*. PhD thesis, Delft University of Technology, Delft.

Sedaghat, A., Liu, X., Whitty, J., and Tang, X. (2012). Wind power of small wind turbines in turbulent open jets. *Scientia Iranica*, 19(2):272–281.

Sethi, J. (2018). *Erosion of sand under high flow velocities - MSc Thesis report*. PhD thesis, Delft University of Technology, Delft.

Shahmohammadi, R., Afzalimehr, H., and Sui, J. (2021). Assessment of critical shear stress and threshold velocity in shallow flow with sand particles. *Water (Switzerland)*, 13(7).

Stuyts, B., Versteele, H., and Cathie, D. (2018). Durban SAPREF MFE Pipeline - Literature review. Technical report.

Van Rhee, C. (2010). Sediment Entrainment at High Flow Velocity. *Journal of Hydraulic Engineering*, 136:572–582.

Van Rijn, L. C., Bisschop, R., and Van Rhee, C. (2019). Modified Sediment Pick-up Function. Technical report.

Wang, B., van Rhee, C., Nobel, A., and Keetels, G. (2021). Modeling the hydraulic excavation of cohesive soil by a moving vertical jet. *Ocean Engineering*, 227.

W.D. Regout (1996). *Flowdredging - Het spuiten van sleuven in zand*. PhD thesis, Delft University of Technology.

Weegenaar, R. A., Keetels, G. H., Winkelman, M. O., and Rhee, C. V. (2015). Sand erosion with a traversing circular jet. *Proceedings of the Institution of Civil Engineers: Maritime Engineering*, 168(2):76–83.

Winterwerp, J. C., Bakker, W. T., Mastbergen, D. R., and Van Rossunv, H. (1992). Hyperconcentrated sand-water mixture flows over erodible bed. *Journal of Hydraulic Engineering*, 118:1508–1525.

W.J. Siteur (2012). *Sedimentation-velocity in jet induced flow - MSc Thesis Report*. PhD thesis, Delft University of Technology, Delft.

Yeh, P. H., Chang, K. A., Henriksen, J., Edge, B., Chang, P., Silver, A., and Vargas, A. (2009). Large-scale laboratory experiment on erosion of sand beds by moving circular vertical jets. *Ocean Engineering*, 36(3-4):248–255.

Yuan, Q., Wang, C., Wang, Y., Peng, C., and Meng, X. (2019). Investigation of Submerged Soil Excavation by High-Velocity Water Jet Using Two-Fluid Smoothed Particle Hydrodynamics Method. *Journal of Hydraulic Engineering*, 145(6).

Yuan, Q., Zhao, M., Wang, C., and Ge, T. (2018). Numerical study of sand scour with a modified Eulerian model based on incipient motion theory. *Marine Georesources and Geotechnology*, 36(7):818–826.

13 Appendices

13.1 Appendix A - Context and background information

In this appendix, the context of the project is described to provide some basic understanding of offshore engineering and its history.

13.1.1 Offshore engineering and cable/pipeline installation

Offshore engineering is the engineering discipline that involves the design and construction of stationary positions in an ocean environment. The main industries of offshore engineering are the oil, gas and offshore windmill parks industries. The stationary positions in offshore engineering can be divided into four categories. The categories are floating structures, bottom-founded platforms, subsea structures and pipelines/cables. The last category is the most relevant for this report and therefore focused on in this section.

The first offshore engineering practices date back more than 120 years ago. In the early 1800s, the demand for oil and natural gas was increasing due to the upcoming rise of heavy industries. Simple construction techniques were adapted to be capable of oil and gas mining in shallow water. Through research in fundamental theories and laws, the increasing environmental factors such as waves and storm activity were overcome. This led to the possibility to ming oil and gas in even deeper waters (Schmidt et al., 2017).

The increasing technologies of building floating and fixed structures for various applications increases the complexity of pipelines and cable installation. The deeper the waters, the harder the installation of pipelines and cables is. Cables and pipelines are used for various reasons with the main function to transport. They transport gasses, fluids, and electricity. The type of transport determines the size and characteristics of the cable/pipeline. Sizes of pipelines and cables can be as big as +450 mm. The current challenge frontier of pipeline/cable installation arises at depths of +3000 meters. The current method for pipeline and cable laying is done by large vessels. An example of a cable laying vessel is the 'Living Stone a DP3 cable installation & multipurpose vessel' and is shown in figure-13.1.

Figure 13.1: Living Stone is a DP3 cable installation & multipurpose vessel
Source: (DEME Offshore, 2022)

The general method of cable and pipeline laying is as follows. The cables or pipelines are loaded onto a vessel upfront and transported to a location where they need to be installed. The cable or pipeline is then gradually dispatched at the back of the vessel, using gravitation to let the cable/pipeline sink subsurface. The pipe/cable curves downwards until it touches the seabed. A side-view of this process imitates an S-shape form (Mamatsopoulos et al., 2020). The weight of the cable determines the angle of the shape. An illustration of this method is shown in figure-13.2. With correct coordination and other external factors such as vessel speed, variations in bending stiffness, weight, buoyancy and forces due to ocean current, the cable/pipeline falls in the designated place.

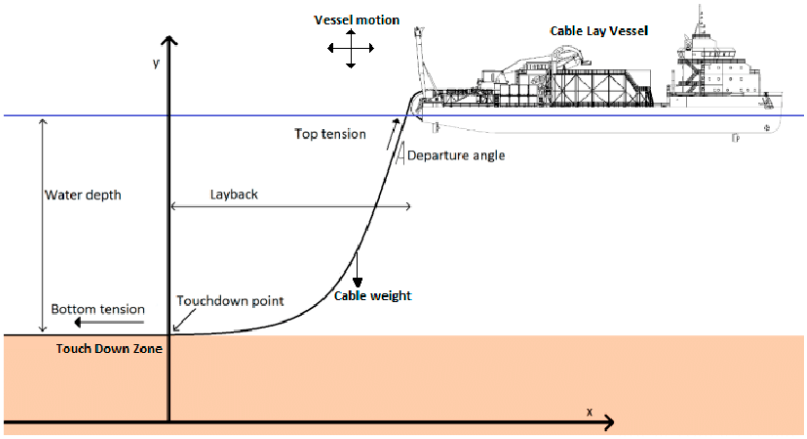

Figure 13.2: Cable/pipeline installation method
Source: (Mamatsopoulos et al., 2020)

It is important that the cables and pipelines are protected. It requires a good weather window and unique vessels to repair cables and pipelines, resulting in expensive processes. There are protection materials and protection methods. The cables and pipelines have specific protection layers, that can prevent damage to a certain extent. However, this protection is not sufficient for some treats. A solution to protect these cables and pipelines is a protection method during the installation of the cables and pipelines. This method is burial using subsea excavation.

13.1.2 Involved parties

DEME Offshore
DEME Offshore is the party that commissioned this assignment. DEME Offshore is one of the four branches of the umbrella company DEME Group. The other branches are dredging, environmental and infra. DEME Group is specialized in engineering subjects such as dredging, land reclamation, marine infrastructure, offshore energy and environmental remediation. Their main vision is to create a sustainable future by tackling global challenges with sustainable solutions (DEME GROUP, 2022). The subbranch DEME's Offshore visions is not to follow, but to lead the market by innovating equipment and technologies that have not been seen in the industry before. This bachelor thesis assignment is a good example that follows this vision.

DEME offshore is one of the pioneers in offshore energy and has an impressive portfolio. DEME offshore is and was involved in the installation of more than 70 windmill parks including more than 2.700 windmills. Their working range started developing in the North Sea, but is currently expanding to windmill parks in Asia and the United States. Not only is DEME offshore involved in the offshore renewable energy sector, but it is also involved in the most iconic and large-scale pipeline projects in recent history (DEME Offshore, 2022). Some of these iconic projects are the installation of Nord Streams 1 & 2. These large-scale pipeline projects are relevant to this report.

One of the core expertise of DEME offshore is the installation of inter-aray/HVDC export cables and pipelines on a seabed. DEME offshore can manage and execute the complete process, from the design table to the actual installation of the cables and pipelines. This includes: "the supply of the cables, accessories and cable protection systems, execution of seabed clearance and route preparation, pre-lay dredging, trenching, cable laying, post-lay burial and protection of crossings and construction of landfalls" (DEME Offshore, 2022). An accurate prediction of the scour depth and width of a CFE tool can be beneficial for most of these activities. DEME offshore is also capable of the removal and testing of cables/pipelines.

Other similar offshore companies
So seabed excavation is a common practice in offshore engineering. It is only understandable that other offshore companies similar to DEME offshore, also do research in this field of subject. They probably have their own methodologies and focus. Since it is a competitive market, the exact details of excavation processes are confidential and therefore unknown to the public.

The model that will be built has the potential to be used in other cases and is not only use full for DEME offshore.

As long as the model provides the opportunity to change the input settings for the CFE tool, this model can be adopted by other parties that have a similar interest in predicting scour depths and widths of controlled flow excavation. However, the final product (the model) will be considered to be confidential and only available for DEME offshore.

13.2 Appendix B - Literature research

13.2.1 Forces on a single grain

The forces on a single grain can be calculated with the following equations Schoen (2014):

$$F_g = \frac{\pi}{6}(\rho_s - \rho_w) * g * D_{50} \tag{13.1}$$

$$\begin{aligned} F_{dv} &= \frac{\pi}{8} * C_D * \rho_w * W_{sp} * D_{50}^3 \\ &\text{Where :} \\ F_g &= \text{Gravitational force [N];} \\ F_{dv} &= \text{Drag force vertical component [N];} \\ W_{sp} &= \text{Submerged particle weight [Kg];} \end{aligned} \tag{13.2}$$

$$\text{Drag force: } F_d h = C_d * \rho_w * u^2 * A_D \tag{13.3}$$

$$\text{Shear force: } F_s = C_s * \rho_w * u^2 * A_s \tag{13.4}$$

$$\begin{aligned} &\text{Lift force: } F_l = C_L * \rho_w * u^2 * A_L \\ &\text{Where :} \\ F_x &= \text{Drag/Shear/Lift force N;} \\ C_x &= \text{Coefficient [-];} \\ u &= \text{Uniform flow velocity [m/s];} \\ A_x &= \text{Area of the particle exposed to the force } [m^2]; \end{aligned} \tag{13.5}$$

13.2.2 Adjustment critical shields parameter

The factor for taking the slope of the bed into account is:

$$f_{slope} = \frac{sin(\phi) + sin(\alpha_{bed})}{sin(\phi)} \tag{13.6}$$

The factor for taking permeability and dilantancy into account is:

$$\begin{aligned} \frac{i}{\Delta * (1 - n_0)} &= \frac{\nu_e}{k} * \frac{n_i - n_0}{1 - n_i} \\ &\text{Where :} \\ i &= \text{Hydraulic gradient [m/s];} \\ \nu_e &= \text{Erosion velocity [m/s];} \\ k &= \text{Permeability [m/s];} \\ n_0 &= \text{in-situ porosity [-];} \\ n_i &= \text{Porosity top layer [-];} \end{aligned} \tag{13.7}$$

By combining equation-13.6 and equation-13.7 and assuming that the porosity of the top layer is equal to the maximum porosity (Schoen, 2014), the adjustment factor of the critical Shield parameter ($\theta_{cr}{}^*$) [-] can be derived. This factor is shown in equation-13.8:

$$\theta_{cr}{}^* = \theta_{cr} * (f_{slope} * \frac{\nu_e}{k} * \frac{n_{max} - n_0}{1 - n_{max}} * \frac{1}{\Delta * (1 - n_0)}) = \theta_{cr} * (\frac{sin(\phi) + sin(\alpha_{bed})}{sin(\phi)} * \frac{\nu_e}{k} * \frac{n_{max} - n_0}{1 - n_{max}} * \frac{1}{\Delta * (1 - n_0)}) \tag{13.8}$$

13.2.3 Sedimentation

There are three types of sediment transport: bed-load, suspended load and wash-load transport (Schoen, 2014). Bed-load is considered to be the transport of the internal sliding of sediment. Bed-load is dependent on the resistance of the seabed sand particles on each other, called the friction force. The equation for the friction force is similar to the equation for the Shields parameter shown in equation-2.1. The Shields parameter can be interpreted as a friction parameter.

$$\begin{aligned} &\tan(\phi) = \frac{\tau}{(\rho_s - \rho_w) * g * D_{50}} \\ &\text{Where :} \\ &\qquad \tau = \text{Shear force [Pa];} \\ &\qquad \phi = \text{Angle of the bed [°];} \end{aligned} \tag{13.9}$$

Bed-load transport occurs when the flow velocity is larger than exceeds the friction force. Based on this theory, it can be expected that a whole layer will be sheared if the flow velocity exceeds the friction force, causing a continuous erosion of layer by layer. This is not realistic and not the case in actual practice. To counter this, the sheared bed-load theory should be taken into account (Schoen, 2014). This theory adds a different resisting force that justifies the lower layers from not eroding.

The suspended load is considered to be the transport caused by the upwards force (pore pressure), causing the sediment to "float". This is called the saltating movement of particles. The saltating movement is settled after the particle has reached a certain height and length and comes to an end after it falls to the seabed again. With this impact, it loses most of its internal momentum. An example of a saltating movement is shown in figure-13.3.

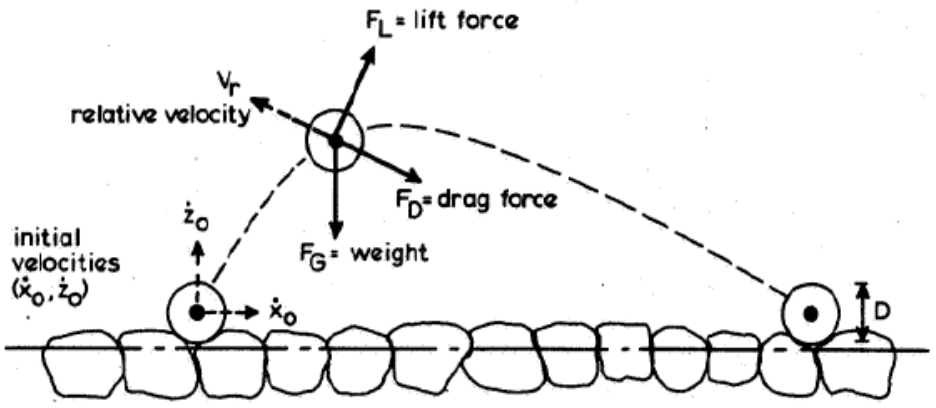

Figure 13.3: Saltating movement
Source: (Leo C. van Rijn, 1984)

The height δ_s and length λ_s of a saltating movement of a sand particle can be derived respectively with equation-13.10 and equation-13.11 (Leo C. van Rijn, 1984).

$$\begin{aligned} &\frac{\delta_s}{D_{50}} = 0.3 * D_*^{0.7} * \sqrt{T} \\ &\text{Where :} \\ &\qquad \delta_s = \text{Saltation height [m];} \end{aligned} \tag{13.10}$$

$$\frac{\lambda_s}{D_{50}} = 3 * D_*^{0.6} * T^{0.9}$$
$$\text{Where :} \tag{13.11}$$
$$\lambda_s = \text{Saltation length [m];}$$

The last transport is related to the sediment transport which is already in the water flow coming from outside of the study area. This wash load transport is not taken into account for this research, because external factors are left out of the scope of the research.

13.2.4 Erosion velocity theories

13.2.4.1 Leo C. van Rijn (1984)

Based on the data obtained from the experiments Leo C. van Rijn (1984) proposed the following equation to calculate the pick-up flux.

$$\phi_p = 0.00033 * \rho_s * \sqrt{\Delta * g * D_{50}} * D_*^{0.3} * T^{1.5} \tag{13.12}$$

in which

$$T = \frac{\theta - \theta_{cr}}{\theta_{cr}} \tag{13.13}$$

The erosion velocity can now be calculated by combining equation-2.6 and equation-13.12. This results in equation-13.14.

$$\nu_e = \frac{0.00033 * \rho_s * \sqrt{\Delta * g * D_{50}} * D_*^{0.3} * T^{1.5} - S}{\rho_s * (1 - n_0 - c_b)} \tag{13.14}$$

13.2.4.2 Bisschop et al. (2010)

Bisschop et al. (2010) continued on the theory of Leo C. van Rijn (1984) and derived equation-13.15.

$$\nu_e = \frac{\phi_p * \sqrt{g * \Delta * D_{50}} - c_b * w_s}{1 - n_0 - c_b}$$
$$\text{Where :}$$
$$\phi_p = \text{Pick-up function according to van Rhee } [kg/m^3 s]; \tag{13.15}$$
$$c_b = \text{The relative concentration level of the jet flow near the soil bed } [kg/m^3];$$
$$w_s = \text{Settling velocity of a single grain in still water } [m/s] \ [kg/m^3 s];$$

$$\phi_p = 0.00033 * D_*^{0.3} * (\frac{\theta - \theta_{cr}^*}{\theta_{cr}^*})^{1.5} \tag{13.16}$$

If equation-13.15 and equation-13.16 are combined then on both sides the erosion velocity (ν_e) is present. The adjusted critical Shields parameter is namely also dependent on the erosion velocity. This problem can't be solved analytically. Bisschop derived a simplification to solve this problem which is shown in the following equations.

$$\nu_e^5 = \alpha^2 * D_*^{0.6} * (\frac{\theta - \theta_{cr}}{\theta_{cr}})^3 * (\frac{k}{\delta})^3 \tag{13.17}$$

in which

$$\alpha = 0.00033 * \frac{\sqrt{\Delta * g * D_{50}}}{(1 - n_0)} \tag{13.18}$$

$$k = 10000 * (\frac{D_{50}}{2})^2 \tag{13.19}$$

(Hazen, 1917)

$$\delta = \frac{n_i - n_0}{(1 - n_i) * \Delta * (1 - n_0)} \tag{13.20}$$

Where :

n_i = Porosity of the sheared layer [-];

Equation-13.17 can be written as follows:

$$\nu_e^5 = \alpha^2 * D_*^{0.6} * (\frac{\theta - \theta_{cr}}{\theta_{cr}})^3 * (\frac{k}{\delta})^3 \rightarrow \nu_e = \alpha^{0.4} * D_*^{0.12} * (\frac{\theta - \theta_{cr}}{\theta_{cr}})^{0.6} * (\frac{k}{\delta})^{0.6} \tag{13.21}$$

13.2.4.3 Winterwerp et al. (1992)

It was found that the maximum pick-up flux due to the hindered settlement can be determined by equation-13.22.

$$\phi_{p_{max}} = 0.033 * (\frac{c_{max}}{c_{avg}} - 1) \tag{13.22}$$

Where :

c_{max} = Maximum sediment-water concentration level [-];

c_{avg} = Average sediment-water concentration level [-];

The average sediment-water concentration can be determined by equation-13.23.

$$c_{avg} = \frac{\rho_j - \rho_w}{\rho_s - \rho_w} \tag{13.23}$$

Steep slopes cause a high flow velocity and result in the erosion of the bar bed. There is an equilibrium slope, where erosion and sedimentation are netto equal to zero. At slopes less steep than the equilibrium slope, bars are formed due to sedimentation. The bars are almost flat and the flow is subcritical. Behind the crest of the bar, erosion takes place and the flow is supercritical. The sedimentation velocity is observed to be around 0.0001 m/s and 0.002 m/s for the conditions mentioned at the beginning of this section. This sedimentation velocity can be calculated with equation-13.24 and equation-13.25. The part $(1 - c_b)^4$ in equation-13.24 represents hindered settlement.

$$S = w_s * c_b * (1 - c_b)^4 * \rho_s \tag{13.24}$$

which can be substituted in:

$$\nu_{sed} = \frac{S}{\rho_s * (1 - n)} = \frac{w_s * c_b * (1 - c_b)^4 * \rho_s}{\rho_s * (1 - n)} \tag{13.25}$$

Where :

ν_{sed} = Sediment velocity $[m/s]$

The dimenionsless pick-up flux form is shown in equation-13.26:

$$\phi_p = \frac{E}{\rho_s * (\Delta * g * D_{50})^{\frac{1}{2}}} \tag{13.26}$$

Using equation-13.26 and the theory by Leo C. van Rijn (1984) it was found that the pick-up flux was overestimating compared to field data, similar to what was found by Bisschop et al. (2010). Sethi (2018) based on the theory of Winterwerp et al. (1992) derived a new empirically based function shown in equation-13.27 to describe the pick-up flux that takes into account the angle between the direction of the flow and the bed of the bar.

$$\begin{aligned} \phi_p * (1 - \frac{tan(\alpha)}{tan(\phi_a)}) =& 0.012 * (\theta^{0.5} - 1.3) * D_*^{0.3} \\ \text{Where :} & \\ \alpha =& \text{Angle difference between direction of the flow and the bed of the bar [°];} \end{aligned} \tag{13.27}$$

In this theory, the Shields parameter and dimensionless grain diameter can be calculated according to equation-2.1 and equation-2.3 stated in section-2.2.2. By subtracting the settle flux from the pick-up flux the erosion rate can be determined.

$$\frac{E - S}{\rho_s * (1 - n) * sin(\alpha)} = \frac{\nu_e}{sin(\alpha)} \tag{13.28}$$

In the scenario that only erosion occurs (S = 0) equations-13.26 and equation-13.27 can be substituted and simplified.

$$\frac{E}{\rho_s * (\Delta * g * D_{50})^{\frac{1}{2}}} * (1 - \frac{tan(\alpha)}{tan(\phi_a)}) = 0.012 * (\theta^{0.5} - 1.3) * D_*^{0.3} \tag{13.29}$$

in which:

$$\frac{E}{\rho_s * (1 - n) * sin(\alpha)} = \frac{\nu_e}{sin(\alpha)} \rightarrow E = \frac{\nu_e}{sin(\alpha)} * (1 - n_0) * \rho_s \tag{13.30}$$

In the case of CFE the jet flow is perpendicular to the bed level. Therefore it can be assumed that the value of $sin(\alpha)$ is equal to 1 since $sin(90°)$ is 1. This results in:

$$\nu_e = \frac{0.012 * (\Delta * g * D_{50})^{0.5} * (\theta^{0.5} - 1.3) * D_*^{0.3}}{(1 - n_0)} \tag{13.31}$$

13.2.4.4 Mastbergen and Van Den Berg (2003)

Mastbergen and Van Den Berg (2003) found that the pick-up flux can be expressed with equation-13.32.

$$\begin{aligned} \phi_p &= A * (\theta - \theta_{cr})^m * D_*^n \\ \text{Where :} & \\ A &= \text{Coefficient [-]} \\ m &= \text{Shear stress power in erosion function [-]} \\ n &= \text{Grain size power in erosion function [-]} \end{aligned} \tag{13.32}$$

Mastbergen and Van Den Berg (2003) derived that the erosion velocity can be calculated with equation-13.33. This equation is shown here:

$$\nu_e = \frac{E - S * cos(\alpha) *}{\rho_s * (1 - n_0)} = \frac{\phi_p * \sqrt{\Delta * g * D_{50}}}{1 - n_0} - \nu_{sed} * cos(\alpha) \tag{13.33}$$

Not only does erosion take place in a vertical direction, but sand bars/dunes also erode in a horizontal direction. This horizontal breaching velocity, ν_{wal} often used in dredging practices is independent of local flow conditions but only dependent on soil properties porosity, permeability and the angle of the bed. It can be expressed as:

$$\nu_{wal} = \frac{(1-n_0) * \Delta * \frac{sin(\phi_a - \alpha)}{sin(\phi_a)}}{\Delta n / k}$$

Where : (13.34)

Δn = porosity increase in the sand bed from undisturbed to loose conditions [-]

To take into account the effect of the generation of the negative pore pressures the pick-up flux is multiplied with a relative erosion velocity factor of $(1 - \frac{\nu_{ero}}{\nu_{wal}})$. Substituting this in equation-2.10 the following equation is derived:

$$\phi_p * (1 - \frac{tan(\alpha)}{tan(\phi_a)}) * (1 - \frac{\nu_e}{\nu_{wal}}) = A * (\theta - \theta_{cr})^m * D_*^n \tag{13.35}$$

Substituting equation-13.33 in equation-13.35 and neglecting the sedimentation velocity this results in:

$$\begin{gathered} \nu_e = \frac{\phi_p * \sqrt{\Delta * g * D_{50}}}{1-n_0} \;\rightarrow\; \phi_p * (\sqrt{\Delta * g * D_{50}}) = \nu_e * (1-n_0) \;\rightarrow\; \phi_p = \frac{\nu_e * (1-n_0)}{\sqrt{\Delta * g * D_{50}}} \\ \downarrow \\ \frac{\nu_e * (1-n_0)}{\sqrt{\Delta * g * D_{50}}} * \frac{sin(\phi_a - \alpha)}{sin(\phi_a)} * (1 - \frac{\nu_e}{\nu_{wal}}) = A * (\theta - \theta_{cr})^m * D_*^n \\ \downarrow \\ \frac{\nu_e}{\sqrt{\Delta * g * D_{50}}} * (1 - \frac{\nu_e}{\nu_{wal}}) = \frac{A * (\theta - \theta_{cr})^m * D_*^n}{(1-n_0) * \frac{sin(\phi_a - \alpha)}{sin(\phi_a)}} \end{gathered} \tag{13.36}$$

If the flow velocity is low, the diameter of the particles is relatively large or has a high permeability and the sand bar has a mild slope, the classic erosion equation-2.10 holds. In this case the ratio of $\frac{\nu_e}{\nu_{wal}}$ is < 1 and therefore can be neglected. In the case that there are high erosion rates or fine sand with relatively low permeability, dilantancy occurs. Then the ratio of $\frac{\nu_e}{\nu_{wal}}$ is > 1 and the value of 1 between the brackets (on the left side of the ratio) can be neglected. Rewriting equation-13.36 and substituting equation-13.34 within the final equation, the erosion velocity can be expressed as:

$$\begin{gathered} \nu_e = \sqrt{\frac{-A * (\theta - \theta_{cr})^m * D_*^n}{(1-n_0) * \frac{sin(\phi_a - \alpha)}{sin(\phi_a)}} * \sqrt{\Delta * g * D_{50}} * \nu_{wal}} \\ \downarrow \\ \nu_e = \sqrt{\frac{A * (\theta - \theta_{cr})^m * D_*^n * k * \sqrt{\Delta^3 * g * D_{50}}}{\Delta n}} \end{gathered} \tag{13.37}$$

13.2.5 Water jet

The water exit velocity of the flow at the nozzle can be calculated with the following equation:

$$u_0 = \zeta * 1.17 * (\frac{P_o}{\rho * d^2})^{\frac{1}{3}}$$

Where :

$$\begin{aligned} u_0 &= \text{Flow velocity at nozzle } [m/s]; \\ \zeta &= \text{factor for energy los [-]}; \\ P_o &= \text{Power of the jet } [kW]; \\ \rho &= \text{Density of the fluid } [kg/m^3]; \\ D_0 &= \text{Nozzle diameter } [m]; \end{aligned} \tag{13.38}$$

13.2.6 Jet regimes

It is not always guaranteed that the water flow will impede the soil. It can also occur that the soil weakly deflects the flow and the soil is not penetrated. There are two different regimes distinguished based on the interaction between the soil and the water flow from the soil. The regimes are shown in figure-13.4.

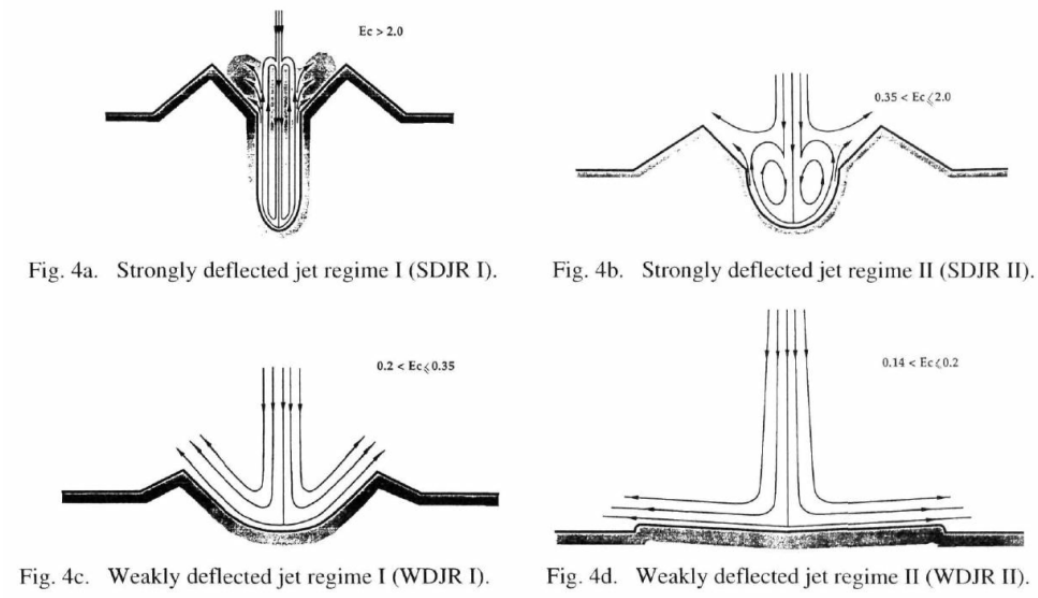

Fig. 4a. Strongly deflected jet regime I (SDJR I).
Fig. 4b. Strongly deflected jet regime II (SDJR II).
Fig. 4c. Weakly deflected jet regime I (WDJR I).
Fig. 4d. Weakly deflected jet regime II (WDJR II).

Figure 13.4: Jet regimes
Source: (Aderibigbe and Rajaratnam, 1996)

In which regime the flow interacts with the soil can be determined with the erosion parameter. For $E_c > 2.0$ the jet regime is in strongly deflected jet regime I, for $0.35 < E_c < 2.0$ it is in strongly deflected jet regime II, for $0.2 < E_c < 0.35$ it is in weakly deflected jet regime I and for $0.13 < E_c < 0.2$ it is in weakly deflected jet regime II. Note that this conditions only hold for a stationary jet (Aderibigbe and Rajaratnam, 1996).

For strongly deflected jet regimes the flow penetrates the bed of the soil. The opening is narrow and the flow is highly turbulent. The flow reaches a relative high depth, but due to depth and slope instabilities a small percentage of sediment is transported outside of the trench. Resulting in a higher dynamic depth than the static depth. In the weakly deflected jet regimes, the flow does not penetrate the soil. The geometries of the static and dynamic depths are almost equal. In the case of weakly deflected jet regime II the deflected flow can be seen as a radial jet. A radial wall jet assumes that the flow is re-directed as it would do when it bounces against an impenetrable plate. Theory about a radial wall jet is not that relevant for this research, because CFE aims to be in strongly deflected regimes.

13.3 Appendices C - Existing model assessment

13.3.1 Boon & Knuuttila technique

Problem context and epistemic purpose
The problem context is similar to the problem context described in section-1.3. During CFE processes trial and error attempts are conducted in order to receive the desired dimensions of a trench. The dimensions of a trench using a CFE process can't be predicted . The phenomenon this model describes is the change in the sea-bed profile caused by the force exerted by the CFE tool. The model predicts the static scour depth and radius of a CFE process after one pass over the seabed. The epistemic purpose of this model is to quantify the influence of a CFE tool on the dimensions of the trench.

Model structure - Parameters and their relations
In this section the model is sketched out and described in a most conceptual manner. The input parameters needed in order to let the model work can be found in table-13.1

Table 13.1: Input parameters - In-house built model

Type of input	Constant	Unit	Description
Environmental	Water Density	$[kg/m^3]$	-
	Gravity	$[m/s^2]$	Acceleration due to gravity
	Solids Density	$[kg/m^3]$	-
	Porosity	[-]	Fraction of empty spaces in a solid
	Submerged Particle Density	$[kg/m^3]$	-
	Grain Size	$[mm]$	-
Jet settings	Nozzle Diameter	[m]	The nozzle diameter of the jet
	Exit Velocity	$[m/s]$	The exit water velocity of the jet
	Distance offset	$[m]$	Height of the nozzle to the seabed
Operational	Transit velocity	$[m/s]$	Horizontal velocity of the jet

In figure-13.5 you can find the steps according to Boon and Knuuttila (2009). The general idea of the steps is followed in the following sections.

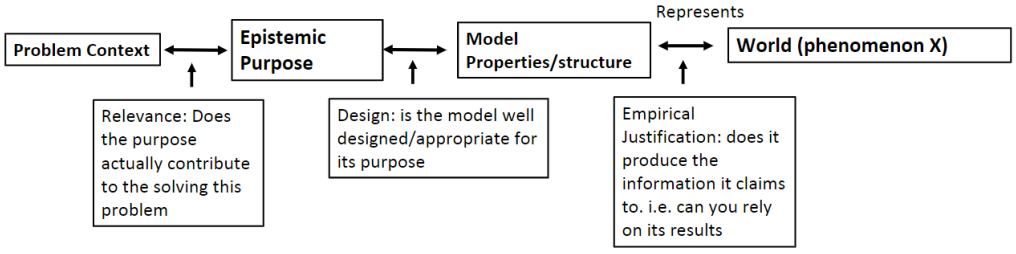

Figure 13.5: Boon and Knuuttilla

The approach that DEME Offshore followed to build the model is shown in figure-13.6.

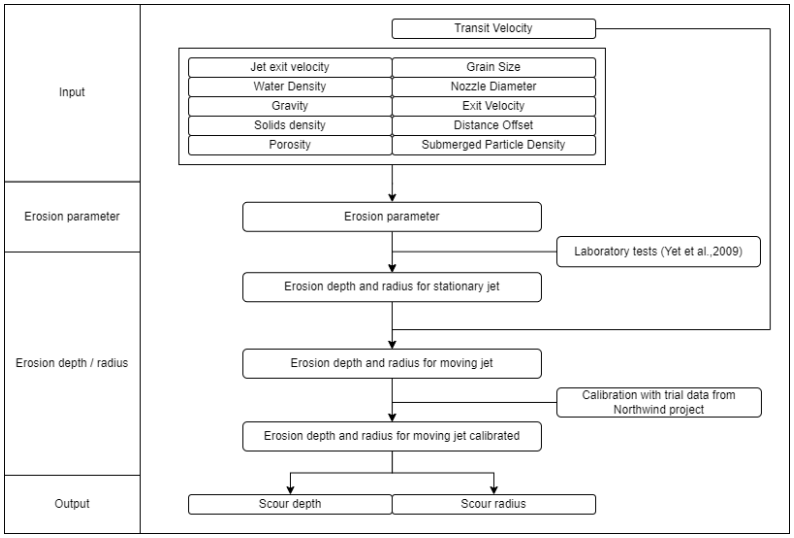

Figure 13.6: Flowchart in-house built model

The papers Aderibigbe and Rajaratnam (1996) and Yeh et al. (2009) both conducted small scale experiments. There were some small differences between the data from both papers. Yeh et al. (2009) provides two logical reasons for this deviation. The first reason is the difference in nozzle diameter. Aderibigbe and Rajaratnam (1996) uses diameters between 4 & 19 mm and Yeh et al. (2009) uses larger diameters of 127mm. The second reason is that Aderibigbe and Rajaratnam (1996) uses impinging distances of $h/d > 8.3$. The impinging ratio distance of Yeh et al. (2009) is fixed at $h/d = 6$. Both papers used this experimental data to derive an equation that predicts the scour depth, radius and ridge height using the erosion parameter. The initial conditions for this model are more similar to the methods used in Yeh et al. (2009). Therefore equation-13.39 form Yeh et al. (2009) was used for the in-house built model:

$$\begin{aligned}
\frac{\epsilon_m}{h} &= 0,64 * (1,26 * E_c^{0,11} - 1) \\
\frac{r_1}{h} &= 0,78 * (1,46 * E_c^{0,15} - 1) \text{ for } E_c < 0,5 \\
\frac{r_1}{h} &= 0,78 * (0,22 + 0,20 * E_c) \text{ for } 0,5 < E_c < 5 \\
\frac{\Delta}{h} &= 0,52 * (-0,02 + 0,044 * E_c)
\end{aligned} \tag{13.39}$$

Where :

ϵ_m = Scour depth [m];
r_1 = Scour radius [m];
Δ = Ridge height [m];

Figure-13.7 provides an illustration to show what the variables mean in the CFE.

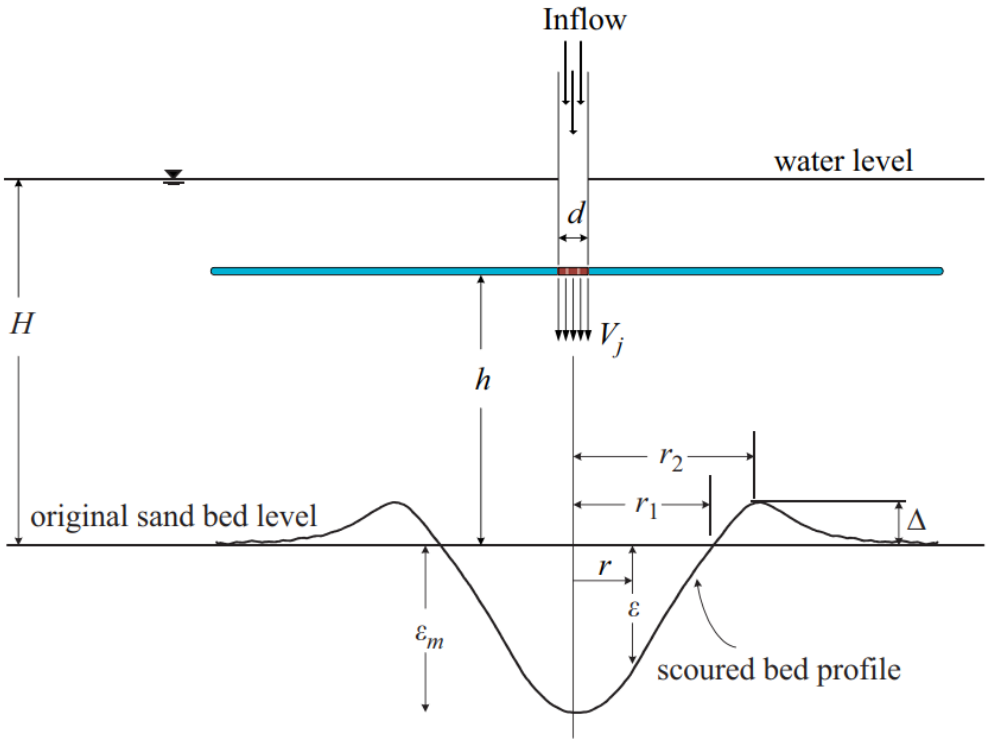

Figure 13.7: Schemization of scour profile
Source: (Yeh et al., 2009)

Note that the equation-13.39 can be used for stationary jets. The influence of the transverse velocity of the jet needs to be taken into account. According to experimental data from Yeh et al. (2009) it was obvious that the scour depth and ridge height was proportional to the transverse velocity of the jet. The scour radius was somewhat constant. The relation between the scour depth and transverse velocity could be described as a parabolic function with the scour depth and radius functioning as asymptotic values for s increasing to infinity. This led to equation-13.40:

$$\begin{aligned} \frac{\epsilon_m}{h} &= \frac{s-4,0}{305,4+3,00*(s-4,0)} \\ \frac{r_1}{h} &= \frac{s}{1930,5+1,07*s}+0,48 \\ \frac{\Delta}{h} &= \frac{s-4,0}{1200,0+12,10*(s-4,0)} \end{aligned} \tag{13.40}$$

Where :

s = Ratio of uniform jet velocity and transverse velocity [m/s];

Equation-13.40 and data from the N project were used to validate this equation. The error margin between the in-house built model and project N field trials for the scour width was between 0 - 8.5 m. The error margin between the in-house built model and project N field trials was between 0.2 - 0.5. These are significant differences. A new empirical model was proposed.

It was mentioned that the scour profile predicted by Aderibigbe and Rajaratnam (1996) had to be scaled down by Yeh et al. (2009). A similar correction was followed by DEME Offshore and is shown in equation-13.41.

EQUATION CONFIDENTIAL (13.41)

Earlier, it was already affirmed that the impingement ratio had no influence on the scour width. In order to predict the scour width, the best fit was calculated through the trial data to predict the static scour width. Also, a new equation was determined for the scour depth based on modifying the parameters of equation-13.40 by hand. The

final equation of the static scours depth and width are shown in equation-13.42. Equation-13.42 can be seen as the final product.

EQUATION CONFIDENTIAL (13.42)

Abstractions, assumptions and simplifications
The model is limited to a certain application. This is caused by abstractions, assumptions and simplifications. The following holds for the model:

- All input parameters are fixed values. They do not change over time. In real life, this is not the case. During CFE projects there are deviations in these input parameters. It is aimed to minimize deviations in these parameters in order to create a smooth trench bed.
- The bathymetry of the seabed is consistently flat. There are no deviations in height of the seabed.
- The soil of the seabed consists of sand and is cohesionless.
- There is no influence of other external factors, such as currents, sedimentation transport caused by other than the jet and physical interference of external (living) objects.
- The erosion parameter can only be used for a large impinging distance ($h > 8.3d$) according to Yeh et al. (2009).

13.3.2 Accuracy

In table-13.2 the input parameters are shown for the validation process of the in-house built model.

Table 13.2: Input parameters - In-house built model

Type of input	Constant	Unit	Value
Environmental	Water Density	$[kg/m^3]$	1025
	Gravity	$[m/s^2]$	9.81
	Solids Density	$[kg/m^3]$	2660.24
	Porosity	[-]	0.34
	Submerged Particle Density	$[kg/m^3]$	1635.24
	Grain Size	$[mm]$	0.26
Jet settings	Nozzle Diameter	[m]	0.65
	Exit Velocity	$[m/s]$	6.08
	Distance offset	$[m]$	3.49
Operational	Transit velocity	$[m/s]$	0.07

13.3.3 Validation and verification

The in-house built model is validated and verified according to the theoretical framework proposed by Sargent (2008). Sargent (2008) mention some tests that could be conducted so that a model can be verified and validated. The tests that are relevant for the in-house built model are Extreme Condition and Parameter Variability-Sensitivity Analysis tests. An Extreme Condition test means that a certain parameter is changed to an extreme value. The outcome is then checked whether the result is logical or not. A Parameter Variability-Sensitivity Analysis test means that a certain parameter is changed either to a lower value or a higher value. The outcome is then checked whether the result is logical or not.

In this section the model will briefly be validated by looking at each parameter separately and the influence on the outcome. This is in order to check whether the model responds and changes in line with the theory. For the fixed variables of water density and gravitational acceleration, no tests are conducted. The tests are conducted with the average of all the input parameters over the available data. These input parameters are shown in appendix-13.3.2 in table-13.2. Each scenario will be compared with this level, now seen as "normal". The results of all the tests are shown in table-13.3.

Table 13.3: Validation and verification according to Sargent

Extreme condition tests					
Parameter	Changed	Expected	Outcome	Correct?	Description:
Nozzle diameter	Zero	Zero	Zero		Error: division by zero
Uniform jet flow velocity	Zero	Zero	Zero		
Standoff distance	Zero	Zero	Zero		Error: division by zero
	>1000	Zero	0<		Result was negative

Parameter Variability-Sensitivity Analysis tests					
Parameter	Changed	Expected	Outcome	Correct?	Description
Density solid	↑	↓	↓		
	↓	↑	↑		
Diameter grain	↑	↓	↓		
	↓	↑	↑		
Diameter nozzle	↑	↑	↑		
	↓	↓	↓		
Uniform jet flow velocity	↑	↑	↑		
	↓	↓	↓		
Distance offset	↑	↓	↑		
	↓	↑	↓		
Trail velocity	↑	↓	↓		
	↓	↑	↑		

The only surprising result that counters the logical outcome derived from the theory is the parameter variability-sensitivity analysis test with the parameter distance offset. It is logical to think that the larger the distance offset, the more water is entrained, the jet width becomes larger and so the jet momentum decreases. Resulting in a lower penetration depth. It also applies the other way around. However, the model determines differently. The test was conducted with minor changes (+50% and -50%). If the distance offset is increased with +1000% only then, the penetration depth starts to decrease compared to the normal. If the distance offset is lowered to 0.0001 then the penetration depth is still lower compared to the normal. It can be concluded that the influence of the distance offset has some flaws in the model and needs more research for future application.

13.4 Appendix D - Available collected trench data

13.4.1 Available data

Table 13.4: Available data

ID #	Power	ρ [Kg/mˆ3]	Porosity [-]	D_{50} [mm]	D_0 [m]	U_n [m/s]	Δ [-]	ν_{trail} [m/s]	s [m]	Static [m]	Dynamic [m]
N.1	1,00	2670,00	0,30	0,30	0,78	7,90	1,60	0,05	1,00	1,20	-
N.2	1,00	2670,00	0,30	0,30	0,78	7,90	1,60	0,10	1,00	0,70	-
N.3	1,00	2670,00	0,30	0,30	0,78	7,90	1,60	0,20	1,00	0,60	-
N.4	1,00	2670,00	0,30	0,30	0,78	7,90	1,60	0,05	3,00	1,20	-
N.5	1,00	2670,00	0,30	0,30	0,78	7,90	1,60	0,10	3,00	1,10	-
N.6	1,00	2670,00	0,30	0,30	0,78	7,90	1,60	0,20	3,00	0,70	-
N.7	1,00	2670,00	0,30	0,30	0,78	7,90	1,60	0,05	5,00	1,40	-
N.8	1,00	2670,00	0,30	0,30	0,78	7,90	1,60	0,10	5,00	0,90	-
N.9	1,00	2670,00	0,30	0,30	0,78	7,90	1,60	0,20	5,00	0,65	-
T.1	0,40	2670,00	0,30	0,30	0,63	3,96	1,60	0,05	2,00	0,50	-
T.2	0,40	2670,00	0,30	0,30	0,63	3,96	1,60	0,10	3,00	0,40	-
T.3	0,40	2670,00	0,30	0,30	0,63	3,96	1,60	0,20	3,00	0,40	-
T.4	0,40	2670,00	0,30	0,30	0,63	3,96	1,60	0,20	5,00	0,35	-
T.5	1,00	2670,00	0,30	0,30	0,63	9,90	1,60	0,02	2,00	0,50	-
T.6	1,00	2670,00	0,30	0,30	0,63	9,90	1,60	0,05	2,00	0,45	-
T.7	1,00	2670,00	0,30	0,30	0,63	9,90	1,60	0,02	2,00	0,60	-
T.8	1,00	2670,00	0,30	0,30	0,63	9,90	1,60	0,02	2,00	0,50	-
T.9	1,00	2670,00	0,30	0,30	0,63	9,90	1,60	0,03	2,00	0,30	-
T.10	1,00	2670,00	0,30	0,30	0,63	9,90	1,60	0,03	2,00	0,30	-
T.11	1,00	2670,00	0,30	0,30	0,63	9,90	1,60	0,03	2,00	0,35	-
T.12	1,00	2670,00	0,30	0,30	0,63	9,90	1,60	0,03	2,00	0,30	-
T.13	0,45	2650,00	0,38	0,21	0,60	4,46	1,59	0,10	4,35	0,15	-
T.14	0,50	2650,00	0,38	0,21	0,60	4,95	1,59	0,10	4,35	0,15	-
D.1	0,60	2650,00	0,38	0,21	0,60	4,20	1,59	0,10	4,35	0,30	0,1
D.2	0,70	2650,00	0,38	0,21	0,60	4,90	1,59	0,10	4,35	0,30	0,3
D.3	0,45	2650,00	0,38	0,21	0,60	3,15	1,59	0,05	4,35	0,10	0,1
D.4	0,50	2650,00	0,38	0,21	0,60	3,50	1,59	0,05	4,35	0,20	0,2
D.5	0,60	2650,00	0,38	0,21	0,60	4,20	1,59	0,05	4,35	0,30	0,3
D.6	0,65	2650,00	0,38	0,21	0,60	4,55	1,59	0,05	4,35	0,40	0,3
D.7	0,70	2650,00	0,38	0,21	0,60	4,90	1,59	0,05	4,35	0,45	0,4
D.8	0,40	2650,00	0,38	0,21	0,60	2,80	1,59	0,03	4,35	0,05	0,1
D.9	0,45	2650,00	0,38	0,21	0,60	3,15	1,59	0,03	4,35	0,20	0,2
D.10	0,50	2650,00	0,38	0,21	0,60	3,50	1,59	0,03	4,35	0,25	0,3
D.11	0,60	2650,00	0,38	0,21	0,60	4,20	1,59	0,03	4,35	0,45	0,5
D.12	0,60	2650,00	0,38	0,21	0,60	4,20	1,59	0,03	4,35	0,35	0,5
D.13	0,60	2650,00	0,38	0,21	0,60	4,20	1,59	0,03	4,35	0,40	0,4
D.14	0,60	2650,00	0,38	0,21	0,60	4,20	1,59	0,03	4,35	0,50	0,65
D.15	0,70	2650,00	0,38	0,21	0,60	4,90	1,59	0,03	4,35	0,30	0,55
D.16	0,70	2650,00	0,38	0,21	0,60	4,90	1,59	0,03	4,35	0,35	0,6
D.17	0,80	2650,00	0,38	0,21	0,60	5,60	1,59	0,03	4,35	0,30	0,7
D.18	0,80	2650,00	0,38	0,21	0,60	5,60	1,59	0,03	4,35	0,50	0,8

13.4.2 Approach assessing data reliability

The data is assessed with the following approach. First, some conclusions are made based on the theory. These conclusions are labeled and later on referred to when they are contradicted based on the data results. The data discrepancies are grouped based on the three projects and causing parameter of deviation.

Theory conclusions

1. **Uniform flow velocity**
   The theory describes that if the uniform flow velocity increases, the shields parameter also increases. A larger force is exposed to a single particle and this results in higher erosion rates. Higher erosion rates mean that more sand is eroded and a larger maximum depth is reached. Thus, to conclude the flow velocity has a positive relationship with the scour depth.

2. **Standoff distance**
   If the standoff distance increases, more water is entrained resulting in a higher discharge. The discharge is negatively related to the uniform flow velocity, based on equation-2.19. This means that the standoff distance has a negative relation to the scour depth.

3. **Trail velocity**
   Based on the theory, the dynamic depth is dependent on the erosion velocity and the trail velocity. The higher the trail velocity, the more the direction of the flow tends to bend backward. So, the higher the trail velocity, the lower the scour depth. Thus, the trail velocity has a negative relation with the scour depth.

4. **Same input parameters**
   It is only logical to conclude that if the input values of each parameter of two data points are equal, the scour depths must be identical.

5. **Same scour depth, but different input parameter**
   If all the parameters are identical except for one, then the scour depth should differ. There might be an exemption to this conclusion. That is when the differing parameter has no influence on the static depth. Based on the sensitivity analysis that is conducted in section-9 it is shown that each parameter has a significant influence on the scour depth if the percentage change falls within a certain range. This is the case for the all mentioned discrepancies. Thus, the conclusion holds in this case.

All the discrepancies in the data set are mentioned below. Note that is possible that there are more discrepancies. These are the ones that are found. The discrepancies that do not match the theory are indicated with the color red and the trends, that match the theory and prove the opposite relation also shown in the data, are indicated with green. A different type of discrepancy is separated with a black horizontal line.

13.4.3 Data assessment - static depth results

Project N

- Data ID: N.7 & N.4 & N.1
  In these three data points all the parameters are the same, except for the standoff distance. The static depth is however not in line with what to expect based on the theory conclusion-2.

- Data ID: N.8 & N.5 & N.2
  In these three data points, all the parameters are the same, except for the standoff distance. Based on these three data points the relation between the stand off distance and static depth a parabolic with the highest depth in the middle of the stand off distance range. This is not in line with theory conclusion-2.

- Data ID: N.9 & N.6 & N.3
  The relation found between these three data points is similar to the discrepancy mentioned above.

  Data ID: T.3 & T.4
  These two data points describe that the higher the standoff distance, the lower the static depth. This meets theory conclusion-2. This shows that the data contradicts itself for all the discrepancies found in the N project.

Project T

- Data ID: T.1 & T.6
  In these two data points all the parameters are identical, except for the uniform flow velocity. As already stated in theory conclusion-1, the uniform flow velocity is positively related to the static depth. These two data points show the opposite.

  Data ID: D.7 & D.8
  In these two data points D.7 has a lower flow velocity, while all the other parameters are the same, than D.8. Based on the theory, D.7 should have a lower static depth than D.8 which is true based on the result. This matches theory conclusion-1.

- Data ID: T.5/T.8 & T.7
  Both ID's have the same input parameters, but different static depths. This is not in line with theory conclusion-4.

  Data ID: T.5 & T.8
  Both ID's have the same input parameters and the same static depth.

- Data ID: T.9/T.10/T.12 & T.11
  Both ID's have the same input parameters, but different static depths. This is not in line with theory conclusion-4.

  Data ID: T.9 & T.10 & T.12
  Both ID's have the same input parameters and the same static depth.

- Data ID: T.2 & T.3
  In these two data points every parameter is the same, except for the trail velocity. Based on the theory conclusion-3 the higher the trail velocity the lower the static depth, which is for these data points not the case.

  Data ID: T.8 & T.9
  In these two data points every parameter is the same, except for the trail velocity. These two data points meet theory conclusion-3.

Project D

- Data ID: D.1 & D.5
  Similar to the discrepancy found in the data points T.2 & T.3. It is not in line with theory conclusion-3.

  Data ID: D.12 & D.2 & D.6
  Similar to the relation of the data points T.8 & T.9

- Data ID: D.13 & D.14 & D.15 & D.16
  All ID's have same input parameters, but also all different static depths. This is not in line with theory conclusion-4.

- Data ID: D.19 & D.20
  Both ID's have same input parameters, but different static depths. This is not in line with theory conclusion-4.

- Data ID: D.17 & D.18
  Both ID's have same input parameters, but different static depths. This is not in line with theory conclusion-4.

  Data ID: x
  There was no relation found within the Project D data set that could prove the opposite relation of the above discrepancies. In the other data sets this relation was found. An example is the relation in the data points T.5 & T.8 or T.9 & T.10 & T.12

- Data ID: D.3 & D.7
  In these two data points the only difference in the parameter is the trail velocity. However, the data point with the higher trail velocity has a higher static depth. This is not in line with theory conclusion-3.

- Data ID: D.17 & D.4
  Similar to the discrepancy found in the data points D.3 & D.7. It is not in line with theory conclusion-3.

  Data ID: D.12 & D.2 & D.6
  These three data points prove that the opposite relation is also shown in the data. The higher the trail velocity, the lower the static depth

---

- Data ID: D.16 & D.20
  These two data points have the same input parameters, except for the uniform flow velocity. It is expected that the data point with the higher uniform flow velocity also has a higher static depth. However, based on the static depth in these data points, the opposite is shown. This is not in line with theory conclusion-1.

- Data ID: D.14 & D.18
  Similar to the discrepancy found in the data points D.16 & D.20. It is not in line with theory conclusion-1.

  Data ID: D.10 & D.11
  These two data points that the opposite relation is also shown in the data. The higher the uniform flow velocity, the higher the static depth

---

For the N project it was found that most of the discrepancies were caused by the standoff distance. The data can be divided into three bins based on the trail velocity (0.05, 0.10 and 0.10 m/s). In each bin, there is a data point with the stand off distance 1, 3 or 5 meters. Each bin shows an incorrect relation of the stand off distance with the static depth. Based on the theory the stand off distance has a negative relation with the static depth.

For the T project it was found that there were some discrepancies caused by the flow and trail velocity. It was also found that there were some data points with equal input parameters with different scour depths. In total there

were found four discrepancies, one based on the flow velocity, one based on the trail velocity and two based on identical input parameters with different static depths. These discrepancies included 11 out of the total 12 data points within the T project.

The most discrepancies were found in the D project. It was found that there were some discrepancies caused by three categories. The three categories that were not found in this project were the categories based on the stand off distance, based on the trail velocity and the same scour depths with one differing parameter. In total there were found eight discrepancies, two based on the uniform flow velocity, three based on the trail velocity and three based on identical parameters with different scour results. These discrepancies included 16 of the total 20 data points within the D project.

Further two large accuracy errors were found in the data set of the D project. For the data points D.5 and D.10, respectively an absolute percentage error was found of 484% and 1156%. These errors are clearly unrealistic. For both the data points, the measured field static depth is relatively low compared to the other results. The input parameters for the two data points are in the same range as the input parameters used in the other data points, which should imply that the static depth must be in the same range as the other data points. However, this is thus not the case. Therefore, the data points D.5 and D.10 are in further analysis scrapped from the data set.

13.4.4 Data assessment - dynamic depth results

Project D

- Data ID: D.11/D.12 & D.13 & D.14
  Both ID's have the same input parameters, but also all different dynamic depths. This is not in line with theory conclusion-4.

- Data ID: D.15 & D.16
  Both ID's have the same input parameters, but different dynamic depths. This is not in line with theory conclusion-4.

- Data ID: D.17 D.18
  Both ID's have the same input parameters, but different dynamic depths. This is not in line with theory conclusion-4.

  Data ID: D.12 & D.12
  These two data points show, that the data also shows the relation that when all parameters are similar, the dynamic depth is also similar.

The only available data for the dynamic depth is coming from the D project. It was found that there were two discrepancies based on the uniform flow velocity and three discrepancies based on identical input parameters width different static scour depths. These five discrepancies included nine out of 18 data points.

13.5 Appendix E - Static model

In this appendix the relations of some of the input parameters with the level of error are plotted in graphs. This appendix adds information to the calibration part of the static model.

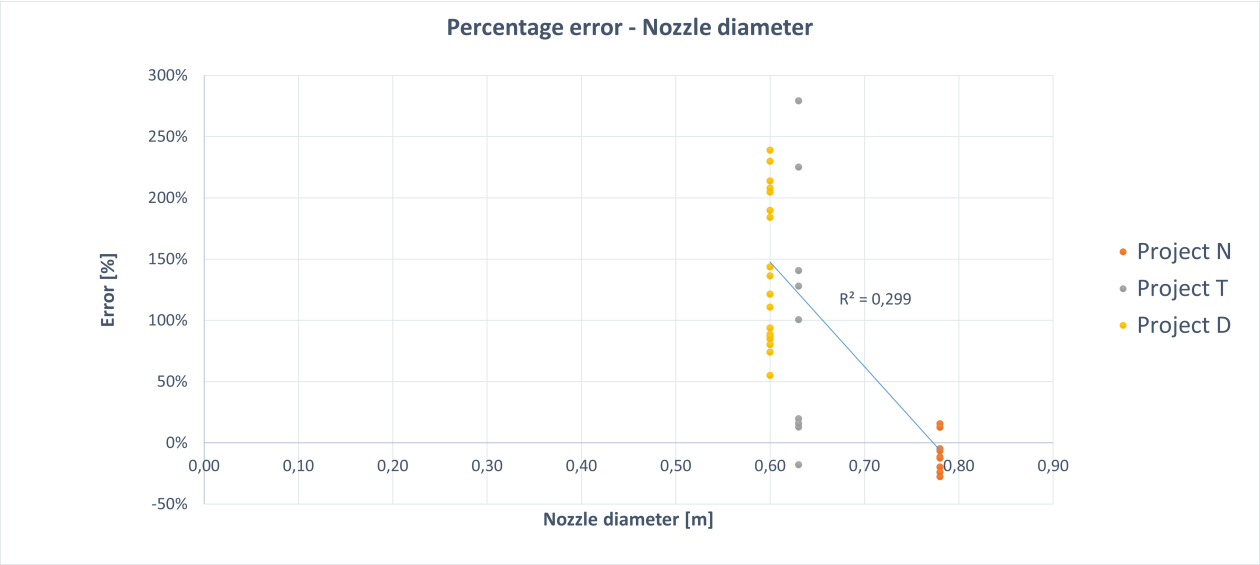

Figure 13.8: Static model - Error against nozzle diameter

Figure 13.9: Static model - Error against impingement ratio

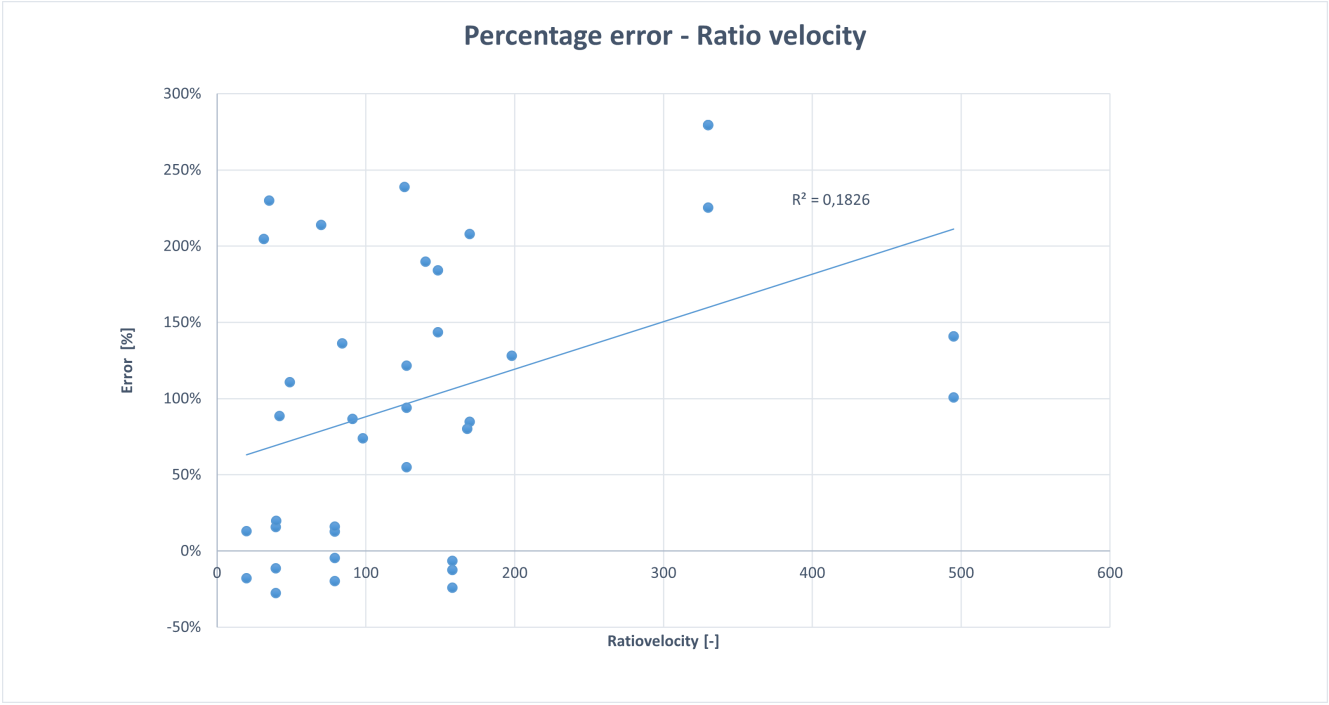

Figure 13.10: Static model - Error against ratio Velocity

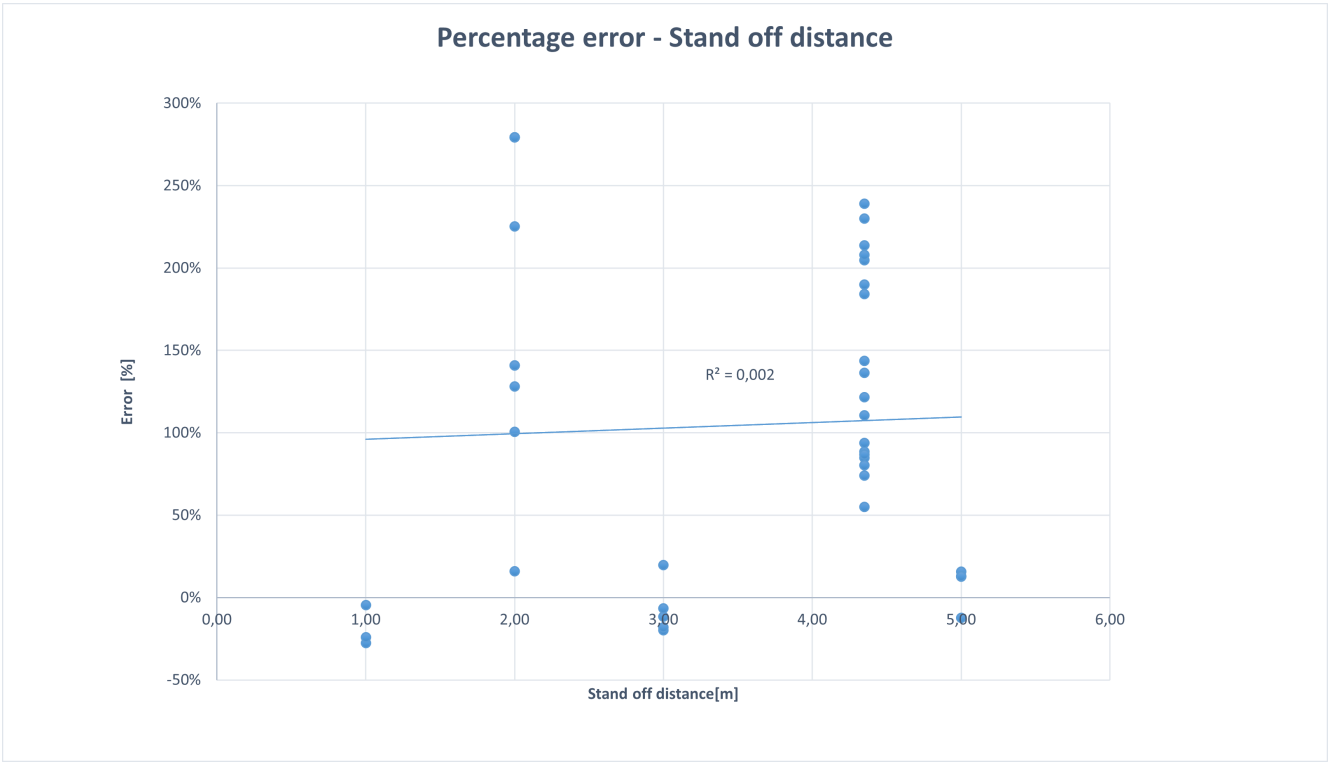

Figure 13.11: Static model - Error against stand off distance

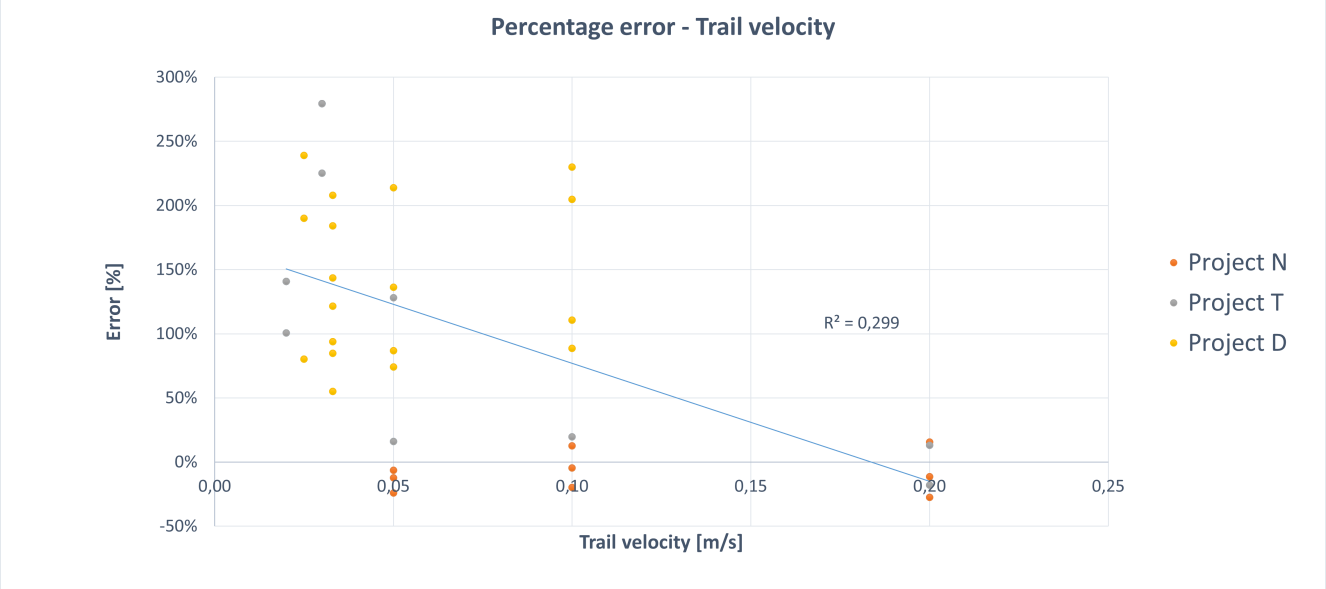

Figure 13.12: Static model - Error against trail velocity

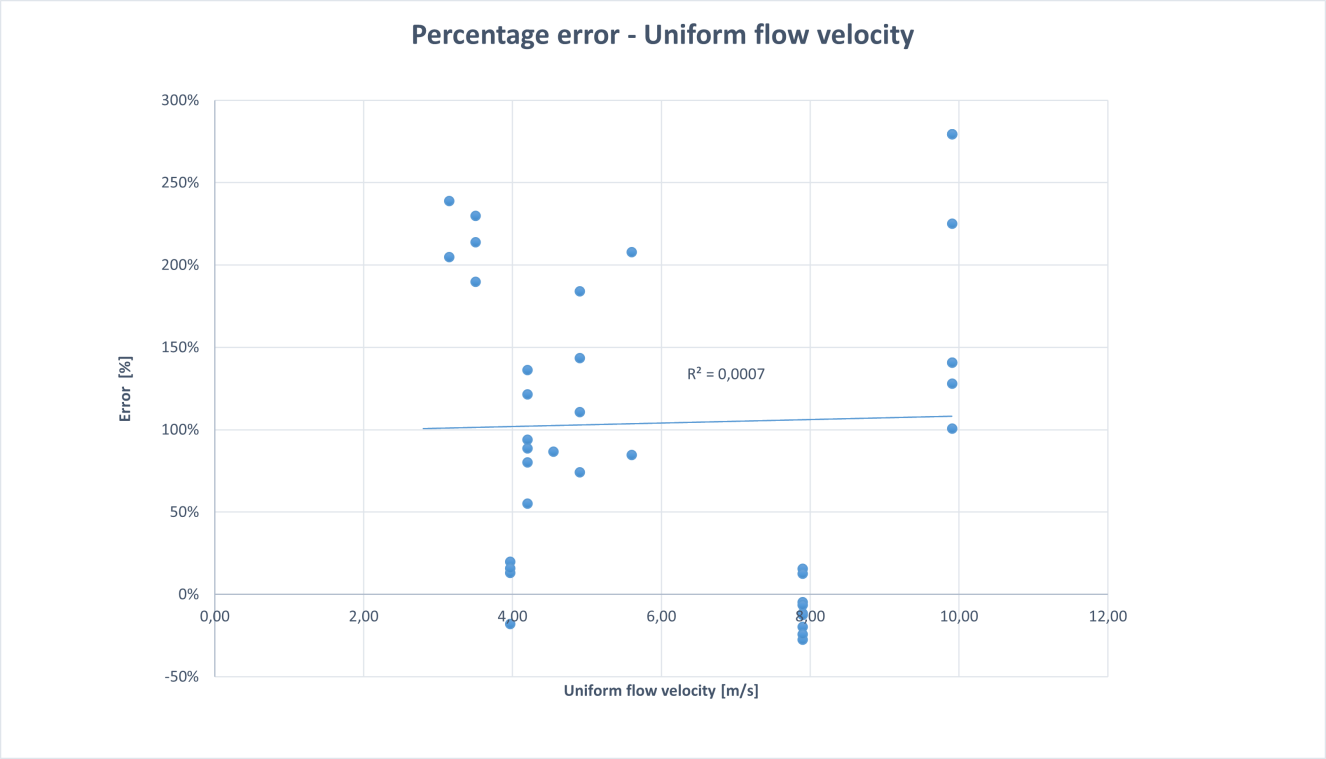

Figure 13.13: Static model - Error against uniform flow velocity

In the following graphs the sensitivity of the calibration coefficient is plotted against a percentage change of the static depth. The data point N.2 is chosen as the basis static depth, to which the other results are compared to. N.2 was chosen because it had the lowest error (-5% figure-6.1) of all the data points before the calibration was conducted. The input parameters for this analysis are similar to the values of data point N.2. The only parameter values that are altered, are the values that determined the different bins. This is for the nozzle diameter; 0.78, 0.63 and 0.60 meter and for the trail velocity; 0.20, 0.10, 0.05, 0.03 and 0.02 m/s.

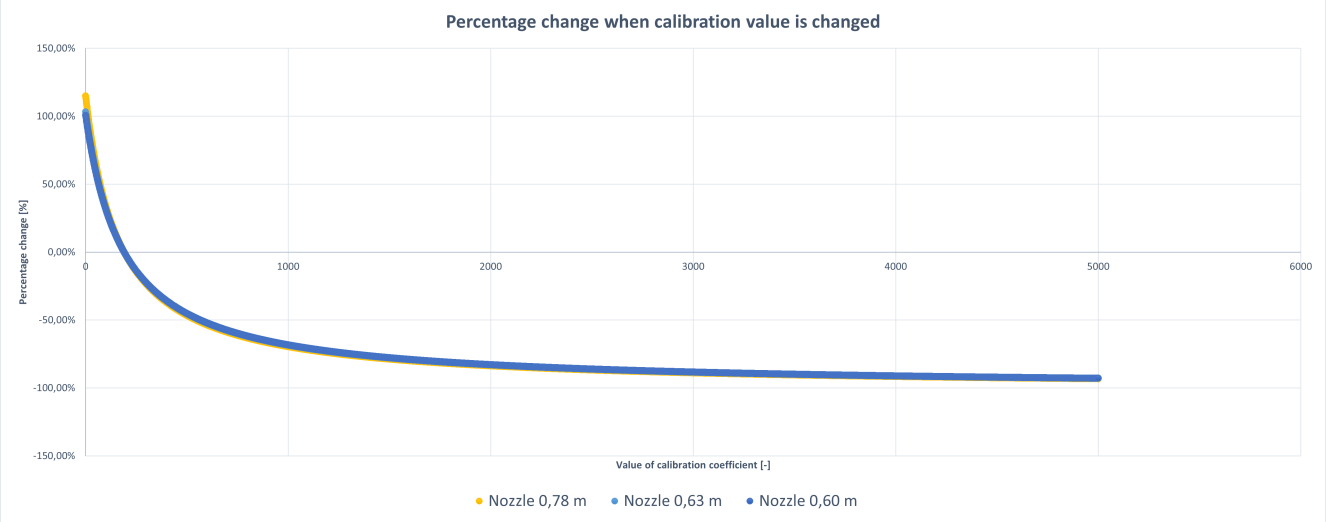

Figure 13.14: Static model - Percentage change when calibration value is changed for different nozzle diameters

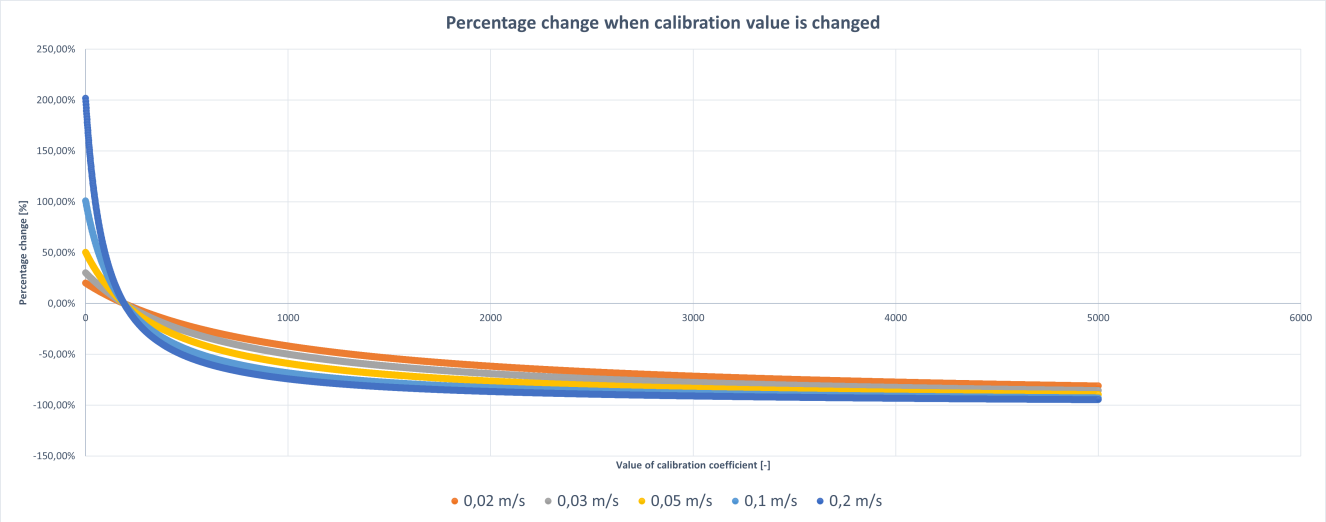

Figure 13.15: Static model - Percentage change when calibration value is changed for different trail velocities

13.6 Appendix F - Sensitivity analysis

13.6.1 Sensitivity analysis static model

In the following figures the sensitivity of the static model is plotted against the field data by altering one parameter.

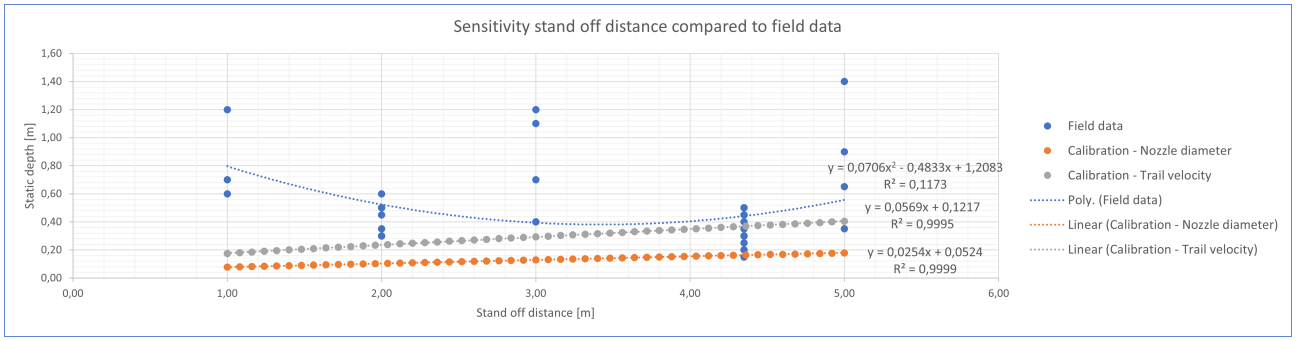

Figure 13.16: Model and field data comparison - Static model - Stand off distance

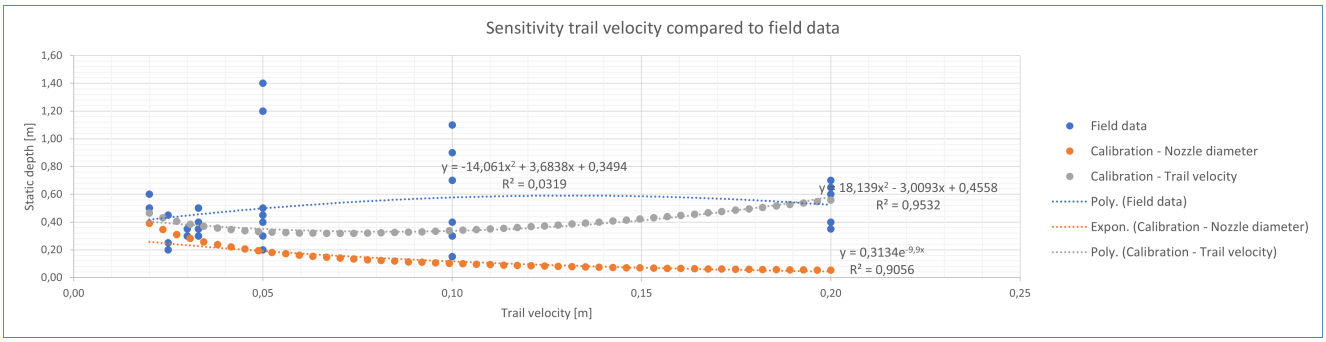

Figure 13.17: Model and field data comparison - Static model - Trail velocity

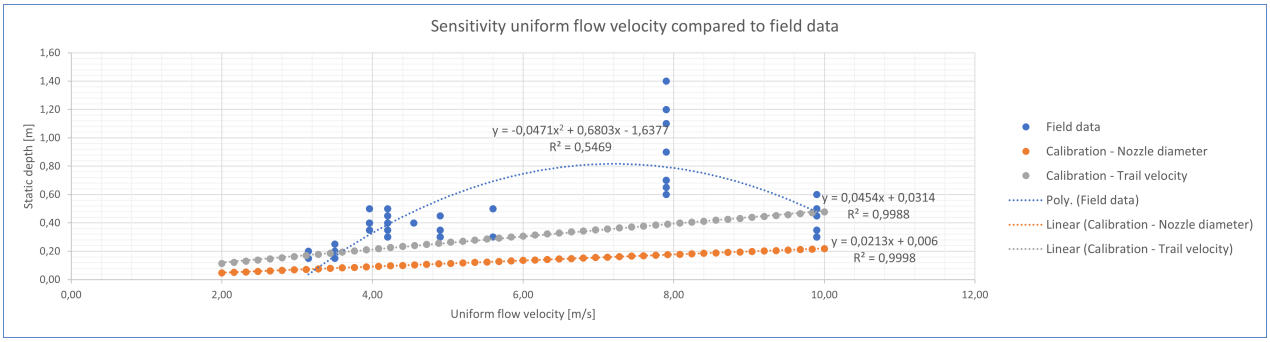

Figure 13.18: Model and field data comparison - Static model - Uniform flow velocity

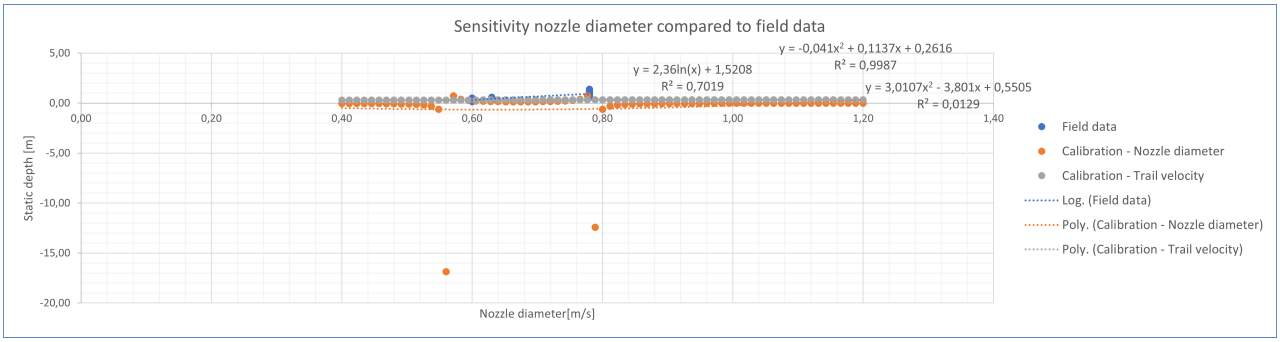

Figure 13.19: Model and field data comparison - Static model - Nozzle diameter

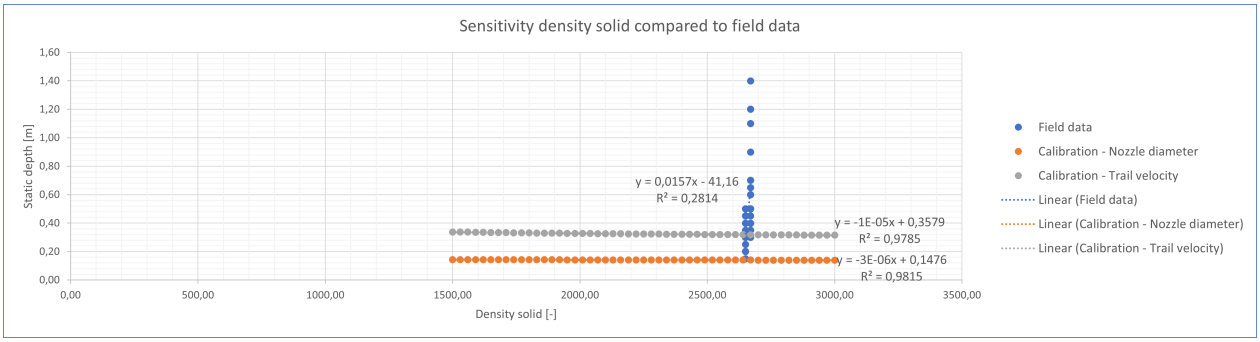

Figure 13.20: Model and field data comparison - Static model - Density solid

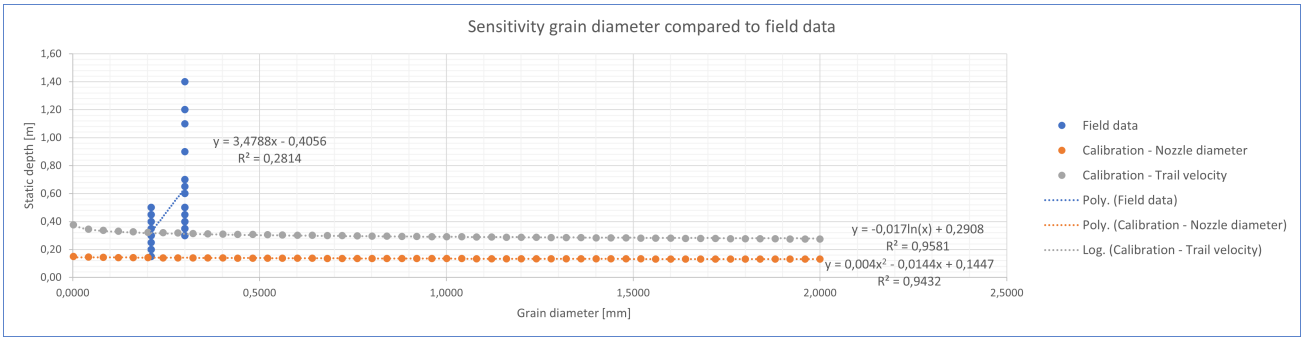

Figure 13.21: Model and field data comparison - Static model - Grain diameter

13.6.2 Sensitivity analysis dynamic model

In the following figures the sensitivity of the dynamic model is plotted against the field data by altering one parameter.

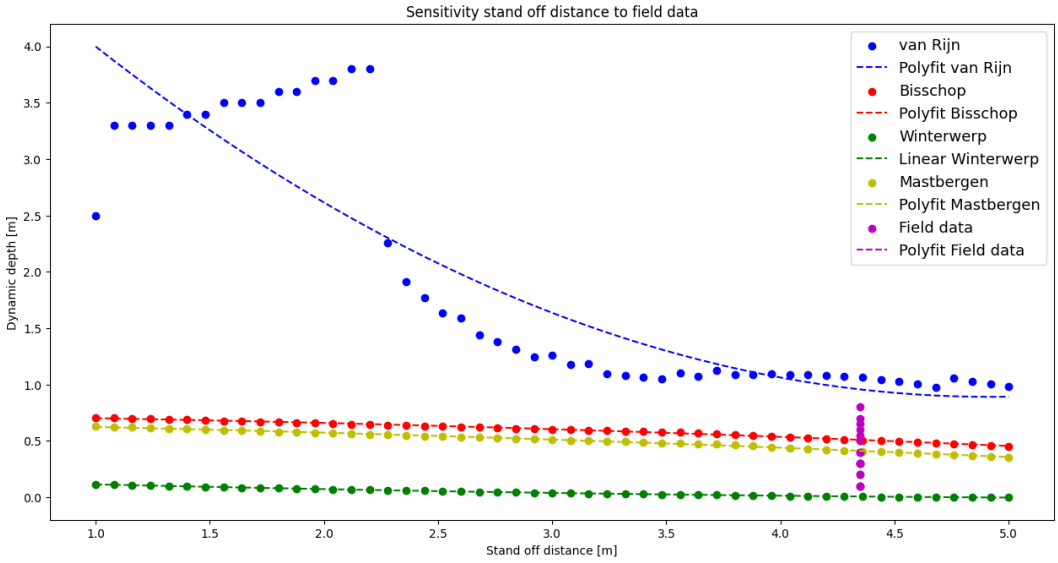

Figure 13.22: Model and field data comparison - Dynamic model - Nozzle diameter

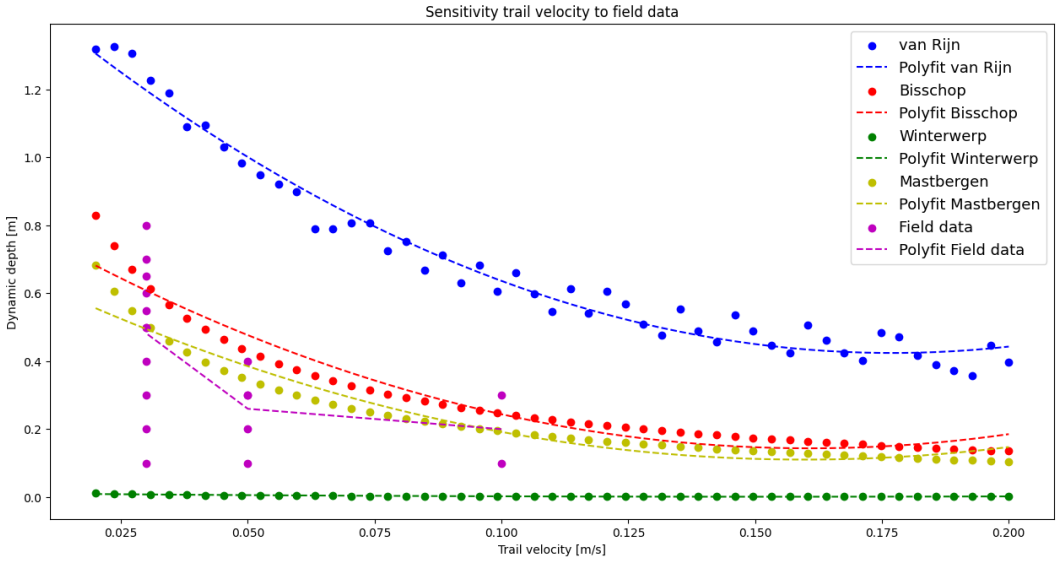

Figure 13.23: Model and field data comparison - Dynamic model - Trail velocity

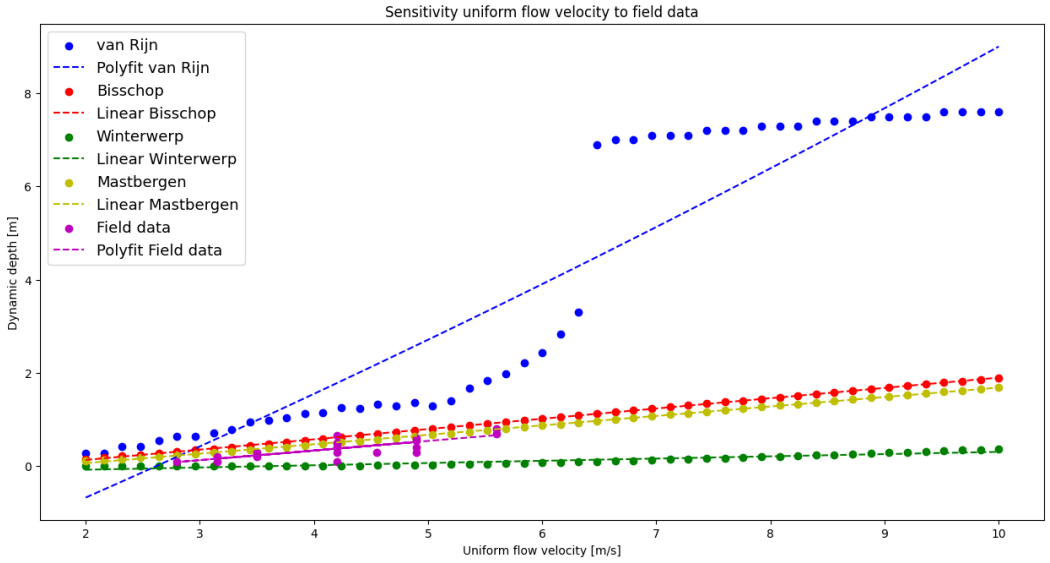

Figure 13.24: Model and field data comparison - Dynamic model - Uniform flow velocity

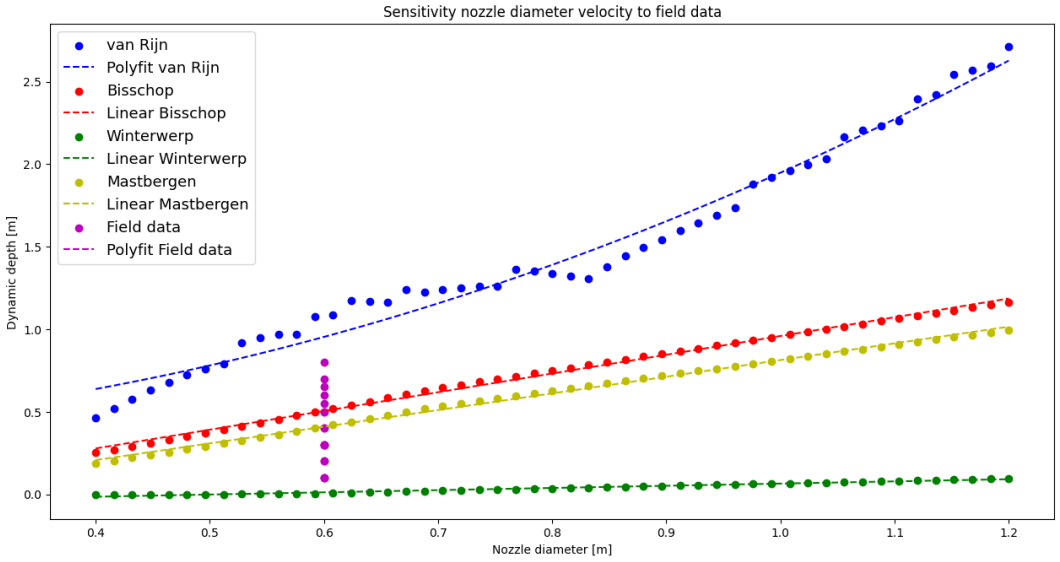

Figure 13.25: Model and field data comparison - Dynamic model - Nozzle diameter

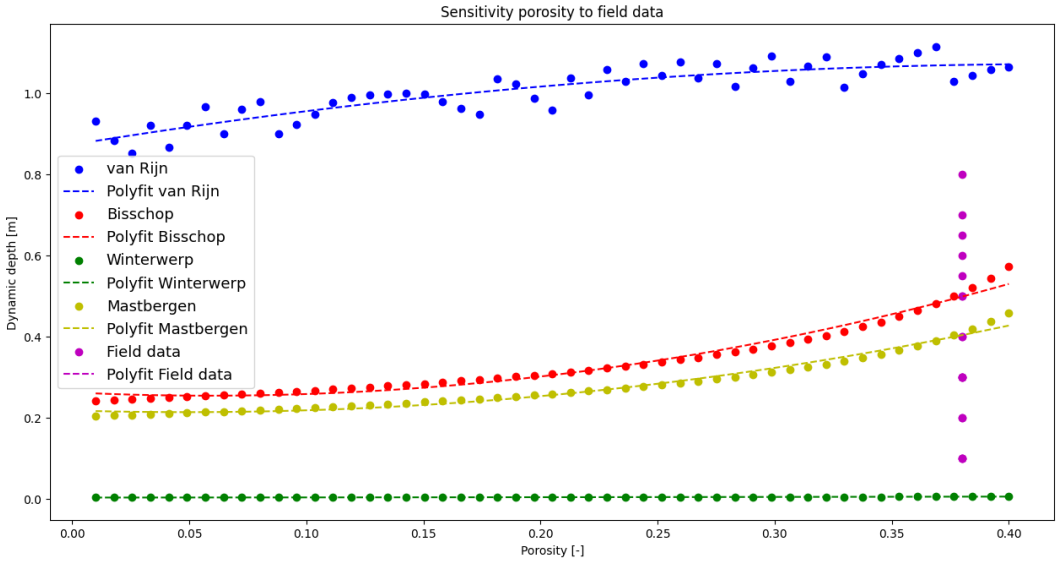

Figure 13.26: Model and field data comparison - Dynamic model - Porosity

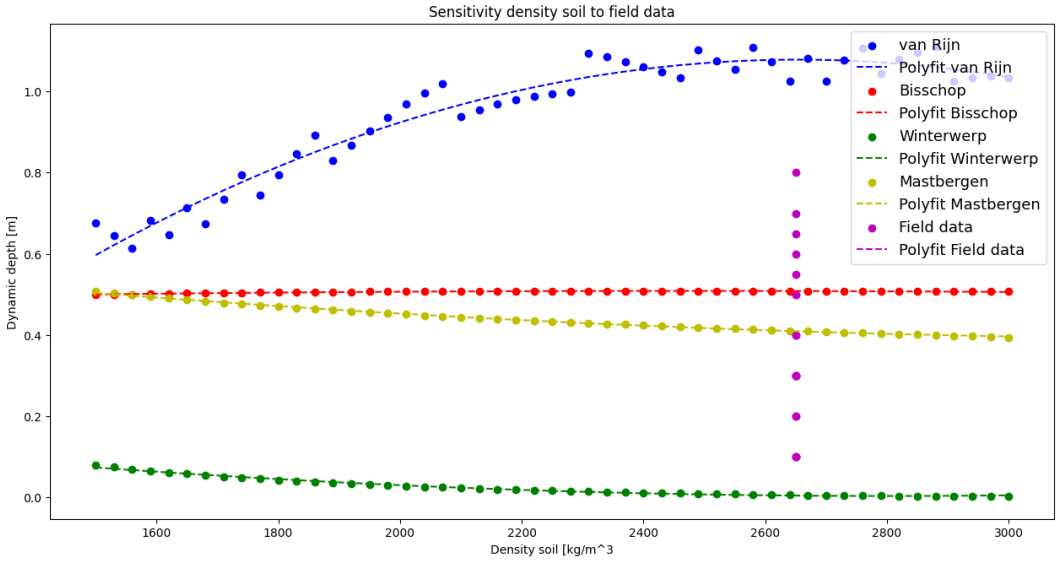

Figure 13.27: Model and field data comparison - Dynamic model - Density soil

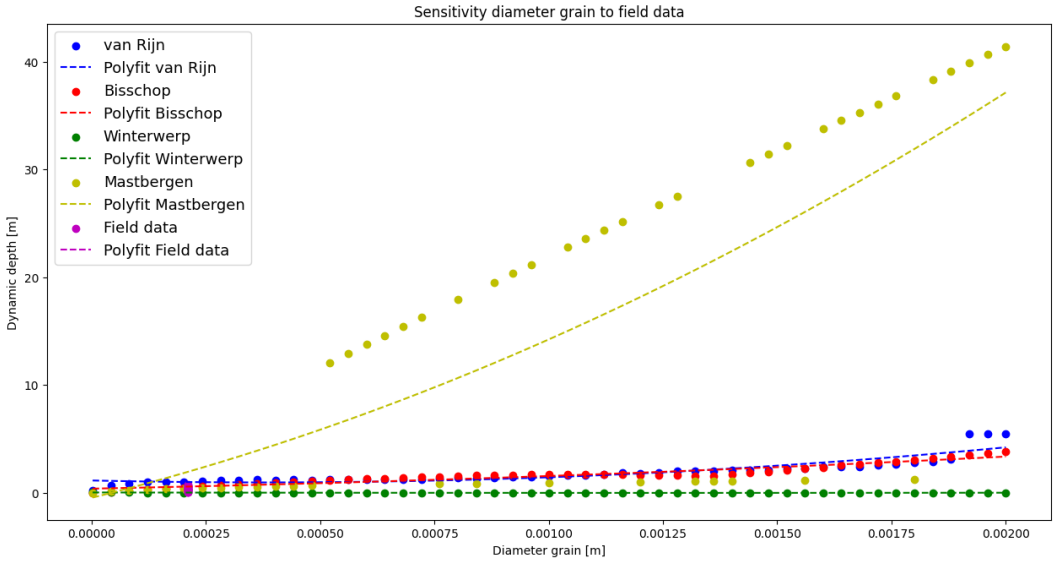

Figure 13.28: Model and field data comparison - Dynamic model - Diameter grain

13.6.3 Critical factors

In the following figures are the critical factors of both models. The figures are separated for the two calibration methods for the static model and for the two erosion velocities for the dynamic model. The first part of the names in the legend indicates the parameter that is assessed and the second part, after the "−" indicate the calibration method/theory.

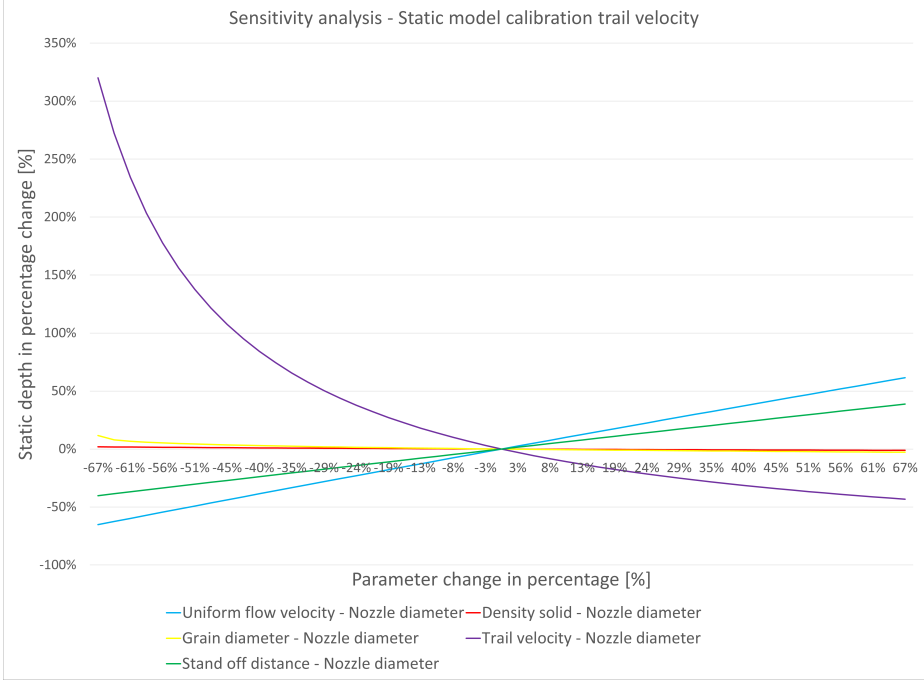

Figure 13.29: Critical parameters - Nozzle diameter

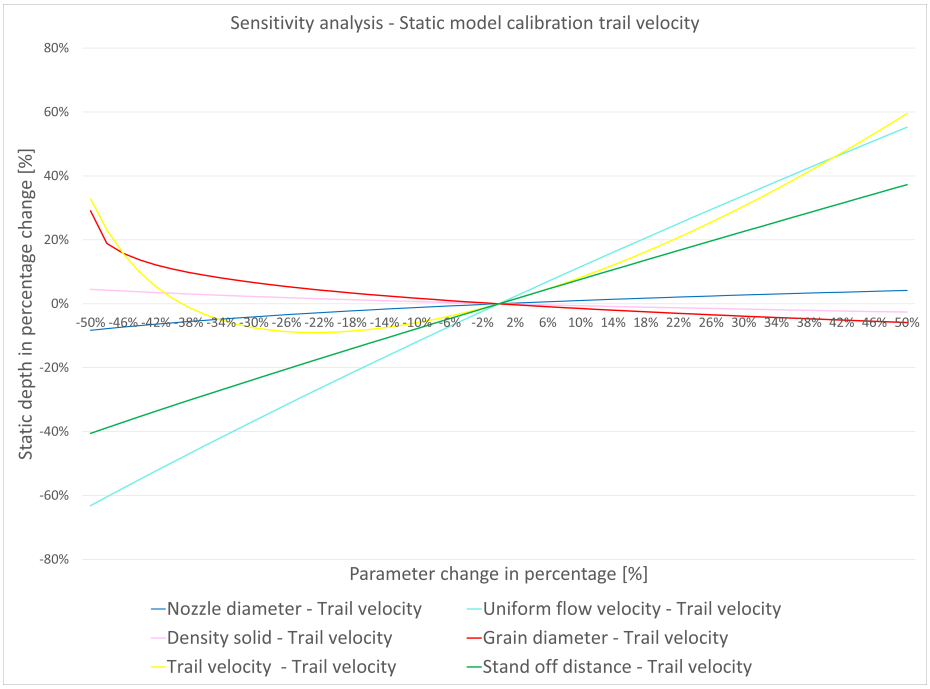

Figure 13.30: Critical parameters - Trail velocity

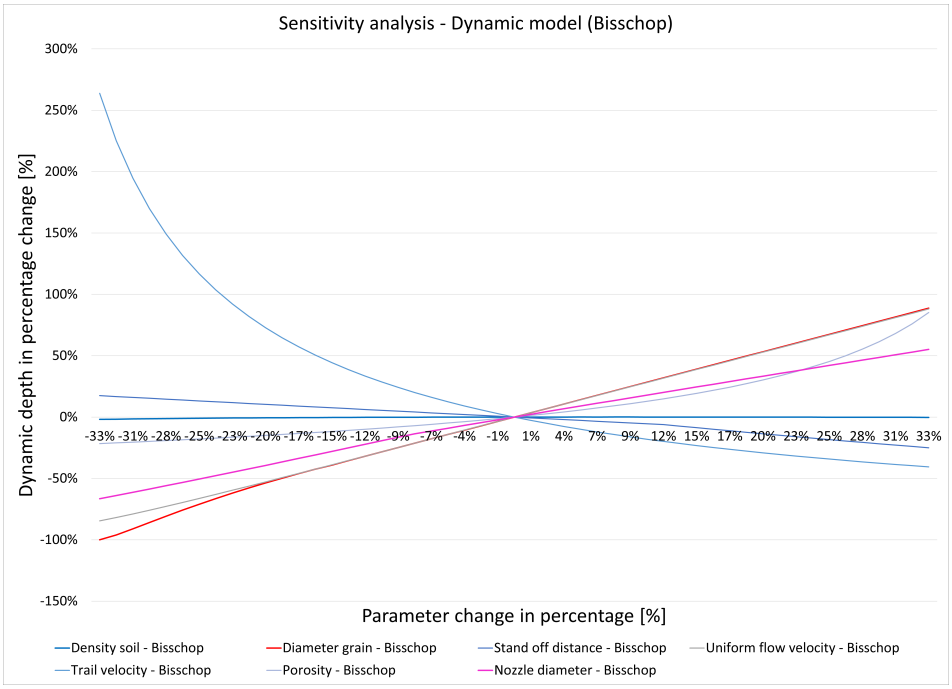

Figure 13.31: Critical parameters - Bisschop et al. (2010)

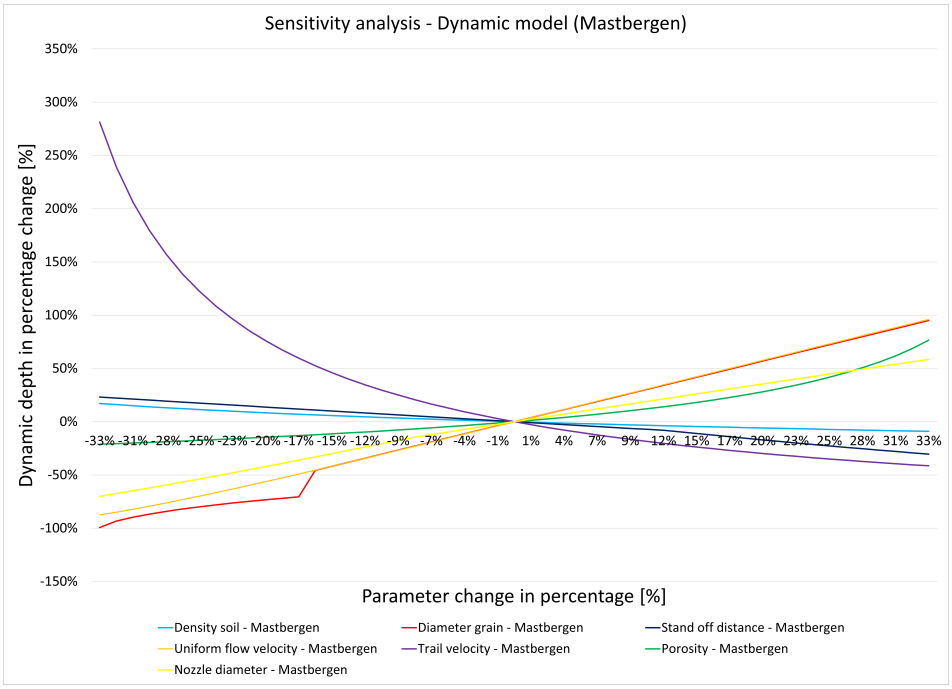

Figure 13.32: Critical parameters - Mastbergen and Van Den Berg (2003)